Structural and biophysical characterization of the mechanism of the inner membrane redox catalyst DsbD from *Escherichia coli*

A dissertation submitted to the

Swiss Federal Institute of Technology Zurich

for the degree of

Doctor of Natural Sciences

Presented by

Anna Rozhkova

Dipl. Biochem. (Moscow State University, Russian Federation)

born on March 27, 1979

citizen of Russian Federation

Accepted on the recommendation of:

Prof. Rudi Glockshuber (examiner)

Prof. Eilika Weber-Ban (co-examiner)

2005

Table of contents

Abbreviations

DTT	dithioteitol
DTNB	dithionitrobenzoic acid
EDTA	ethylenediaminetetraacetic acid
GdmCl	guanidinium chloride
GSH	reduced glutathione
GSSG	oxidized glutathione
HEPES	N-2-hydroxyethylpiperazine-N'-2'-ethanesulfonic acid
HPLC	high performance liquid chromatography
IAM	iodoacetamide
NTB	nitrobenzoic acid
PEG	polyethilenglycol
TCEP	Tris(2-carboxyethyl)phosphine hydrochloride
Tris	Tris-hydroximethyl-aminomethane

1. Abstract

In the periplasm of *Escherichia coli*, Dsb proteins catalyze di̲sulfide b̲ond formation, isomerisation, and reduction. DsbA and DsbB constitute the oxidative pathway that is responsible for the formation of disulfide bonds. DsbD has a central function in the reductive pathway: it transfers electrons from the cytosolic thioredoxin system across the inner membrane to the periplasm. These reducing equivalents are utilized for disulfide bond isomerization (involving DsbC and DsbG) and for reduction of the *c*-type apocytochromes prior to heme ligation (involving CcmG and CcmH). DsbD consists of three domains: two periplasmic domains in the N- and C-terminal region (nDsbD and cDsbD) and a central transmembrane (TM) domain. Each of these domains contains a pair of essential cysteines: C103/C109 in nDsbD, C163/C285 in the TM domain, and C461/C464 in cDsbD. It was postulated that the catalytic mechanism of DsbD is based exclusively on intra- and intermolecular disulfide exchange reactions. According to the existing model, electrons flow successively from thioredoxin to the TM domain of DsbD, then to cDsbD, nDsbD, and finally to the periplasmic substrate proteins. Available structural information on DsbD included the crystal structure of oxidized nDsbD and of the mixed disulfide between nDsbD and DsbC. In addition, a crystal structure of oxidized cDsbD had been reported.

In this thesis, the catalytic mechanism of DsbD was studied using biophysical and biochemical techniques. To study the intrinsic physical properties of the individual periplasmic domains of DsbD, isolated nDsbD and cDsbD were overexpressed and purified to homogeneity. The determined redox potentials of -232 mV and -235 mV, respectively, demonstrate that electron transfer from thioredoxin ($E_0` = -270$ mV) *via* DsbD to DsbC ($E_0` = -140$ mV) is thermodynamically driven. The direction of the electron flow from the periplasmic domains of DsbD to DsbC was confirmed *in vitro* by reversed phase HPLC analysis of acid-quenched reaction products. The overall electron flow from cDsbD$_{red}$ to nDsbD$_{ox}$ and finally to DsbC$_{ox}$ is rapid at 25°C and pH 7.0. Complete reduction of DsbC is achieved within about 500 s when low initial protein concentrations of 0.25 µM are used. Direct reduction of DsbC by cDsbD is extremely slow ($k_{app} = 57$ M^{-1}s^{-1}). As expected, reverse electron transfer from DsbC$_{red}$ to nDsbD$_{ox}$ or cDsbD$_{ox}$ does not occur.

We then measured the kinetics of all functional and non-functional disulfide exchange reactions between different Dsb proteins. The very fast electron transfer from nDsbD$_{red}$ to DsbC$_{ox}$ or DsbG$_{ox}$ ($k_{app} = 4$ x 10^6 M^{-1}s^{-1} and $k_{app} = 2$ x 10^6 M^{-1}s^{-1}, respectively) ensures effective reduction of these proteins by DsbD *in vivo*. In contrast, one of the fastest nonfunctional reactions, reduction of DsbA by nDsbD, is >1000-fold slower ($k_{app} = 900$ M^{-1}s^{-}

[1]). Based on the kinetic data, we can conclude that large kinetic barriers separate the oxidative DsbA/B and the reductive DsbC/D systems and guarantee their independence.

We next showed that C109 and C461 form an inter-domain disulfide bond between nDsbD and cDsbD. This finding allowed crystallization and structure determination of the kinetically stabilized mixed disulfide complex between the C103S variant of nDsbD and the C464S variant of cDsbD (nDsbD-SS-cDsbD) that represents an essential intermediate in the catalytic cycle of DsbD. Comparison of the crystal structure of nDsbD-SS-cDsbD with the known structure of the complex between nDsbD and DsbC revealed a strong overlap between the surface areas of nDsbD that interact with DsbC and cDsbD. Consequently, electron transfer from cDsbD to DsbC via nDsbD must involve large relative domain movements. We also solved crystal structures of oxidized and reduced cDsbD and compared them with the cDsbD structure in the nDsbD-SS-cDsbD complex. cDsbD appears to be a very rigid protein that does not undergo significant conformational changes upon disulfide exchange.

Finally, we proved that DsbD rapidly and directly transfers electrons to the reductase CcmG, and showed that another Ccm protein, CcmH, is not required for this process. For kinetic and structural studies, we produced CcmG as a soluble protein that lacks the N-terminal transmembrane helix. Using stopped-flow fluorescence measurements, we showed fast electron transfer from nDsbD to soluble CcmG *in vitro* ($k_{app} = 4 \times 10^5 \text{ M}^{-1}\text{s}^{-1}$). We also synthesized the mixed disulfide complex between the C103S variant of nDsbD and the C83S variant of soluble CcmG (nDsbD-SS-CcmG) and determined its crystal structure. Comparison of the X-ray structures of all three mixed disulfide complexes of nDsbD (nDsbD-SS-DsbC, nDsbD-SS-cDsbD, and nDsbD-SS-CcmG) revealed the structural basis for the intriguing ability of nDsbD to interact specifically and very rapidly with different target proteins such as the membrane-anchored monomer CcmG and the periplasmic dimers DsbC and DsbG.

2. Introduction

2.1 Oxidative protein folding in bacteria

Oxidative protein folding is a composite process by which a reduced, unfolded protein acquires both its native disulfide bonds and native structure (Narayan *et al.*, 2000). Failure to form proper disulfide bonds, or their slow formation in the cell, is likely to lead to protein aggregation and degradation by proteases. In gram-negative bacteria, disulfide bonds are formed in the oxidizing environment of the periplasm. It has been estimated that more than half of the periplasmic and membrane proteins contain at least one disulfide bond (Haebel *et al.*, 2002; Hiniker and Bardwell, 2004; Kim *et al.*, 2003). *In vitro*, disulfide bonds can be formed spontaneously by molecular oxygen, but the rate of this spontaneous formation is much slower than the rate of disulfide bond formation *in vivo* (Anfinsen, 1973; Saxena and Wetlaufer, 1970). Moreover, the number of possible disulfide cross-links increases by around one order of magnitude with each additional cysteine pair. This means that a protein with four pairs of cysteine residues has less than a 1% chance of attaining the correct four disulfides by random oxidation. Indeed, oxidative protein folding *in vivo* is catalyzed by a variety of thiol-disulfide oxidoreductases and requires two enzymatic activities: disulfide bond formation and isomerization of non-native disulfide bonds.

2.2 The superfamily of thioredoxin-like proteins

Thiol-disulfide oxidoreductases that catalyze disulfide bond formation and isomerization in *Escherichia coli* belong to the thioredoxin superfamily. These proteins share two common features: they contain an active site with a C-X-X-C motif (where X is any amino acid) and an overall structure known as the thioredoxin fold. The thioredoxin fold was named after thioredoxin, in which it was first observed (Martin, 1995). However, the thioredoxin fold is somewhat smaller than thioredoxin itself and consists of a central four-stranded β-sheet with three flanking α-helices (Fig. 1). The thioredoxin fold comprises about 80 core residues, but each of the proteins containing it possesses extra residues in addition to the core. Certain sites in the thioredoxin fold can tolerate insertions without disruption of the overall structure (indicated with asterisks in Fig. 1). Thioredoxin is a monomeric 108-residue single-domain protein that, in addition to the thioredoxin fold, has a β-strand and a *α*-helix at the N-terminus (Fig. 2) (Katti *et al.*, 1990). The periplasmic dithiol oxidase DsbA from *E. coli* is a 189-residue monomer with two distinct domains – a thioredoxin domain and an α-helical domain, which is inserted into the thioredoxin fold between β2 and α2 (Martin *et al.*, 1993).
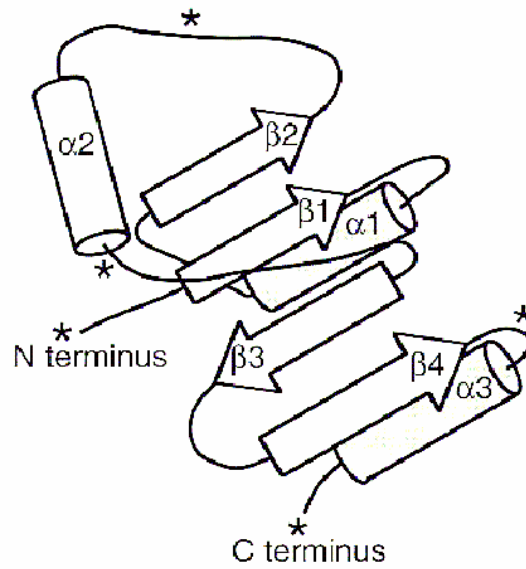
Figure 1. Architecture of the thioredoxin fold. Astrisks indicate sites in the structure at which insertions of residues are found. (Martin, 1995)
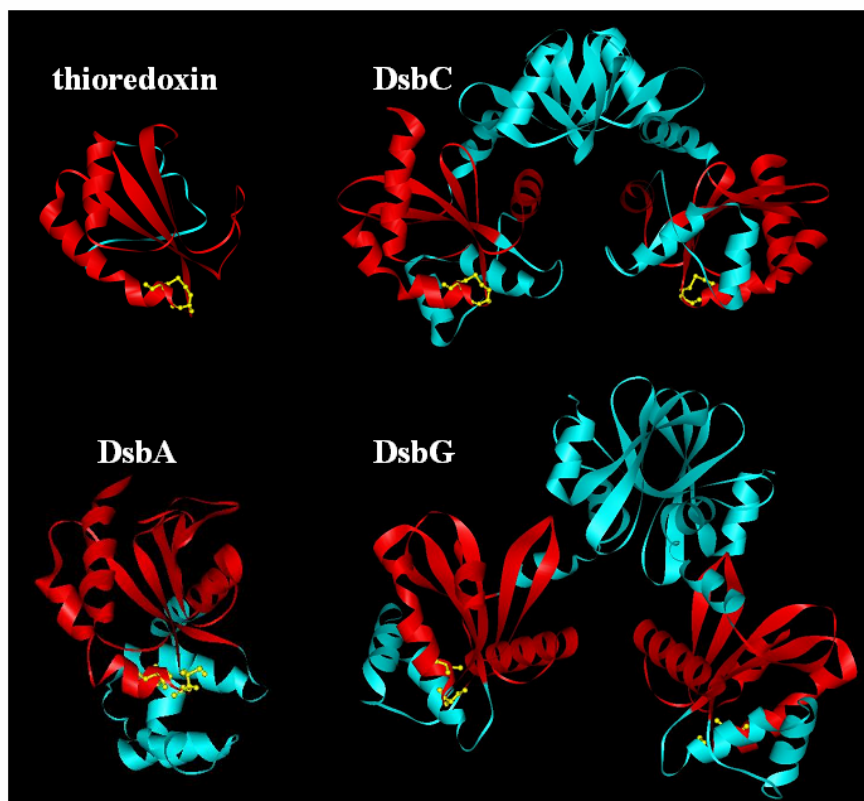
Figure 2. Crystal structures of *E.coli* cytoplasmic thioredoxin and the periplamic thiol-disulfide oxidoreductases: DsbA, DsbC, and DsbG. The thioredoxin fold is depicted in red. Active site cysteine residues are shown in yellow. (Heras *et al.*, 2004; Katti *et al.*, 1990; Martin *et al.*, 1993; McCarthy *et al.*, 2000)

Finally, the periplasmic disulfide isomerase DsbC and its homologue DsbG are homodimers of 216 and 231-residue subunit, respectively, consisting of a N-terminal dimerization domain and a C-terminal thioredoxin domain (Heras *et al.*, 2004; McCarthy *et al.*, 2000). Despite the common C-X-X-C active site motif and the overall structural similarity, the individual members of the thioredoxin superfamily show low sequence identity and vary widely in their oxidizing power and therefore in their function (Martin, 1995).

2.3 Mechanism of thiol-disulfide exchange

Oxidation and reduction of disulfide bonds is mediated by fast thiol-disulfide exchange between the active site cysteines of an enzyme and the cysteines of a substrate protein. The catalytic mechanism of thioredoxin-like thiol-disulfide oxidoreductases involves cycling of their active site cysteine residues between the reduced and disulfide-bonded forms, *via* an intermediate with a mixed disulfide bond between the catalyst and the substrate protein (Fig. 3) (Darby and Creighton, 1995; Frech *et al.*, 1996; Kallis and Holmgren, 1980).
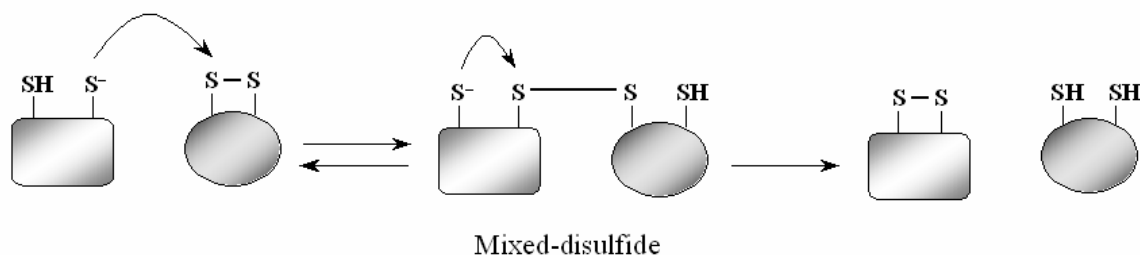
Figure 3. Thiol-disulfide exchange reaction between proteins. (Sevier and Kaiser, 2002)

In the C-X-X-C motif of thioredoxin-like proteins, only the N-terminal cysteine is exposed to solvent, and able to form mixed disulfide with protein substrates. The reaction rates of disulfide exchange between a thiol-disulfide oxidoreductase and a peptide substrate vary between 10^3-10^7 $M^{-1}s^{-1}$ (Darby *et al.*, 1998), which is several orders of magnitude faster than disulfide exchange between alkyl thiols (10-10^3 $M^{-1}s^{-1}$)(Shaked *et al.*, 1980; Szajewski and Whitesides, 1980). Factors that determine the reaction rates are the pK_a of the N-terminal active site cysteine, the effective concentration and accessibility of the thiol or disulfide groups in the substrate, and the chemical enviroment of the active site.

2.4 pK_a values, redox properties, and C-X-X-C motifs of thioredoxin-like proteins

Only deprotonated thiols can act as nucleophiles in disulfide exchange reactions. The extent of thiol ionization at any particular pH and, consequently, its intrinsic chemical reactivity are determined by the pK_a of the thiol (Holmgren, 1985; Kortemme and Creighton, 1995; Nelson and Creighton, 1994). Moreover, the *pK_a* values also determine the intrinsic reactivity of the sulfur atoms even when they are involved in a disulfide bond (Creighton, 1975; Szajewski and Whitesides, 1980). Thus the pK_a values of all sulfurs affect the rates and direction of disulfide exchange reactions. Biophysical studies on DsbA (Grauschopf *et al.*, 1995; Hennecke *et al.*, 1997; Huber-Wunderlich and Glockshuber, 1998; Jacobi *et al.*, 1997; Nelson and Creighton, 1994) and thioredoxin (Chivers *et al.*, 1996; Dyson *et al.*, 1997; Mossner *et al.*, 1998) revealed that the pK_a value of the nucleophilic, N-terminal cysteine thiol of the C-X-X-C motif is a critical factor for the redox properties of thiol-disulfide oxidoreductases. In DsbA, the extremely low pK_a value (~3.5 compared to a value of 9.5 for a normal cysteine) of the nucleophilic thiol stabilizes the reduced state of the active site and explains the observation that reduced DsbA is 23 kJ/mol more stable than oxidized DsbA (Grauschopf *et al.*, 1995; Hennecke *et al.*, 1997; Nelson and Creighton, 1994; Wunderlich and Glockshuber, 1993; Zapun *et al.*, 1993). The very low pK_a implicates that the nucleophilic thiol of DsbA is fully ionized and reactive at physiological pH, explaining the high rate of disulfide interchange. These features make DsbA a very strong oxidase. In contrast, thioredoxin is the most reducing member of the family and its nucleophilic thiol possesses a pK_a value of about 7.1 (Mossner *et al.*, 1998). For various DsbA and thioredoxin active site variants and also for the wild type proteins, a correlation between increased redox potentials and decreased pK_a values of the nucleophilic active site thiols was observed (Grauschopf *et al.*, 1995; Huber-Wunderlich and Glockshuber, 1998; Mossner *et al.*, 1998). It has been demonstrated that the dipeptide sequence between the active-site cysteines strongly influences the pK_a values and redox properties of thioredoxin-like thiol-disulfide oxidoreductases (Chivers *et al.*, 1996; Grauschopf *et al.*, 1995; Holst *et al.*, 1997; Huber-Wunderlich and Glockshuber, 1998; Krause *et al.*, 1991; Mossner *et al.*, 1998; Mossner *et al.*, 1999; Rossmann *et al.*, 1997). For example, a proline that follows the nucleophilic cysteine in the active site motif of DsbA (Table 1) seems to be responsible for the oxidizing power of DsbA, whereas a proline residue at the second position of the dipeptide is typical for the reductant thioredoxin (Kortemme and Creighton, 1995; Mossner *et al.*, 1998).

protein	C-X-X-C motif	E_0', mV	pK_a
thioredoxin	C-G-P-C	- 270[a]	7.1[g]
DsbA	C-P-H-C	- 122[b]	3.5[h]
DsbC	C-G-Y-C	- 140[c]	4.1[i]
DsbD	C-V-A-C	- 235[d]	-
DsbG	C-P-Y-C	- 129[e]	-
CcmG	C-P-T-C	- 210[f]	6.7[f]

Table 1. Active site C-X-X-C motifs, redox potentials, and p*Ka* values of *E. coli* thioredoxin proteins. ([a] – (Krause *et al.*, 1991); [b] – (Wunderlich and Glockshuber, 1993; Zapun *et al.*, 1993); [c] – (Rozhkova *et al.*, 2004; Zapun *et al.*, 1995); [d] – (Collet *et al.*, 2002; Rozhkova *et al.*, 2004); [e] – (Bessette *et al.*, 1999; van Straaten *et al.*, 1998); [f] – (Li *et al.*, 2001); [g] –(Mossner *et al.*, 1998); [h] – (Nelson and Creighton, 1994); [i] – (Sun and Wang, 2000)

In addition, a histidine residue at the second position of dipeptide appears to stabilize the thiolate anion of DsbA and contribute to its low pK_a (Guddat *et al.*, 1998). Indeed, replacement of the X-X dipeptide in DsbA or thioredoxin by the active site sequence of other thiol-disulfide oxidoreductases shifts the pK_a values towards the corresponding value of related enzyme. The X-X dipeptides are characteristic for the individual members of the thioredoxin superfamily (Table 1).

2.5 Disulfide bond formation and isomerization in *Escherichia coli*

2.5.1 The Dsb protein family

In the periplasm of *E. coli*, formation and isomerisation of d̲i̲s̲ulfide b̲onds is catalyzed by Dsb proteins that constitute two independent pathways (Fig. 4). The oxidative DsbA/DsbB pathway is responsible for disulfide bond formation (Bardwell *et al.*, 1991; Bardwell *et al.*, 1993; Dailey and Berg, 1993). The oxidizing power utilized by this pathway comes from the membrane-embedded electron transport system. The reductive DsbC/DsbD pathway
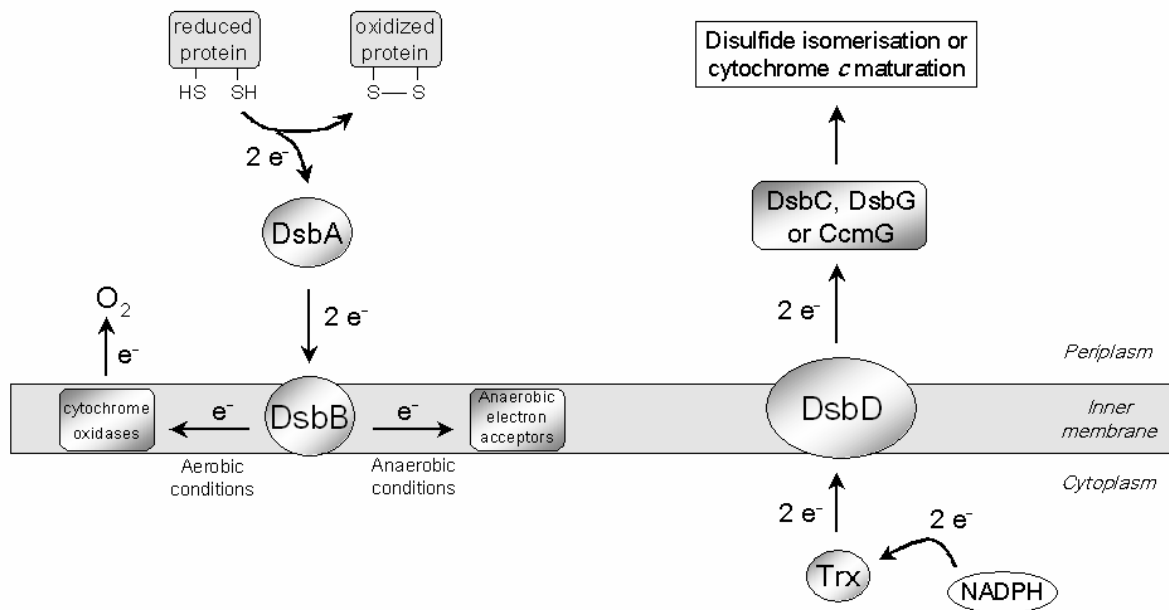
Figure 4. Oxidative DsbB and reductive DsbD pathways in *Escherichia coli*. Arrows indicate the direction of electron flow.

guaranties efficient disulfide bond isomerization (Bolhuis *et al.*, 1999; Krupp *et al.*, 2001; Missiakas *et al.*, 1995; Rietsch *et al.*, 1997; Stewart *et al.*, 1999). The reducing equivalents required for maintance of the catalytically active, reduced state of DsbC originate from the cytosolic thioredoxin system.

2.5.2 The periplasmic dithiol oxidase DsbA

 DsbA was the first identified bacterial protein required for disulfide bond formation *in vivo* (Bardwell *et al.*, 1991; Kamitani *et al.*, 1992). It was observed that *dsbA⁻* strains are hypersensitive to benzylpenicillin, dithiothreitol and metals (Missiakas *et al.*, 1993; Stafford *et al.*, 1999). They show reduced levels of several secreted proteins such as the outer-membrane protein OmpA, alkaline phosphatase, and β-lactamase (Bardwell *et al.*, 1991). They do not exhibit motility because of lack of the properly assembled flagellar motor (Dailey and Berg, 1993). In addition, *dsbA* mutants of many pathogenic bacteria are avirulent since virulence components such as pili and toxins are not properly folded and/or assembled (Peek and Taylor, 1992). DsbA is a strong oxidase that very rapidly and randomly introduces disulfide bonds into a wide variety of substrate proteins. Recently, Hiniker and Bardwell identified 10 cysteine-containing proteins from the *E. coli* periplasm that are *in vivo* substrates

of DsbA. Six of these proteins (PhoA, DppA, Rnase I, FlgI, HisJ, and LivJ) contain at least one known structural disulfide bond (Hiniker and Bardwell, 2004). Upon oxidation of substrate polypeptides, DsbA becomes reduced and is re-oxidized by DsbB (Bardwell *et al.*, 1993; Guilhot *et al.*, 1995; Kishigami *et al.*, 1995; Kishigami and Ito, 1996).

2.5.3 DsbB recycles oxidized DsbA

In 1993, three groups independently identified and characterized the *E. coli dsbB* gene, whose protein product was required for disulfide bond formation in periplasmic proteins (Bardwell *et al.*, 1993; Dailey and Berg, 1993; Missiakas *et al.*, 1993). *dsbB* mutants exhibit the same pleotropic phenotype as *dsbA* mutants, suggesting that both proteins belong to the same oxidation pathway (Missiakas *et al.*, 1993). This hypothesis was confirmed by the observation that in *dsbB⁻* strains DsbA accumulates in the reduced state, while in wild type strains DsbA is completely oxidized (Kishigami *et al.*, 1995). The isolation of a DsbA-DsbB mixed-disulfide complex confirmed that DsbA and DsbB interact directly (Guilhot *et al.*, 1995; Kishigami *et al.*, 1995). In addition, Bader and coworkers showed rapid direct re-oxidation of DsbA by DsbB *in vitro* (Bader *et al.*, 1998). DsbB is a 20 kDa inner membrane protein (Fig. 5), predicted to have four transmembrane helices and two periplasmic loops (Jander *et al.*, 1994). DsbB has four essential cysteine residues – one pair in each of the periplasmic loops (Guilhot *et al.*, 1995; Kishigami *et al.*, 1995; Kishigami and Ito, 1996; Kobayashi *et al.*, 1997; Kobayashi and Ito, 1999). The electrons from reduced DsbA first flow to the DsbB C-
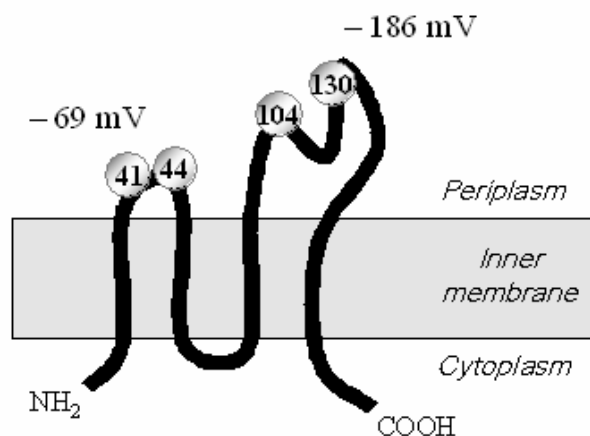

Figure 5. Membrane topology of DsbB. DsbB is predicted to consist of four transmembrane helices and two periplasmic loops each containing a pair of essential cysteines. The redox potentials of cysteine pairs C41-C44 and C104-C130 are – 69 mV and – 186 mV, respectively (Grauschopf *et al.*, 2003).

terminal cysteine pair (C104-C130), which has a redox potential of –186 mV, and then to the

N-terminal cysteine pair (C41-C44) with a redox potential of –69 mV (Grauschopf *et al.*, 2003). Re-oxidation of the N-terminal cysteine pair occurs through ubiquinone, which, under aerobic conditions, donates the electrons to cytochrome oxidases and finally to oxygen (Bader *et al.*, 1999; Bader *et al.*, 2000). Under anaerobic conditions the electrons are passed from DsbB to menaquinone and then to fumarate or nitrate reductase (Bader *et al.*, 1999). Using purified components, Bader and coworkers showed that quinones could act as direct recipients of electrons from DsbB (Bader *et al.*, 1999). Thus, DsbB has the novel ability to generate a disulfide bond in DsbA by reduction of quinones.

2.5.4 The protein disulfide isomerase DsbC

It has been demonstrated that DsbA can introduce wrong disulfide bonds into substrate proteins and therefore trap the proteins in nonnative conformations both *in vitro* and *in vivo* (Bader *et al.*, 2000; Hiniker and Bardwell, 2004). The incorrectly formed disulfides must be isomerized to the native conformation to allow proper folding of the proteins. The first step in the discovery of the isomerization pathway in prokaryotes was the identification of the periplasmic protein disulfide isomerase DsbC (Missiakas *et al.*, 1994; Shevchik *et al.*, 1994). The *E. coli dsbC* gene was isolated independently by screening for dithiothreitol-sensitive mutations (Missiakas *et al.*, 1994) and as a suppressor of a *dsbA* null phenotype (Shevchik *et al.*, 1994). Like *dsbA⁻* and *dsbB⁻* strains, *dsbC* mutants are defective in disulfide bond formation, but the defect in absence of DsbC is much milder (Rietsch *et al.*, 1996). For instance, mutations in DsbC neither affect cell motility nor the formation of OmpA and β-lactamase. The function of DsbC was established using *in vitro* folding assays with model substrate polypeptides and confirmed in expression studies of exogenous proteins in various *dsb⁻* backgrounds (Darby *et al.*, 1998; Joly and Swartz, 1997; Rietsch *et al.*, 1996; Rietsch *et al.*, 1997; Sone *et al.*, 1997; Zapun *et al.*, 1995). It was found that DsbC is required for the correct folding of proteins with multiple disulfide bonds. Moreover, Joly and Schwartz (1997) demonstrated that overproduction in *E. coli* of heterologous proteins with consecutive disulfide bonds did not require DsbC, whereas the yield of proteins with nonconsecutive bridges was decreased by 50% in *dsbC⁻* strains (Joly and Swartz, 1997). Recently, Hiniker and Bardwell have shown that two *E. coli* periplasmic proteins, RNase I (4 disulfide bonds) and MepA (6 conserved cysteines), are *in vivo* substrates of DsbA and DsbC (Hiniker and Bardwell, 2004). The quantity of RNase I and MepA was dramatically decreased in *dsbA⁻* and *dsbC⁻* strains. In contrast, the levels of two other DsbA-dependent proteins (PhoA and DppA) were unchanged in *dsbC⁻* strains. PhoA and DppA contain only consecutive disulfide

bonds, whereas RNase I contains one non-consecutive disulfide bond in addition to three consecutive ones. So far the disulfide connectivity of MepA remains unknown. These findings suggest that DsbC is required for the folding of proteins with at least one non-consecutive disulfide bond, whereas DsbA is important for disulfide bond formation in all disulfide-containing proteins translocated to the periplasm. The proposal that disulfide bond connectivity determines whether a protein requires DsbC for its proper folding got further support in the work of Berkmen and colleagues (Berkmen *et al.*, 2005). The authors showed that acid phosphatase phytase (AppA) that has one non-consecutive disulfide bond requires DsbC for its proper folding. However, the activity of an AppA variant lacking the non-consecutive bond is DsbC-independent. Additionally, a homolog of AppA that contains only consecutive bonds and does not need DsbC becomes DsbC-dependent upon engineering of a non-consecutive bond.

DsbC is a V-shaped homodimeric isomerase that belongs to the thioredoxin superfamily. Each DsbC subunit consists of an N-terminal dimerization domain and a C-terminal thioredoxin domain with a C-G-Y-C motif. Sun and Wang (2000) showed that the dimerization of DsbC is required for its function *in vivo* (Sun and Wang, 2000). The crystal structure (Fig.6) revealed that DsbC combines two basic features required for disulfide bond isomerase activity, namely a thiolate active site that can attack and reshuffle substrate

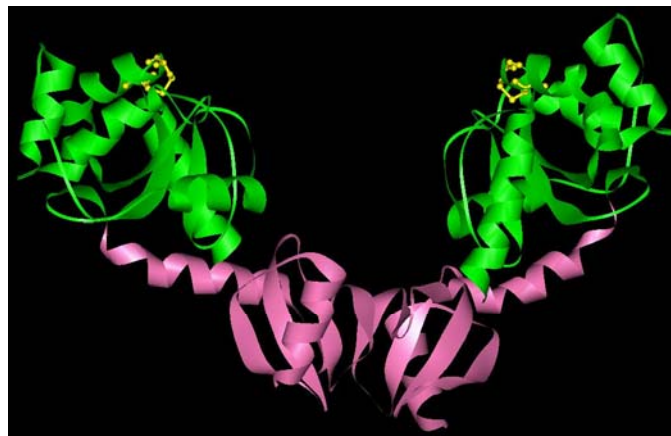**Figure 6. Ribbon diagram of the DsbC homodimer.** The N-terminal dimerisation domain and the C-terminal catalytic domain are depicted in pink and green, respectively. Active site cysteine residues are shown in yellow. (McCarthy *et al.*, 2000)

disulfide bonds, and an uncharged surface to bind folding substrate peptides (McCarthy *et al.*, 2000). Both active sites of DsbC are separated by ~40 Å and oriented towards the inside of

the "V". The surface of the cleft between the two arms of the V is lined with hydrophobic and uncharged residues, enabling non-covalent binding of substrate proteins. It was proposed that the cleft can switch between open and closed conformations in order to adjust to the binding partner (Haebel *et al.*, 2002). Substrate binding appears to play a significant role in catalysis by DsbC (Darby *et al.*, 1998). The reactions between DsbC and substrate peptides occur at rates up to 10^5-fold faster than those involving DsbC and glutathione. Such rate enhancement might be due to considerably increased effective concentrations of the reacting groups upon peptide binding to the catalyst. In fact, mixed-disulfide complexes of DsbC and the peptides are 10^4-fold more stable than the corresponding mixed-disulfides with glutathione. In addition, the stability of the enzyme-peptide mixed-disulfide relative to the stability of a disulfide bond in a folding protein favours breakage of unstable substrate disulfide bonds and provides the opportunity for the formation of new more stable disulfides. The intramolecular thiol-disulfide exchange reaction between DsbC and a scrambled protein can occur only if the active site cysteines of DsbC are reduced (Joly and Swartz, 1997; Rietsch *et al.*, 1997). *In vivo*, reduction of DsbC is carried out by DsbD (Missiakas *et al.*, 1995; Rietsch *et al.*, 1997). In the absence of DsbD, cytoplasmic thioredoxin or cytoplasmic thioredoxin reductase, DsbC is found completely oxidized *in vivo* (Chung *et al.*, 2000; Katzen and Beckwith, 2000; Missiakas *et al.*, 1995; Rietsch *et al.*, 1997).

2.5.5 The inner membrane electron transporter DsbD

DsbD is a 59 kDa inner membrane protein that consists of three domains: a periplasmic N-terminal domain (nDsbD), a central transmembrane (TM) domain with eight predicted TM helices, and a C-terminal domain (cDsbD) that is again oriented towards the periplasm. The suggested topological structure of DsbD (Fig. 7) was derived from a combination of *in vivo* experiments with alkaline phosphatase fusions and computational algorithms for transmembrane sequences prediction (Chung *et al.*, 2000; Gordon *et al.*, 2000; Stewart *et al.*, 1999). Mutational analyses showed that each of the domains contains one pair of conserved cysteine residues essential for DsbD activity *in vivo* (Chung *et al.*, 2000; Gordon *et al.*, 2000; Stewart *et al.*, 1999). The two invariant cysteines of the TM domain are located within the membrane-spanning region, C163 in TM helix 1 and C285 in TM helix 4 (Fig. 7). DsbD can be split into its three structural domains without loss of *in vivo* activity (Katzen and Beckwith, 2000): simultaneous expression of the three separated DsbD domains restores reduction of DsbC and cytochrome *c* maturation. However, when any of the three domains is removed from the system, oxidized DsbC accumulates and the formation of holocytochromes is
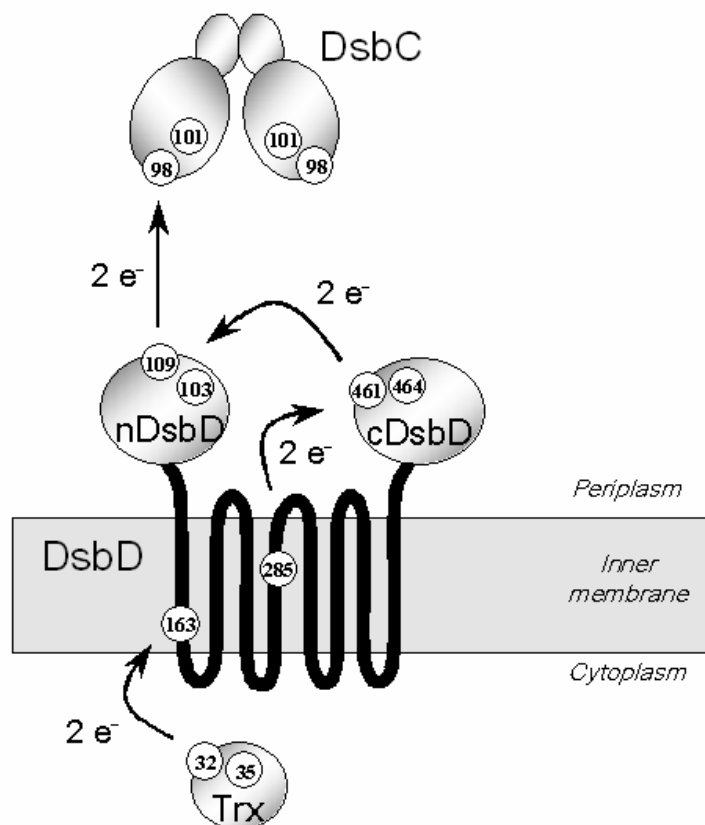
Figure 7. Model of the electron flow from thioredoxin (Trx) to DsbC via DsbD. Electron transport is proposed to occur exclusively through inter- and intramolecular disulfide exchange. Arrows indicate the direction of electron flow. Essential cysteines are depicted as circles with corresponding numbers.

abolished. These results indicate that all three domains are required for DsbD activity, but do not need to be part of a single polypeptide. Additionally, it has been shown that both nDsbD and cDsbD are oxidized when the TM domain is not present, whereas absence of nDsbD does not affect the redox state of the other two domains. cDsbD is required for the reduction of nDsbD, but not the TM domain. Taken together these results demonstrate that electrons within the DsbD molecule flow from the TM domain to cDsbD and finally to nDsbD. The detection of apparent reaction intermediates in the form of mixed disulfides indicated direct electron flow from thioredoxin via DsbD to DsbC or CcmG (Katzen and Beckwith, 2000; Krupp *et al.*, 2001). *In vivo*, the TM domain forms a mixed disulfide with thioredoxin, and nDsbD forms a mixed disulfide with DsbC or CcmG. This demonstrates that DsbD utilizes at least two thiol-disulfide exchange reactions during the electron transfer from cytoplasmic thioredoxin to the periplasmic substrates. The direct reduction of DsbC by nDsbD was confirmed *in vitro* (Goldstone *et al.*, 2001). Studies on mixed disulfides combined with mutational analyses allowed the specification of DsbD cysteines involved in the reaction.

C163 of the TM domain forms a disulfide bond with C32 of thioredoxin, and C109 of nDsbD interacts with periplasmic substrate proteins. It was proposed that the catalytic mechanism of DsbD is exclusively based on inter- and intra-molecular disulfide exchange reactions. According to the existing model (Fig. 7), the TM domain accepts electrons from cytoplasmic thioredoxin and transfers them across the inner membrane to cDsbD, followed by successive reduction of nDsbD and finally of DsbC, DsbG or CcmG (Chung *et al.*, 2000; Katzen and Beckwith, 2000; Katzen *et al.*, 2002; Krupp *et al.*, 2001). It is likely that a significant conformational change takes place during the interconvertions of oxidized and reduced forms of the TM domain (Katzen and Beckwith, 2003; Krupp *et al.*, 2001; Porat *et al.*, 2004), making the membrane-embedded cysteines alternatively accessible to the cytoplasm or to the periplasm. It is assumed that in the reduced state, the catalytic cysteines of the TM domain are accessible from the periplasm and available for interaction with oxidized cDsbD, while in the oxidized state, the disulfide bonds are accessible from the cytoplasm and interact with reduced thioredoxin (Katzen and Beckwith, 2003; Porat *et al.*, 2004).

Recently, crystal structures of both soluble periplasmic domains of DsbD and of the nDsbD-DsbC mixed disulfide complex were solved. The crystal structure of oxidized nDsbD revealed an immunoglobulin-like fold consisting of a β-sandwich formed by two antiparallel β–sheets and a catalytic subdomain that is inserted into the immunoglobulin-like fold (Fig. 8A) (Goulding *et al.*, 2002). In the oxidized form of nDsbD, the two active site cyteines form a disulfide bond between two β-strands. The active site disulfide is completely shielded from the environment by the active-site cap-loop region. Importantly, the nDsbD-SS-DsbC complex exhibits a stoichiometry of one nDsbD monomer per DsbC homodimer (Fig. 8B) (Haebel *et al.*, 2002). This is due to the fact that nDsbD binds into the central cleft of the V-shaped DsbC dimer and forms specific contacts with both catalytic domains of DsbC. Comparison of the complex with oxidized nDsbD revealed large conformational changes in the cap structure that regulates the accessibility of the nDsbD active site. In addition, Haebel and coworkers proposed that nDsbD exploits changes in the charge distribution of the active site to distinguish between oxidized and reduced forms of DsbC. cDsbD is a thioredoxin-like protein with a C-V-A-C active site motif. It possesses a thioredoxin fold and shares 28% sequence identity with thioredoxin. cDsbD consists of six α-helices and 4 β-strands, with an extended N-terminal stretch (Fig. 8C) (Kim *et al.*, 2003). This N-terminal stretch might serve as a flexible linker between the TM domain and cDsbD, allowing physical movement of cDsbD during electron shuttling.
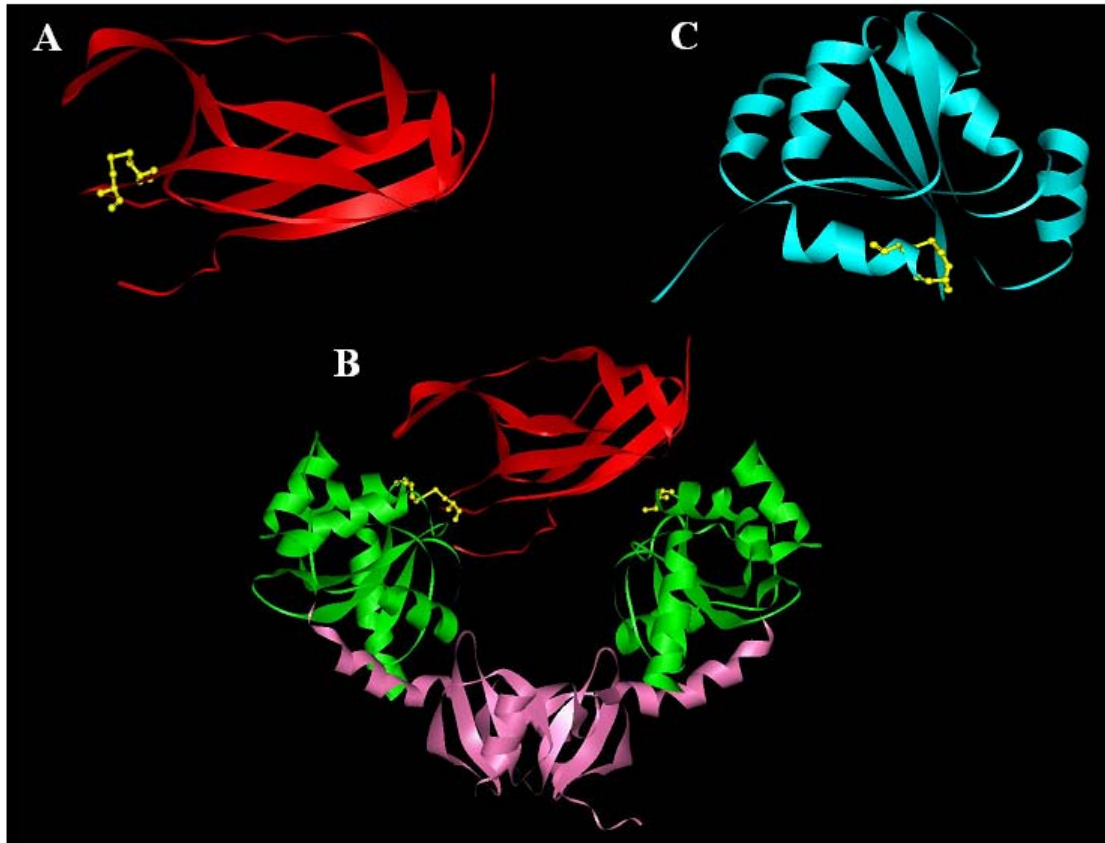
Figure 8. Crystal structures of nDsbD (A), nDsbD-SS-DsbC complex (B), and cDsbD (C). nDsbD is depicted in red. The N-terminal dimerization domain and the C-terminal catalytic domain of DsbC are in pink and green, respectively. cDsbD is depicted in cyan. Active site cysteine residues are shown in yellow. (Goulding *et al.*, 2002; Haebel *et al.*, 2002; Kim *et al.*, 2003)

2.5.6 DsbG is a homologue of DsbC

DsbG is another periplasmic substrate of DsbD (Bessette *et al.*, 1999; Chung *et al.*, 2000). It was recently discovered on the basis of its ability to confer resistance to high concentrations of DTT, when encoded by a multicopy plasmid (Andersen *et al.*, 1997). DsbG is the least abundant of the periplasmic Dsb proteins (Bessette *et al.*, 1999). DsbG is a homodimeric protein that shows 28% sequence identity and 56% sequence similarity to DsbC (Andersen *et al.*, 1997; McCarthy *et al.*, 2000). The redox potentials of DsbC (–140 mV) and DsbG (–129 mV) are also similar (Bessette *et al.*, 1999; Rozhkova *et al.*, 2004; van Straaten *et al.*, 1998; Zapun *et al.*, 1995). Based on *in vivo* and *in vitro* data, it was proposed that DsbG has disulfide isomerase and chaperone activities (Bessette *et al.*, 1999; Shao *et al.*, 2000). Bessette

and colleagues showed that overexpression of DsbG can partially rescue the formation of multidisulfide proteins in a *dsbC* mutant background. However, DsbG was inactive in the classical insulin-reduction assay and, unlike DsbC, it does not catalyze oxidative refolding of RNaseA (Bessette *et al.*, 1999). Moreover, in contrast to DsbC, no *in vivo* substrates of DsbG were found (Hiniker and Bardwell, 2004). These findings suggest that DsbG is a specialized disulfide isomerase with considerably different substrate specificity compared to DsbC. Comparison of the recently solved structure of DsbG (Heras *et al.*, 2004) with the structure of DsbC (McCarthy *et al.*, 2000) offered clues to the differing substrate specificity of DsbG and DsbC. The uncharged surface of the DsbC cleft is consistent with binding of unfolded proteins. In contrast, the size and surface charge of the DsbG binding sites indicate that its substrates are likely to be much larger than those of DsbC and that they could be partially or completely folded.

2.6 The *Escherichia coli* thioredoxin system

The thioredoxin system supplies a variety of substrate proteins both in the cytosol and in the periplasm with reducing power (Holmgren, 1985). It is composed of cytosolic thioredoxin, thioredoxin reductase, and NADPH. Thioredoxin is a ubiquitous disulfide reductase responsible for maintaining proteins in their reduced state (Holmgren, 1985). It was first discovered as a hydrogen donor for ribonucleotide reductase (Laurent *et al.*, 1964), but later recognized as a general protein disulfide reductase that contributes to the cellular thiol-disulfide equilibrium (Derman *et al.*, 1993; Holmgren, 1985; Russel and Model, 1986). In the periplasm of *E. coli*, two different systems depend on the reducing potential of thioredoxin: disulfide bond isomerization and cytochrome *c* maturation pathways (Bolhuis *et al.*, 1999; Fabianek *et al.*, 1999; Krupp *et al.*, 2001; Missiakas *et al.*, 1995; Rietsch *et al.*, 1997; Stewart *et al.*, 1999). Upon reduction of a target protein, thioredoxin becomes oxidized and its reduced form is regenerated by thioredoxin reductase. Thioredoxin reductase is a dimeric FAD-containing enzyme that catalyzes the NADPH-dependent reduction of thioredoxin (for a review see (Williams, 1995)). The enzymatic mechanism of the thioredoxin system involves the transfer of electrons from NADPH via a system of redox-active disulfides. Electrons flow from NADPH to FAD, then to the active site disulfide of thioredoxin reductase, and finally to thioredoxin (for reviews see (Holmgren, 1985; Williams, 1995)). *In vitro*, reduction of thioredoxin by NADPH is very efficiently catalysed by thioredoxin reductase with a k_{cat}/K_m value of about 10^7 M^{-1}s^{-1} (Mossner *et al.*, 1999). As thioredoxin is mainly in the reduced state

in *E. coli* cells (Holmgren and Fagerstedt, 1982), it appears that NADPH-dependent reduction of thioredoxin is not rate-limiting for the catalytic cycle of thioredoxin *in vivo*.

2.7 Cytochrome *c* maturation

2.7.1 General

The *c*-type cytochromes are soluble or membrane-anchored electron transfer proteins that are components of various photosynthetic and/or respiratory chains in bacteria, mitochondria, and chloroplasts. A special feature of the *c*-type cytochromes is the covalent attachment of the vinyl side groups of heme *via* two thioether bonds to the cysteine residues of the conserved C-X-X-C-H motif in apocytochrome *c* (Sambongi *et al.*, 1996). In the bacterial *c*-type cytochromes, the heme domain is located on the outer side of the cytoplasmic membrane (Thony-Meyer *et al.*, 1994). Synthesis of both the apocytochrome and the heme occurs in the cytoplasm followed by their separate export across the cytoplasmic membrane (Page and Ferguson, 1990) and covalent attachment of heme to the polypeptide. The heme-iron and the cysteines in the heme-binding motif of apocytochrome must be reduced prior to heme ligation (Sambongi *et al.*, 1996). The overall post-translational process that leads to the formation of properly folded cytochrome *c* with one (or more) covalently attached heme is called cytochrome *c* maturation or biogenesis.

2.7.2 Cytochrome c maturation in Escherichia coli

In *E. coli*, *c*-type cytochromes are synthesized exclusively under anaerobic conditions, under which the expression of the *ccm* genes is induced (Choe and Reznikoff, 1993; Rabin and Stewart, 1993; Tanapongpipat *et al.*, 1998). Eight genes called *ccmABCDEFGH* are specifically required for cytochrome c maturation in *E. coli* (Grove *et al.*, 1996; Thony-Meyer *et al.*, 1995). In addition, it was shown that gene products of the general secretion pathway (Sec-system) and cellular redox control system (the thioredoxin system and Dsb proteins) contribute to efficient cytochrome *c* biogenesis (Crooke and Cole, 1995; Grove *et al.*, 1996; Metheringham *et al.*, 1995; Sambongi and Ferguson, 1994, 1996). Lack of DsbA, DsbB, or DsbD results in a cytochrome *c* negative phenotype (Crooke and Cole, 1995; Metheringham *et al.*, 1995; Metheringham *et al.*, 1996; Sambongi and Ferguson, 1994, 1996), underlining the importance of balanced redox conditions for cytochrome *c* biogenesis. Ccm proteins are believed to form a membrane protein complex that coordinates delivery and attachment of heme to apocytochromes (for a review, see (Thony-Meyer, 2000, 2002)). CcmA is a peripheral membrane protein with a well-conserved ATP binding cassette (Goldman *et al.*,

1997a; Goldman *et al.*, 1997b). CcmB, an integral membrane protein with six transmembrane helices, is believed to be a permease. CcmA and CcmB seem to be the subunits of an ABC transporter. CcmC is an integral membrane protein with six predicted transmembrane helices that catalyze covalent attachment of heme to CcmE (Ahuja and Thony-Meyer, 2003; Ren and Thony-Meyer, 2001; Schulz *et al.*, 1998). Formation of the heme-binding form of CcmE is significantly enhanced in the presence of the small integral membrane protein CcmD, which apparently stabilizes CcmE in the membrane and influences the interaction between CcmC and CcmE (Ahuja and Thony-Meyer, 2005; Schulz *et al.*, 1999). The subsequent heme transfer from the holo-CcmE intermediate to apocytochrome *c* involves further integral membrane proteins, CcmF and CcmH, and also the membrane-anchored thioredoxin-like reductase CcmG (Fabianek *et al.*, 1998, 2000; Reid *et al.*, 2001; Schulz *et al.*, 1999). Co-immunoprecipitation experiments revealed that CcmF interacts directly with CcmE and CcmH, but not with apocytochrome *c*. This is in agreement with the view that CcmF and CcmH form a heme lyase complex in which CcmH recruits the apocytochrome and CcmF recruits the heme moieties for ligation (Ren *et al.*, 2002). As the ligation occurs in the oxidizing environment of the periplasm, the heme-binding cysteines of apocytochromes are likely to be oxidized and must be re-reduced for heme attachment. Bacteria have evolved a specific reductive pathway that utilizes the reducing power of cytoplasmic NADPH for the reduction of apocytochromes. In *E. coli*, electrons originating from NADPH are thought to flow from DsbD *via* CcmG and CcmH to apocytochromes *c* (Chung *et al.*, 2000; Crooke and Cole, 1995; Fabianek *et al.*, 1998; Fabianek *et al.*, 1999; Reid *et al.*, 1998; Reid *et al.*, 2001; Sambongi and Ferguson, 1994).

2.7.3 CcmG is a specific reductase from Escherichia coli

CcmG is a 20 kDa periplasmic, membrane-anchored thioredoxin-like protein essential for cytochrome *c* maturation (Fabianek *et al.*, 1998; Page and Ferguson, 1997; Reid *et al.*, 1998). The hydrophilic C-terminal domain of CcmG contains a C-P-T-C active site motif and has a redox potential of about –210 mV (Li *et al.*, 2001). CcmG active site cysteine residues are important for cytochrome *c* maturation (Fabianek *et al.*, 1998). It has been shown that strains, expressing CcmG variants with one or both active site cysteine residues replaced by serine, produce strongly decreased amounts of holocytochrome *c*. The restoration of cytochrome *c* biogenesis was achieved by addition of thiol reductants to the medium. In contrast to various other bacterial oxidoreductases, CcmG does not show reductase activity in the classical insulin reduction assay, and its absence does not affect the activity of alkaline phosphatase,

suggesting that reductase activity of CcmG is highly specialized and limited to the pathway of cytochrome *c* maturation (Fabianek *et al.*, 1997; Monika *et al.*, 1997; Page and Ferguson, 1997).

The recently solved crystal structure of a CcmG homologue from *Bradyrhizobium japonicum* (Edeling *et al.*, 2002) revealed a thioredoxin fold with several distinguishing features essential for cytochrome *c* maturation (Fig. 9). One of these features is a characteristic groove formed by two inserts in the fold, the N-terminal β-hairpin-like structure and the central insert. It was
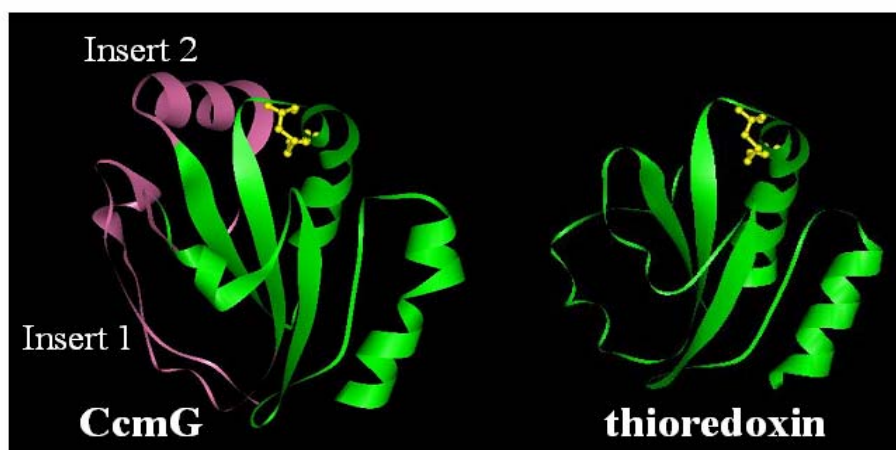
Figure 9. Crystal structure comparison of CcmG (A) and thioredoxin (B). The characteristic groove of CcmG, formed by the N-terminal β-hairpin-like structure (insert 1) and the central insert (insert 2), is depicted in pink. Active site cysteine residues are shown in yellow. (Edeling *et al.*, 2002)

shown that deletion of any of the two inserts suppresses cytochrome *c* formation (Edeling *et al.*, 2002; Edeling *et al.*, 2004). Another CcmG-specific feature is an unusually acidic active site of CcmG compared with those of other thioredoxin-like proteins. Several conserved acidic residues contribute to the negative charge and are required for efficient cytochrome *c* maturation (Edeling *et al.*, 2004).

2.7.4 DsbD-dependent reduction of apocytochromes in Escherichia coli

The reducing power required for cytochrome *c* maturation in the periplasm of *E. coli* comes from the cytoplasmic thioredoxin system *via* the inner membrane redox catalyst DsbD and the periplasmic reductase CcmG (Fig. 4). Indeed, genetic studies showed that in the absence of DsbD, thioredoxin or thioredoxin reductase, cytochrome *c* maturation is suppressed and CcmG accumulates in the oxidized state (Chung *et al.*, 2000; Crooke and Cole, 1995; Metheringham *et al.*, 1996; Reid *et al.*, 1998; Sambongi and Ferguson, 1994). Detection of

the mixed-disulfide intermediate between DsbD and CcmG *in vivo* (Katzen and Beckwith, 2000) is strong evidence in favour of direct electron transfer from DsbD to CcmG. The mechanism of further electron transfer from CcmG to apocytochromes is not yet established, and several models exit (Reid *et al.*, 2001). According to the first model, electrons sequentially flow from reduced CcmG to CcmH and then to apocytochromes (Monika *et al.*, 1997; Page *et al.*, 1998; Reid *et al.*, 2001). The observation that only the second (but not the first) cysteine in the C-X-X-C active site motif of CcmH is important for cytochrome *c* maturation led to another model for apocytochrome *c* reduction (Fabianek *et al.*, 1999). First, a disulfide bond of oxidized apocytochrome *c* is broken by a nucleophilic attack of the second CcmH active site thiol, leading to a mixed disulfide between apocytochrome *c* and CcmH. This disulfide is then resolved by reduced CcmG, resulting in CcmG oxidation and release of reduced apocytochrome *c* and CcmH. In the last step, DsbD regenerates reduced CcmG. Accumulating data suggest that the role of CcmG in cytochrome *c* maturation is more complex than solely reduction of apocytochromes. It has been shown that CcmG active site cysteine mutants are still able to produce some holocytochrome *c*, whereas *ccmG*⁻ strains are completely defective in cytochrome *c* maturation even in the presence of reductants (Fabianek *et al.*, 1998; Fabianek *et al.*, 1999; Grove *et al.*, 1996; Reid *et al.*, 2001; Thony-Meyer *et al.*, 1995). These results led to the conclusion that, apart from the reduction of apocytochromes, CcmG might also be required for stabilization of one or several proteins involved in cytochrome *c* maturation (Fabianek *et al.*, 1998).

2.8 Aim of the thesis

This thesis was focused on the investigation of the catalytic mechanism of the inner membrane protein DsbD from *E. coli*. First, we addressed the issue of the intrinsic biophysical properties and reactivity of nDsbD and cDsbD, and of the kinetic parameters of disulfide exchange between nDsbD and the three DsbD substrate proteins, DsbC, DsbG, and CcmG.

The second step was to establish a protocol for the synthesis of nDsbD-SS-cDsbD and nDsbD-SS-CcmG mixed-disulfide complexes, which would allow their crystallization and structure determination. The kinetic and structural data should provide an insight into the adaptability of nDsbD to its very different binding partners.

The coexistence of the oxidative DsbA/B and the reductive DsbC/D pathways within the same periplasmic compartment raised the question of how the two pathways are kept separate. If barriers did not exist, there would be a futile cycle in which, for instance, DsbD

would reduce DsbA, or DsbB would oxidize DsbC. Therefore, we have undertaken a kinetic analysis of all disulfide exchange reactions that may occur between protein from the oxidative DsbA/B and the reductive DsbC/D pathways.

Finally, we were interested to obtain the structures of oxidized and reduced cDsbD and to compare them with the structure of cDsbD in the nDsbD-SS-cDsbD complex.

2.9 References

Ahuja, U., and Thony-Meyer, L. (2003) Dynamic features of a heme delivery system for cytochrome C maturation. *J Biol Chem* **278**: 52061-52070.

Ahuja, U., and Thony-Meyer, L. (2005) CcmD is involved in complex formation between CcmC and the heme chaperone CcmE during cytochrome c maturation. *J Biol Chem* **280**: 236-243.

Andersen, C.L., Matthey-Dupraz, A., Missiakas, D., and Raina, S. (1997) A new Escherichia coli gene, dsbG, encodes a periplasmic protein involved in disulphide bond formation, required for recycling DsbA/DsbB and DsbC redox proteins. *Mol Microbiol* **26**: 121-132.

Anfinsen, C.B. (1973) Principles that govern the folding of protein chains. *Science* **181**: 223-230.

Bader, M., Muse, W., Zander, T., and Bardwell, J. (1998) Reconstitution of a protein disulfide catalytic system. *J Biol Chem* **273**: 10302-10307.

Bader, M., Muse, W., Ballou, D.P., Gassner, C., and Bardwell, J.C. (1999) Oxidative protein folding is driven by the electron transport system. *Cell* **98**: 217-227.

Bader, M.W., Xie, T., Yu, C.A., and Bardwell, J.C. (2000) Disulfide bonds are generated by quinone reduction. *J Biol Chem* **275**: 26082-26088.

Bardwell, J.C., McGovern, K., and Beckwith, J. (1991) Identification of a protein required for disulfide bond formation in vivo. *Cell* **67**: 581-589.

Bardwell, J.C., Lee, J.O., Jander, G., Martin, N., Belin, D., and Beckwith, J. (1993) A pathway for disulfide bond formation in vivo. *Proc Natl Acad Sci U S A* **90**: 1038-1042.

Berkmen, M., Boyd, D., and Beckwith, J. (2005) The non-consecutive disulfide bond of Echerichia coli phytase (AppA) renders it dependent on the protein disulfide isomerase, DsbC. *J Biol Chem*.

Bessette, P.H., Cotto, J.J., Gilbert, H.F., and Georgiou, G. (1999) In vivo and in vitro function of the Escherichia coli periplasmic cysteine oxidoreductase DsbG. *J Biol Chem* **274**: 7784-7792.

Bolhuis, A., Venema, G., Quax, W.J., Bron, S., and van Dijl, J.M. (1999) Functional analysis of paralogous thiol-disulfide oxidoreductases in Bacillus subtilis. *J Biol Chem* **274**: 24531-24538.

Chivers, P.T., Laboissiere, M.C., and Raines, R.T. (1996) The CXXC motif: imperatives for the formation of native disulfide bonds in the cell. *Embo J* **15**: 2659-2667.

Choe, M., and Reznikoff, W.S. (1993) Identification of the regulatory sequence of anaerobically expressed locus aeg-46.5. *J Bacteriol* **175**: 1165-1172.

Chung, J., Chen, T., and Missiakas, D. (2000) Transfer of electrons across the cytoplasmic membrane by DsbD, a membrane protein involved in thiol-disulphide exchange and protein folding in the bacterial periplasm. *Mol Microbiol* **35**: 1099-1109.

Collet, J.F., Riemer, J., Bader, M.W., and Bardwell, J.C. (2002) Reconstitution of a disulfide isomerization system. *J Biol Chem* **277**: 26886-26892.

Creighton, T. (1975) Reactivities of the cysteine residues of the reduced pancreatic trypsin inhibitor. *J Mol Biol* **96**: 777-782.

Crooke, H., and Cole, J. (1995) The biogenesis of c-type cytochromes in Escherichia coli requires a membrane-bound protein, DipZ, with a protein disulphide isomerase-like domain. *Mol Microbiol* **15**: 1139-1150.

Dailey, F.E., and Berg, H.C. (1993) Mutants in disulfide bond formation that disrupt flagellar assembly in Escherichia coli. *Proc Natl Acad Sci U S A* **90**: 1043-1047.

Darby, N.J., and Creighton, T.E. (1995) Characterization of the active site cysteine residues of the thioredoxin-like domains of protein disulfide isomerase. *Biochemistry* **34**: 16770-16780.

Darby, N.J., Raina, S., and Creighton, T.E. (1998) Contributions of substrate binding to the catalytic activity of DsbC. *Biochemistry* **37**: 783-791.

Derman, A.I., Prinz, W.A., Belin, D., and Beckwith, J. (1993) Mutations that allow disulfide bond formation in the cytoplasm of Escherichia coli. *Science* **262**: 1744-1747.

Dyson, H.J., Jeng, M.F., Tennant, L.L., Slaby, I., Lindell, M., Cui, D.S., Kuprin, S., and Holmgren, A. (1997) Effects of buried charged groups on cysteine thiol ionization and reactivity in Escherichia coli thioredoxin: structural and functional characterization of mutants of Asp 26 and Lys 57. *Biochemistry* **36**: 2622-2636.

Edeling, M.A., Guddat, L.W., Fabianek, R.A., Thony-Meyer, L., and Martin, J.L. (2002) Structure of CcmG/DsbE at 1.14 A resolution: high-fidelity reducing activity in an indiscriminately oxidizing environment. *Structure (Camb)* **10**: 973-979.

Edeling, M.A., Ahuja, U., Heras, B., Thony-Meyer, L., and Martin, J.L. (2004) The acidic nature of the CcmG redox-active center is important for cytochrome c maturation in Escherichia coli. *J Bacteriol* **186**: 4030-4033.

Fabianek, R.A., Huber-Wunderlich, M., Glockshuber, R., Kunzler, P., Hennecke, H., and Thony-Meyer, L. (1997) Characterization of the Bradyrhizobium japonicum CycY protein, a membrane-anchored periplasmic thioredoxin that may play a role as a reductant in the biogenesis of c-type cytochromes. *J Biol Chem* **272**: 4467-4473.

Fabianek, R.A., Hennecke, H., and Thony-Meyer, L. (1998) The active-site cysteines of the periplasmic thioredoxin-like protein CcmG of Escherichia coli are important but not essential for cytochrome c maturation in vivo. *J Bacteriol* **180**: 1947-1950.

Fabianek, R.A., Hofer, T., and Thony-Meyer, L. (1999) Characterization of the Escherichia coli CcmH protein reveals new insights into the redox pathway required for cytochrome c maturation. *Arch Microbiol* **171**: 92-100.

Fabianek, R.A., Hennecke, H., and Thony-Meyer, L. (2000) Periplasmic protein thiol:disulfide oxidoreductases of Escherichia coli. *FEMS Microbiol Rev* **24**: 303-316.

Frech, C., Wunderlich, M., Glockshuber, R., and Schmid, F.X. (1996) Preferential binding of an unfolded protein to DsbA. *Embo J* **15**: 392-398.

Goldman, B.S., Beckman, D.L., Bali, A., Monika, E.M., Gabbert, K.K., and Kranz, R.G. (1997a) Molecular and immunological analysis of an ABC transporter complex required for cytochrome c biogenesis. *J Mol Biol* **268**: 724-738.

Goldman, B.S., Sherman, D.A., and Kranz, R.G. (1997b) Comparison of the bacterial HelA protein to the F508 region of the cystic fibrosis transmembrane regulator. *J Bacteriol* **179**: 7869-7871.

Goldstone, D., Haebel, P.W., Katzen, F., Bader, M.W., Bardwell, J.C., Beckwith, J., and Metcalf, P. (2001) DsbC activation by the N-terminal domain of DsbD. *Proc Natl Acad Sci U S A* **98**: 9551-9556.

Gordon, E.H., Page, M.D., Willis, A.C., and Ferguson, S.J. (2000) Escherichia coli DipZ: anatomy of a transmembrane protein disulphide reductase in which three pairs of

cysteine residues, one in each of three domains, contribute differentially to function. *Mol Microbiol* **35**: 1360-1374.

Goulding, C.W., Sawaya, M.R., Parseghian, A., Lim, V., Eisenberg, D., and Missiakas, D. (2002) Thiol-disulfide exchange in an immunoglobulin-like fold: structure of the N-terminal domain of DsbD. *Biochemistry* **41**: 6920-6927.

Grauschopf, U., Winther, J.R., Korber, P., Zander, T., Dallinger, P., and Bardwell, J.C. (1995) Why is DsbA such an oxidizing disulfide catalyst? *Cell* **83**: 947-955.

Grauschopf, U., Fritz, A., and Glockshuber, R. (2003) Mechanism of the electron transfer catalyst DsbB from Escherichia coli. *Embo J* **22**: 3503-3513.

Grove, J., Tanapongpipat, S., Thomas, G., Griffiths, L., Crooke, H., and Cole, J. (1996) Escherichia coli K-12 genes essential for the synthesis of c-type cytochromes and a third nitrate reductase located in the periplasm. *Mol Microbiol* **19**: 467-481.

Guddat, L.W., Bardwell, J.C., and Martin, J.L. (1998) Crystal structures of reduced and oxidized DsbA: investigation of domain motion and thiolate stabilization. *Structure* **6**: 757-767.

Guilhot, C., Jander, G., Martin, N.L., and Beckwith, J. (1995) Evidence that the pathway of disulfide bond formation in Escherichia coli involves interactions between the cysteines of DsbB and DsbA. *Proc Natl Acad Sci U S A* **92**: 9895-9899.

Haebel, P.W., Goldstone, D., Katzen, F., Beckwith, J., and Metcalf, P. (2002) The disulfide bond isomerase DsbC is activated by an immunoglobulin-fold thiol oxidoreductase: crystal structure of the DsbC-DsbDalpha complex. *Embo J* **21**: 4774-4784.

Hennecke, J., Spleiss, C., and Glockshuber, R. (1997) Influence of acidic residues and the kink in the active-site helix on the properties of the disulfide oxidoreductase DsbA. *J Biol Chem* **272**: 189-195.

Heras, B., Edeling, M.A., Schirra, H.J., Raina, S., and Martin, J.L. (2004) Crystal structures of the DsbG disulfide isomerase reveal an unstable disulfide. *Proc Natl Acad Sci U S A* **101**: 8876-8881.

Hiniker, A., and Bardwell, J.C. (2004) In vivo substrate specificity of periplasmic disulfide oxidoreductases. *J Biol Chem* **279**: 12967-12973.

Holmgren, A., and Fagerstedt, M. (1982) The in vivo distribution of oxidized and reduced thioredoxin in Escherichia coli. *J Biol Chem* **257**: 6926-6930.

Holmgren, A. (1985) Thioredoxin. *Annu Rev Biochem* **54**: 237-271.

Holst, B., Tachibana, C., and Winther, J.R. (1997) Active site mutations in yeast protein disulfide isomerase cause dithiothreitol sensitivity and a reduced rate of protein folding in the endoplasmic reticulum. *J Cell Biol* **138**: 1229-1238.

Huber-Wunderlich, M., and Glockshuber, R. (1998) A single dipeptide sequence modulates the redox properties of a whole enzyme family. *Fold Des* **3**: 161-171.

Jacobi, A., Huber-Wunderlich, M., Hennecke, J., and Glockshuber, R. (1997) Elimination of all charged residues in the vicinity of the active-site helix of the disulfide oxidoreductase DsbA. Influence of electrostatic interactions on stability and redox properties. *J Biol Chem* **272**: 21692-21699.

Jander, G., Martin, N.L., and Beckwith, J. (1994) Two cysteines in each periplasmic domain of the membrane protein DsbB are required for its function in protein disulfide bond formation. *Embo J* **13**: 5121-5127.

Joly, J.C., and Swartz, J.R. (1997) In vitro and in vivo redox states of the Escherichia coli periplasmic oxidoreductases DsbA and DsbC. *Biochemistry* **36**: 10067-10072.

Kallis, G.B., and Holmgren, A. (1980) Differential reactivity of the functional sulfhydryl groups of cysteine-32 and cysteine-35 present in the reduced form of thioredoxin from Escherichia coli. *J Biol Chem* **255**: 10261-10265.

Kamitani, S., Akiyama, Y., and Ito, K. (1992) Identification and characterization of an Escherichia coli gene required for the formation of correctly folded alkaline phosphatase, a periplasmic enzyme. *Embo J* **11**: 57-62.

Katti, S.K., LeMaster, D.M., and Eklund, H. (1990) Crystal structure of thioredoxin from Escherichia coli at 1.68 A resolution. *J Mol Biol* **212**: 167-184.

Katzen, F., and Beckwith, J. (2000) Transmembrane electron transfer by the membrane protein DsbD occurs via a disulfide bond cascade. *Cell* **103**: 769-779.

Katzen, F., Deshmukh, M., Daldal, F., and Beckwith, J. (2002) Evolutionary domain fusion expanded the substrate specificity of the transmembrane electron transporter DsbD. *Embo J* **21**: 3960-3969.

Katzen, F., and Beckwith, J. (2003) Role and location of the unusual redox-active cysteines in the hydrophobic domain of the transmembrane electron transporter DsbD. *Proc Natl Acad Sci U S A* **100**: 10471-10476.

Kim, J.H., Kim, S.J., Jeong, D.G., Son, J.H., and Ryu, S.E. (2003) Crystal structure of DsbDgamma reveals the mechanism of redox potential shift and substrate specificity(1). *FEBS Lett* **543**: 164-169.

Kishigami, S., Kanaya, E., Kikuchi, M., and Ito, K. (1995) DsbA-DsbB interaction through their active site cysteines. Evidence from an odd cysteine mutant of DsbA. *J Biol Chem* **270**: 17072-17074.

Kishigami, S., and Ito, K. (1996) Roles of cysteine residues of DsbB in its activity to reoxidize DsbA, the protein disulphide bond catalyst of Escherichia coli. *Genes Cells* **1**: 201-208.

Kobayashi, T., Kishigami, S., Sone, M., Inokuchi, H., Mogi, T., and Ito, K. (1997) Respiratory chain is required to maintain oxidized states of the DsbA-DsbB disulfide bond formation system in aerobically growing Escherichia coli cells. *Proc Natl Acad Sci U S A* **94**: 11857-11862.

Kobayashi, T., and Ito, K. (1999) Respiratory chain strongly oxidizes the CXXC motif of DsbB in the Escherichia coli disulfide bond formation pathway. *Embo J* **18**: 1192-1198.

Kortemme, T., and Creighton, T.E. (1995) Ionisation of cysteine residues at the termini of model alpha-helical peptides. Relevance to unusual thiol pKa values in proteins of the thioredoxin family. *J Mol Biol* **253**: 799-812.

Krause, G., Lundstrom, J., Barea, J.L., Pueyo de la Cuesta, C., and Holmgren, A. (1991) Mimicking the active site of protein disulfide-isomerase by substitution of proline 34 in Escherichia coli thioredoxin. *J Biol Chem* **266**: 9494-9500.

Krupp, R., Chan, C., and Missiakas, D. (2001) DsbD-catalyzed transport of electrons across the membrane of Escherichia coli. *J Biol Chem* **276**: 3696-3701.

Laurent, T.C., Moore, E.C., and Reichard, P. (1964) Enzymatic Synthesis of Deoxyribonucleotides. Iv. Isolation and Characterization of Thioredoxin, the Hydrogen Donor from Escherichia Coli B. *J Biol Chem* **239**: 3436-3444.

Li, Q., Hu, H., and Xu, G. (2001) Biochemical characterization of the thioredoxin domain of Escherichia coli DsbE protein reveals a weak reductant. *Biochem Biophys Res Commun* **283**: 849-853.

Martin, J.L., Bardwell, J.C., and Kuriyan, J. (1993) Crystal structure of the DsbA protein required for disulphide bond formation in vivo. *Nature* **365**: 464-468.

Martin, J.L. (1995) Thioredoxin--a fold for all reasons. *Structure* **3**: 245-250.

McCarthy, A.A., Haebel, P.W., Torronen, A., Rybin, V., Baker, E.N., and Metcalf, P. (2000) Crystal structure of the protein disulfide bond isomerase, DsbC, from Escherichia coli. *Nat Struct Biol* **7**: 196-199.

Metheringham, R., Griffiths, L., Crooke, H., Forsythe, S., and Cole, J. (1995) An essential role for DsbA in cytochrome c synthesis and formate-dependent nitrite reduction by Escherichia coli K-12. *Arch Microbiol* **164**: 301-307.

Metheringham, R., Tyson, K.L., Crooke, H., Missiakas, D., Raina, S., and Cole, J.A. (1996) Effects of mutations in genes for proteins involved in disulphide bond formation in the periplasm on the activities of anaerobically induced electron transfer chains in Escherichia coli K12. *Mol Gen Genet* **253**: 95-102.

Missiakas, D., Georgopoulos, C., and Raina, S. (1993) Identification and characterization of the Escherichia coli gene dsbB, whose product is involved in the formation of disulfide bonds in vivo. *Proc Natl Acad Sci U S A* **90**: 7084-7088.

Missiakas, D., Georgopoulos, C., and Raina, S. (1994) The Escherichia coli dsbC (xprA) gene encodes a periplasmic protein involved in disulfide bond formation. *Embo J* **13**: 2013-2020.

Missiakas, D., Schwager, F., and Raina, S. (1995) Identification and characterization of a new disulfide isomerase-like protein (DsbD) in Escherichia coli. *Embo J* **14**: 3415-3424.

Monika, E.M., Goldman, B.S., Beckman, D.L., and Kranz, R.G. (1997) A thioreduction pathway tethered to the membrane for periplasmic cytochromes c biogenesis; in vitro and in vivo studies. *J Mol Biol* **271**: 679-692.

Mossner, E., Huber-Wunderlich, M., and Glockshuber, R. (1998) Characterization of Escherichia coli thioredoxin variants mimicking the active-sites of other thiol/disulfide oxidoreductases. *Protein Sci* **7**: 1233-1244.

Mossner, E., Huber-Wunderlich, M., Rietsch, A., Beckwith, J., Glockshuber, R., and Aslund, F. (1999) Importance of redox potential for the in vivo function of the cytoplasmic disulfide reductant thioredoxin from Escherichia coli. *J Biol Chem* **274**: 25254-25259.

Narayan, M., Welker, E., Wedemeyer, W.J., and Scheraga, H.A. (2000) Oxidative folding of proteins. *Acc Chem Res* **33**: 805-812.

Nelson, J.W., and Creighton, T.E. (1994) Reactivity and ionization of the active site cysteine residues of DsbA, a protein required for disulfide bond formation in vivo. *Biochemistry* **33**: 5974-5983.

Page, M.D., and Ferguson, S.J. (1990) Apo forms of cytochrome c550 and cytochrome cd1 are translocated to the periplasm of Paracoccus denitrificans in the absence of haem incorporation caused either mutation or inhibition of haem synthesis. *Mol Microbiol* **4**: 1181-1192.

Page, M.D., and Ferguson, S.J. (1997) Paracoccus denitrificans CcmG is a periplasmic protein-disulphide oxidoreductase required for c- and aa3-type cytochrome biogenesis; evidence for a reductase role in vivo. *Mol Microbiol* **24**: 977-990.

Page, M.D., Sambongi, Y., and Ferguson, S.J. (1998) Contrasting routes of c-type cytochrome assembly in mitochondria, chloroplasts and bacteria. *Trends Biochem Sci* **23**: 103-108.

Peek, J.A., and Taylor, R.K. (1992) Characterization of a periplasmic thiol:disulfide interchange protein required for the functional maturation of secreted virulence factors of Vibrio cholerae. *Proc Natl Acad Sci U S A* **89**: 6210-6214.

Porat, A., Cho, S.H., and Beckwith, J. (2004) The unusual transmembrane electron transporter DsbD and its homologues: a bacterial family of disulfide reductases. *Res Microbiol* **155**: 617-622.

Rabin, R.S., and Stewart, V. (1993) Dual response regulators (NarL and NarP) interact with dual sensors (NarX and NarQ) to control nitrate- and nitrite-regulated gene expression in Escherichia coli K-12. *J Bacteriol* **175**: 3259-3268.

Reid, E., Eaves, D.J., and Cole, J.A. (1998) The CcmE protein from Escherichia coli is a haem-binding protein. *FEMS Microbiol Lett* **166**: 369-375.

Reid, E., Cole, J., and Eaves, D.J. (2001) The Escherichia coli CcmG protein fulfils a specific role in cytochrome c assembly. *Biochem J* **355**: 51-58.

Ren, Q., and Thony-Meyer, L. (2001) Physical interaction of CcmC with heme and the heme chaperone CcmE during cytochrome c maturation. *J Biol Chem* **276**: 32591-32596.

Ren, Q., Ahuja, U., and Thony-Meyer, L. (2002) A bacterial cytochrome c heme lyase. CcmF forms a complex with the heme chaperone CcmE and CcmH but not with apocytochrome c. *J Biol Chem* **277**: 7657-7663.

Rietsch, A., Belin, D., Martin, N., and Beckwith, J. (1996) An in vivo pathway for disulfide bond isomerization in Escherichia coli. *Proc Natl Acad Sci U S A* **93**: 13048-13053.

Rietsch, A., Bessette, P., Georgiou, G., and Beckwith, J. (1997) Reduction of the periplasmic disulfide bond isomerase, DsbC, occurs by passage of electrons from cytoplasmic thioredoxin. *J Bacteriol* **179**: 6602-6608.

Rossmann, R., Stern, D., Loferer, H., Jacobi, A., Glockshuber, R., and Hennecke, H. (1997) Replacement of Pro109 by His in TlpA, a thioredoxin-like protein from Bradyrhizobium japonicum, alters its redox properties but not its in vivo functions. *FEBS Lett* **406**: 249-254.

Rozhkova, A., Stirnimann, C.U., Frei, P., Grauschopf, U., Brunisholz, R., Grutter, M.G., Capitani, G., and Glockshuber, R. (2004) Structural basis and kinetics of inter- and intramolecular disulfide exchange in the redox catalyst DsbD. *Embo J* **23**: 1709-1719.

Russel, M., and Model, P. (1986) The role of thioredoxin in filamentous phage assembly. Construction, isolation, and characterization of mutant thioredoxins. *J Biol Chem* **261**: 14997-15005.

Sambongi, Y., and Ferguson, S.J. (1994) Specific thiol compounds complement deficiency in c-type cytochrome biogenesis in Escherichia coli carrying a mutation in a membrane-bound disulphide isomerase-like protein. *FEBS Lett* **353**: 235-238.

Sambongi, Y., and Ferguson, S.J. (1996) Mutants of Escherichia coli lacking disulphide oxidoreductases DsbA and DsbB cannot synthesise an exogenous monohaem c-type cytochrome except in the presence of disulphide compounds. *FEBS Lett* **398**: 265-268.

Sambongi, Y., Stoll, R., and Ferguson, S.J. (1996) Alteration of haem-attachment and signal-cleavage sites for Paracoccus denitrificans cytochrome C550 probes pathway of c-type cytochrome biogenesis in Escherichia coli. *Mol Microbiol* **19**: 1193-1204.

Saxena, V., and Wetlaufer, D. (1970) Formation of three dimentional structure in proteins. I. Rapid nonenzymatic reactivation of reduced lyzozyme. *biochemistry* **9**: 5015-5022.

Schulz, H., Hennecke, H., and Thony-Meyer, L. (1998) Prototype of a heme chaperone essential for cytochrome c maturation. *Science* **281**: 1197-1200.

Schulz, H., Fabianek, R.A., Pellicioli, E.C., Hennecke, H., and Thony-Meyer, L. (1999) Heme transfer to the heme chaperone CcmE during cytochrome c maturation requires the CcmC protein, which may function independently of the ABC-transporter CcmAB. *Proc Natl Acad Sci U S A* **96**: 6462-6467.

Sevier, C.S., and Kaiser, C.A. (2002) Formation and transfer of disulphide bonds in living cells. *Nat Rev Mol Cell Biol* **3**: 836-847.

Shaked, Z., Szajewski, R.P., and Whitesides, G.M. (1980) Rates of thiol-disulfide interchange reactions involving proteins and kinetic measurements of thiol pKa values. *Biochemistry* **19**: 4156-4166.

Shao, F., Bader, M.W., Jakob, U., and Bardwell, J.C. (2000) DsbG, a protein disulfide isomerase with chaperone activity. *J Biol Chem* **275**: 13349-13352.

Shevchik, V.E., Condemine, G., and Robert-Baudouy, J. (1994) Characterization of DsbC, a periplasmic protein of Erwinia chrysanthemi and Escherichia coli with disulfide isomerase activity. *Embo J* **13**: 2007-2012.

Sone, M., Akiyama, Y., and Ito, K. (1997) Differential in vivo roles played by DsbA and DsbC in the formation of protein disulfide bonds. *J Biol Chem* **272**: 10349-10352.

Stafford, S.J., Humphreys, D.P., and Lund, P.A. (1999) Mutations in dsbA and dsbB, but not dsbC, lead to an enhanced sensitivity of Escherichia coli to Hg2+ and Cd2+. *FEMS Microbiol Lett* **174**: 179-184.

Stewart, E.J., Katzen, F., and Beckwith, J. (1999) Six conserved cysteines of the membrane protein DsbD are required for the transfer of electrons from the cytoplasm to the periplasm of Escherichia coli. *Embo J* **18**: 5963-5971.

Sun, X.X., and Wang, C.C. (2000) The N-terminal sequence (residues 1-65) is essential for dimerization, activities, and peptide binding of Escherichia coli DsbC. *J Biol Chem* **275**: 22743-22749.

Szajewski, R.P., and Whitesides, G.M. (1980) Rate constants and equilibrium constants of thioldisulfide interchange reactions involving oxidized glutathione. *J Am Chem Soc* **102**: 2011-2026.

Tanapongpipat, S., Reid, E., Cole, J.A., and Crooke, H. (1998) Transcriptional control and essential roles of the Escherichia coli ccm gene products in formate-dependent nitrite reduction and cytochrome c synthesis. *Biochem J* **334 (Pt 2)**: 355-365.

Thony-Meyer, L., Ritz, D., and Hennecke, H. (1994) Cytochrome c biogenesis in bacteria: a possible pathway begins to emerge. *Mol Microbiol* **12**: 1-9.

Thony-Meyer, L., Fischer, F., Kunzler, P., Ritz, D., and Hennecke, H. (1995) Escherichia coli genes required for cytochrome c maturation. *J Bacteriol* **177**: 4321-4326.

Thony-Meyer, L. (2000) Haem-polypeptide interactions during cytochrome c maturation. *Biochim Biophys Acta* **1459**: 316-324.

Thony-Meyer, L. (2002) Cytochrome c maturation: a complex pathway for a simple task? *Biochem Soc Trans* **30**: 633-638.

van Straaten, M., Missiakas, D., Raina, S., and Darby, N.J. (1998) The functional properties of DsbG, a thiol-disulfide oxidoreductase from the periplasm of Escherichia coli. *FEBS Lett* **428**: 255-258.

Williams, C.H., Jr. (1995) Mechanism and structure of thioredoxin reductase from Escherichia coli. *Faseb J* **9**: 1267-1276.

Wunderlich, M., and Glockshuber, R. (1993) Redox properties of protein disulfide isomerase (DsbA) from Escherichia coli. *Protein Sci* **2**: 717-726.

Zapun, A., Bardwell, J.C., and Creighton, T.E. (1993) The reactive and destabilizing disulfide bond of DsbA, a protein required for protein disulfide bond formation in vivo. *Biochemistry* **32**: 5083-5092.

Zapun, A., Missiakas, D., Raina, S., and Creighton, T.E. (1995) Structural and functional characterization of DsbC, a protein involved in disulfide bond formation in Escherichia coli. *Biochemistry* **34**: 5075-5089.

3. Results

3.1 Structural basis and kinetics of inter- and intramolecular disulfide exchange in the redox catalyst DsbD

Anna Rozhkova, Christian U. Stirnimann, Patrick Frei, Ulla Grauschopf, René Brunisholz,

Markus G. Grütter, Guido Capitani and Rudi Glockshuber

Structural basis and kinetics of inter- and intramolecular disulfide exchange in the redox catalyst DsbD

**Anna Rozhkova[1,4],
Christian U Stirnimann[2,4], Patrick Frei[1],
Ulla Grauschopf[1], René Brunisholz[3],
Markus G Grütter[2], Guido Capitani[2,*]
and Rudi Glockshuber[1,*]**

[1]Institut für Molekularbiologie und Biophysik, Eidgenössische Technische Hochschule Hönggerberg, Zürich, Switzerland, [2]Biochemisches Institut, Universität Zürich, Winterthurerstrasse, Zürich, Switzerland and [3]Protein-Servicelabor, Departement Biologie, Eidgenössische Technische Hochschule Hönggerberg, Zürich, Switzerland

DsbD from *Escherichia coli* catalyzes the transport of electrons from cytoplasmic thioredoxin to the periplasmic disulfide isomerase DsbC. DsbD contains two periplasmically oriented domains at the N- and C-terminus (nDsbD and cDsbD) that are connected by a central transmembrane (TM) domain. Each domain contains a pair of cysteines that are essential for catalysis. Here, we show that Cys109 and Cys461 form a transient interdomain disulfide bond between nDsbD and cDsbD in the reaction cycle of DsbD. We solved the crystal structure of this catalytic intermediate at 2.85 Å resolution, which revealed large relative domain movements in DsbD as a consequence of a strong overlap between the surface areas of nDsbD that interact with DsbC and cDsbD. In addition, we have measured the kinetics of all functional and nonfunctional disulfide exchange reactions between redox-active, periplasmic proteins and protein domains from the oxidative DsbA/B and the reductive DsbC/D pathway. We show that both pathways are separated by large kinetic barriers for nonfunctional disulfide exchange between components from different pathways.

*Corresponding authors. Rudi Glockshuber, Institut für Molekularbiologie und Biophysik, Eidgenössische Technische Hochschule Hönggerberg, CH-8093 Zürich, Switzerland.
Tel.: +41 1 633 6819; Fax: +41 1 633 1036;
E-mail: rudi@mol.biol.ethz.ch or Guido Capitani, Biochemisches Institut, Universität Zürich, Winterthurerstrasse 190, CH-8057 Zürich, Switzerland. Tel.: +41 1 635 5587; Fax: +41 1 635 6834;
E-mail: capitani@bioc.unizh.ch
[4]These authors contributed equally to this work

Introduction

Disulfide bonds are a typical post-translational modification of secretory proteins. In bacteria, disulfide bond formation occurs in the oxidizing environment of the periplasm and is catalyzed by redox enzymes of the Dsb family. Two types of reactions are primarily required for correct formation of disulfide bonds in proteins with multiple disulfide bonds: disulfide bond formation and disulfide bond isomerization (Ritz and Beckwith, 2001; Collet and Bardwell, 2002; Hiniker and Bardwell, 2003). Each of these reactions is linked with an independent electron transfer pathway in *Escherichia coli*. The pathway of disulfide bond formation involves the oxidation of reduced, newly translocated proteins by the periplasmic dithiol oxidase DsbA. DsbA belongs to the thioredoxin family and has a very reactive disulfide bond (active site: Cys-Pro-His-Cys), which is transferred randomly and extremely rapidly to reduced polypeptide substrates by disulfide exchange (Wunderlich *et al*, 1993; Zapun and Creighton, 1994; Darby and Creighton, 1995). Polypeptide oxidation generates reduced DsbA, which is reoxidized by ubiquinone from the respiratory chain, a two-electron transfer reaction catalyzed by the inner membrane protein DsbB (Bardwell *et al*, 1993; Dailey and Berg, 1993; Bader *et al*, 2000; Grauschopf *et al*, 2003). The reduced quinone (ubiquinol) is then reoxidized by molecular oxygen via terminal cytochrome oxidases (Bader *et al*, 1999; Kobayashi and Ito, 1999). The pathway of disulfide isomerization copes with wrong disulfide bonds randomly introduced by DsbA. The disulfide isomerase DsbC, a homodimeric, periplasmic protein with the active site Cys-Gly-Tyr-Cys, attacks wrong disulfide bonds in scrambled polypeptide substrates, and catalyzes their rearrangement to the native conformation (Missiakas *et al*, 1994; Zapun *et al*, 1995; McCarthy *et al*, 2000; Maskos *et al*, 2003). Consequently, for being active as a catalyst, DsbC has to be kept in a reduced state in an otherwise oxidizing cellular compartment. This is achieved through a specific electron transfer cascade in which two electrons from cytoplasmic NADPH flow to cytoplasmic thioredoxin, then to the inner membrane protein DsbD, and then to periplasmic DsbC (Rietsch *et al*, 1997; Chung *et al*, 2000; Krupp *et al*, 2001).

DsbD consists of 546 amino acids and is composed of a periplasmically oriented, N-terminal domain with immunoglobulin-like fold (nDsbD), a central transmembrane (TM) domain predicted to be composed of eight TM helices, and a C-terminal domain with thioredoxin fold (cDsbD) that is again oriented toward the periplasm (Gordon *et al*, 2000). Each of the three domains contains one pair of invariant cysteines that are essential for electron transport from thioredoxin to DsbC (Stewart *et al*, 1999). It was hence postulated that the catalytic mechanism of DsbD is exclusively based on disulfide exchange reactions between DsbD and its substrate proteins, and intramolecular disulfide interchange between
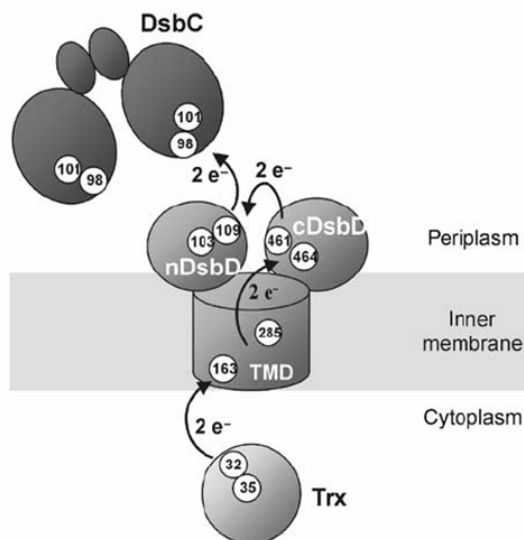
Figure 1 Proposed electron flow from reduced thioredoxin in the cytoplasm to oxidized, homodimeric DsbC in the periplasm via DsbD. According to this mechanism, electron transport occurs exclusively through intermolecular and intramolecular disulfide exchange. DsbD consists of an N-terminal domain (nDsbD, residues 1–143) and a C-terminal domain (cDsbD; residues 419–546), which are oriented toward the periplasm, and a central TM domain (residues 144–418). Numbered circles represent essential cysteine residues in the respective protein.

the three DsbD domains (Goldstone *et al*, 2001; Krupp *et al*, 2001; Collet *et al*, 2002; Katzen and Beckwith, 2003). According to this model, oxidizing equivalents are transferred from oxidized DsbC to the Cys103/Cys109 pair of nDsbD, then to Cys461/Cys464 of the cDsbD, followed by oxidation of the Cys163/Cys285 pair of the TM domain, which eventually oxidizes thioredoxin in the cytoplasm (Figure 1). Besides DsbC, the proteins DsbG and CcmG (DsbE) are further known *in vivo* substrates of DsbD that are kept in a reduced state in the periplasm. DsbG is a homodimeric homolog of DsbC (26% sequence identity) of unknown function (Andersen *et al*, 1997; van Straaten *et al*, 1998; Bessette *et al*, 1999), and CcmG is a membrane-anchored enzyme with thioredoxin fold that is required for cytochrome *c* biogenesis (Reid *et al*, 2001).

Available structural information on DsbD includes the X-ray structure of oxidized nDsbD and the X-ray structure of the mixed disulfide between the Cys103Ala variant of nDsbD and the Cys101Ser variant of DsbC (Goulding *et al*, 2002; Haebel *et al*, 2002). In addition, a crystal structure of oxidized cDsbD has been reported (Kim *et al*, 2003). Importantly, the nDsbD-SS-DsbC complex exhibits a stoichiometry of one nDsbD monomer per DsbC homodimer. This is due to the fact that nDsbD does not only interact with residues around the active site disulfide of a DsbC subunit, but forms specific, additional contacts with the second subunit in the DsbC dimer that prevent binding of a second nDsbD equivalent in a symmetry-related manner.

Several aspects of the above model for the DsbD cycle raise questions regarding the structure of DsbD. In particular, it is not obvious how two cysteines in the TM domain should suffice to transport electrons over a distance of about 60 Å (membrane thickness) via a 'disulfide ladder' from the cytoplasm to the periplasm. In addition, the cysteine residues that
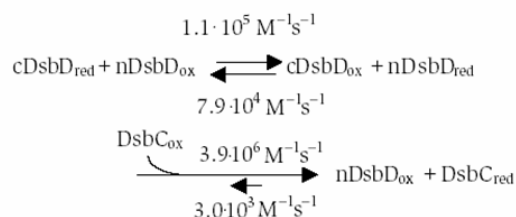
are involved in intramolecular disulfide interchange between the three domains in DsbD have not yet been identified. Here, we show that Cys109 and Cys461 mediate disulfide interchange between nDsbD and cDsbD. In addition, we solved the crystal structure of the kinetically stabilized mixed disulfide between both domains. The mixed disulfide complex represents a trapped intermediate in the catalytic cycle of DsbD, and reveals that large domain movements must occur during catalysis of electron transfer. Moreover, we demonstrate that both the reduction of DsbC by nDsbD, and disulfide interchange between nDsbD and cDsbD are very rapid processes. Finally, we show that the DsbA/B and DsbC/D redox systems are separated by large kinetic barriers that appear exclusively caused by steric block of disulfide exchange.

Results

Physical properties of the isolated periplasmic domains nDsbD and cDsbD

We expressed and purified the isolated periplasmic domains of DsbD, nDsbD (residues 1–143 of mature DsbD), and a C-terminally (His)$_6$-tagged variant of cDsbD (residues 419–546). To test the intrinsic reactivity of the individual domains, we analyzed the kinetics of electron transfer from reduced cDsbD via oxidized nDsbD to oxidized DsbC by reversed-phase HPLC separation of acid-quenched reactions products (Figure 2A). We found that the overall reaction is very rapid at pH 7.0 and 25°C, and yields reduced DsbC, oxidized nDsbD, and oxidized cDsbD within about 500 s when low initial concentrations of 0.25 μM were used for all proteins (monomer concentration in the case of DsbC). No mixed disulfides between nDsbD and DsbC, or nDsbD and cDsbC were detected. This indicates that these mixed disulfides are kinetically unstable and dissociate very rapidly by intramolecular disulfide exchange. As a control, we showed that the reverse reaction is not observed (Figure 2B). In addition, we measured the redox potentials of cDsbD, nDsbD, and DsbC at pH 7.0 and 25°C in identical buffer conditions, and obtained values of −0.235, −0.232, and −0.140 V, respectively (Figure 2F). The redox potential of DsbC and the practically identical potentials of cDsbD and nDsbD are in good agreement with previous measurements (Zapun *et al*, 1995; Collet *et al*, 2002) and confirm that complete electron transfer from cDsbD to DsbC via nDsbD is thermodynamically driven.

We next measured the individual microscopic rate constants of electron transfer from cDsbD to nDsbD, and from nDsbD to DsbC. Figures 2C and D show that reduction of DsbC by nDsbD is extremely rapid ($3.9 \times 10^6 \, \mathrm{M^{-1} s^{-1}}$), while intermolecular disulfide exchange between cDsbD and nDsbD is more than one order of magnitude slower. Thus, electron transfer between cDsbD and nDsbD is rate-limiting for the overall *in vitro* reaction according to the following scheme.

$$\mathrm{cDsbD_{red} + nDsbD_{ox}} \underset{7.9 \cdot 10^4 \, \mathrm{M^{-1} s^{-1}}}{\overset{1.1 \cdot 10^5 \, \mathrm{M^{-1} s^{-1}}}{\rightleftharpoons}} \mathrm{cDsbD_{ox} + nDsbD_{red}}$$

$$\mathrm{DsbC_{ox}} \underset{3.0 \cdot 10^3 \, \mathrm{M^{-1} s^{-1}}}{\overset{3.9 \cdot 10^6 \, \mathrm{M^{-1} s^{-1}}}{\longrightarrow}} \mathrm{nDsbD_{ox} + DsbC_{red}}$$
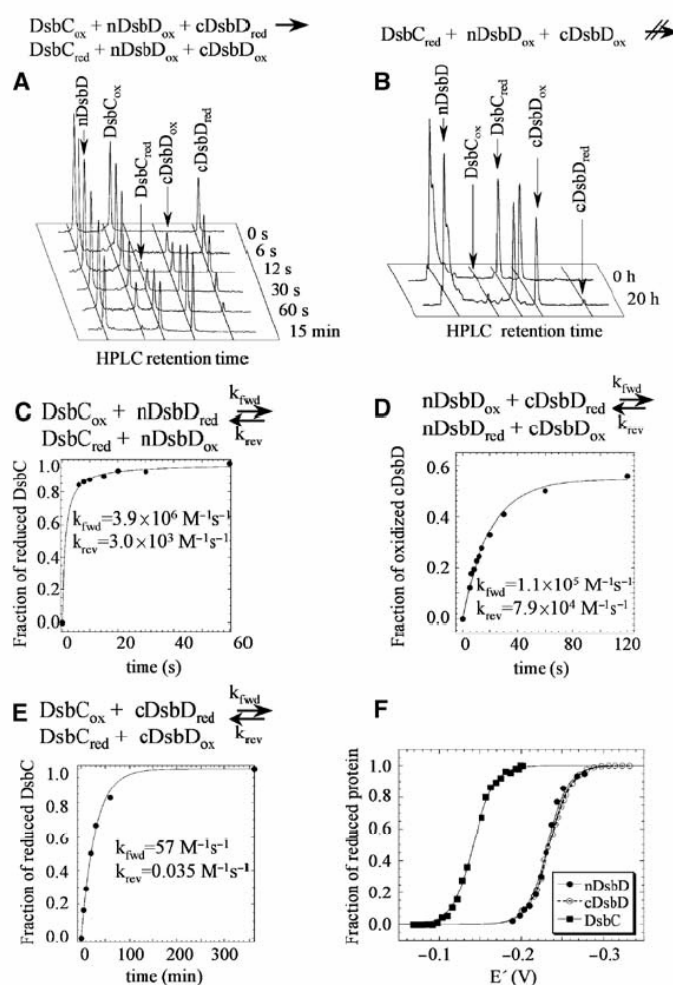
Figure 2 Kinetics of electron transport from cDsbD via nDsbD to DsbC at 25°C and pH 7.0. The reactions were acid-quenched after different incubation times, and products were separated on a C_{18} reverse-phase HPLC column. (**A**) $DsbC_{ox}$, $nDsbD_{ox}$, and $cDsbD_{red}$ (0.25 μM each) were mixed at a 1:1:1 ratio. Note that $nDsbD_{ox}$ and $nDsbD_{red}$ cannot be separated under these conditions. (**B**) No electron flow from $DsbC_{red}$ to $cDsbD_{ox}$ or $nDsbD_{ox}$ is observed. (**C**) Reduction of $DsbC_{ox}$ by $nDsbD_{red}$. Initial protein concentrations were 0.25 μM. The solid line corresponds to a second-order fit, with a rate constant of $3.9 \times 10^6\,M^{-1}\,s^{-1}$. The rate constant of the reverse reaction ($3.0 \times 10^3\,M^{-1}\,s^{-1}$) was deduced from the equilibrium constant of 1300 for the reduction of DsbC by nDsbD. (**D**) Disulfide exchange kinetics between isolated nDsbD and cDsbD. $nDsbD_{red}$ and $cDsbD_{ox}$ (0.25 μM each) were mixed, and the attainment of the equilibrium was fitted according to second-order kinetics for the forward and the reverse reaction with the program *Berkeley Madonna*. The obtained equilibrium constant of 1.4 agrees well with the calculated equilibrium constant of 1.3 from the redox potential measurements (see panel F). The fit (solid line) yielded rate constants of 1.1×10^5 and $7.9 \times 10^4\,M^{-1}\,s^{-1}$ for the forward and reverse reactions, respectively. (**E**) Direct reduction of $DsbC_{ox}$ by $cDsbD_{red}$ in the absence of nDsbD. The reaction was performed under pseudo-first-order conditions, with initial concentrations of 1 μM for $DsbC_{ox}$ (monomer) and 10 μM for $cDsbD_{red}$. The fit (solid line) yields a rate constant of $57\,M^{-1}\,s^{-1}$. The rate constant for the reverse reaction was calculated from the equilibrium constant (1600) for the reduction of DsbC by DsbD. (**F**) Determination of the redox potentials of nDsbD, cDsbD, and DsbC at pH 7.0 and 25°C by equilibration of proteins with thiol-disulfide redox buffers (see Materials and methods for details). All concentrations of DsbC refer to the DsbC monomer.

However, disulfide exchange between nDsbD and cDsbD is most likely not rate-limiting for the reaction cycle of intact DsbD, where nDsbD and cDsbD are covalently linked and thus expected to have very high effective concentrations. As an additional control, we showed that direct reduction of DsbC by cDsbD is almost five orders of magnitude slower ($k_2 = 57\,M^{-1}\,s^{-1}$) compared to the reduction by nDsbD (Figures 2E and 6). This result explains why both periplasmic domains of DsbD are required for shuffling electrons from the TM domain of DsbD to DsbC.

Cys109 and Cys461 form a mixed disulfide between nDsbD and cDsbD

To identify the cysteine residues that form a transient mixed disulfide between nDsbD and cDsbD in the DsbD reaction cycle, we purified the single-cysteine variants Cys103Ser and Cys109Ser of nDsbD, and Cys461Ser and Cys464Ser of cDsbD. Free thiol groups in the purified proteins were quantified with Ellman's assay both at the level of the native and denatured states. Table I shows that only Cys109 of nDsbD and Cys461 of cDsbD are reactive and solvent accessible, while Cys103

and Cys464 are buried in the folded domains. Consequently, disulfide exchange between nDsbD and cDsbD can only occur via a transient disulfide bond between Cys109 and Cys461. To prepare a kinetically stable mixed disulfide between nDsbD and cDsbD, we first synthesized the activated mixed disulfide between nDsbD-C103S and thionitrobenzoic acid by incubation of nDsbD-C103S with excess of Ellman's reagent. The activated mixed disulfide was then purified and mixed with equimolar amounts of the variant cDsbD-C464S, which resulted in almost quantitative formation of the mixed disulfide between nDsbD-C103S and cDsbD-C464S (Supplementary Figure S1). The reaction product was purified to homogeneity by chromatography on Ni-NTA agarose and gel filtration, concentrated to 40 mg/ml, and crystallized.

Structure determination of the mixed disulfide between nDsbD and cDsbD

The X-ray structure of the mixed disulfide between nDsbD and cDsbD (termed nDsbD-SS-cDsbD in the following) was

Table 1 Accessible thiols in single-cysteine variants of nDsbD and cDsbD

Domain variant	Free thiols/polypeptide	
	Denatured[a]	Native
nDsbD-C103S	0.98	1.04
nDsbD-C109S	1.02	0.07
cDsbD-C461S	1.04	0.12
cDsbD-C464S	1.07	0.98

[a]In the presence of 6 M guanidinium chloride.

solved at a resolution of 2.85 Å (PDB entry 1SE1). The crystals belong to space group C2 and contain three nDsbD-SS-cDsbD complexes (A–C) per asymmetric unit. The structure reveals in full detail how the N-terminal immunoglobulin-like domain of DsbD interacts with the C-terminal thioredoxin-like domain.

The final electron density map is well defined throughout the structure, which was refined to an R-factor of 0.224 and a free R-factor of 0.284 (Table II). The Ramachandran plot statistics is very good (Table II) with only one residue (Asp79 from nDsbD) in the disallowed region. The electron density of Asp79 is well defined and was found to be identical in the structure of noncomplexed nDsbD (Goulding *et al* (2002), PDB entry 1L6P (1.65 Å), Haebel *et al* (2002), PDB entry 1JPE (1.9 Å)) and for the complex between nDsbD and DsbC (nDsbD-SS-DsbC, Haebel *et al* (2002), PDB entry 1JZD (2.3 Å)), respectively.

The average B-factor for the final nDsbD-SS-cDsbD model is 38.4 Å^2, which compares with a Wilson B-factor of 68.8 Å^2 for the data and with an average B-factor of 43.3 Å^2 for the structure of nDsbD-SS-DsbC (PDB entry 1JZD).

Overall structure of nDsbD-SS-cDsbD

nDsbD possesses an immunoglobulin-like fold (Goulding *et al*, 2002), and cDsbD a thioredoxin-like fold (Kim *et al*, 2003). Each nDsbD-SS-cDsbD complex has dimensions of about 34 Å × 43 Å × 75 Å (Figure 3A). Comparison of the nDsbD-SS-DsbC complex with nDsbD-SS-cDsbD reveals similarities and differences in the binding mode and interfaces. As Cys109 of nDsbD forms a mixed disulfide with the solvent-exposed, nucleophilic cysteine of its reaction partner in both

Table 2 Crystallographic data and refinement statistics

Data collection				
Radiation source	SLS Villigen, CH beamline X06SA			
Wavelength (Å)	0.7514			
Space group	C2			
Unit cell (Å^3)	188.5 × 52.6 × 107.9, β = 100.4°			
Resolution range (Å)	20–2.85			
No. of reflections	109 492			
No. of unique reflections	24 676			
Completeness (%)	99.3 (97.3)[a]			
R_{sym}	8.0 (36.2)[a]			
Average I/σ	16.1 (3.6)[a]			
Redundancy	4.4 (3.3)[a]			
Refinement statistics				
Resolution (Å)	20–2.85			
No. of reflections (test)	24 336 (707)			
No. of atoms	Complex A	Complex B	Complex C	Total
nDsbD	979	915	927	2821
CDsbD	1000	931	922	2853
Water molecules				284
R-factor	0.224 (0.349)[b]			
Free R-factor	0.284 (0.443)[b]			
R.m.s.d. bonds (Å)	0.0076			
R.m.s.d. angles (deg)	1.24			
Average B-factor (Å^2)	38.4			
Ramachandran plot regions (%)				
Most favored	89.7%			
Additional allowed	9.2%			
Generously allowed	0.6%			
Disallowed region	0.5%			

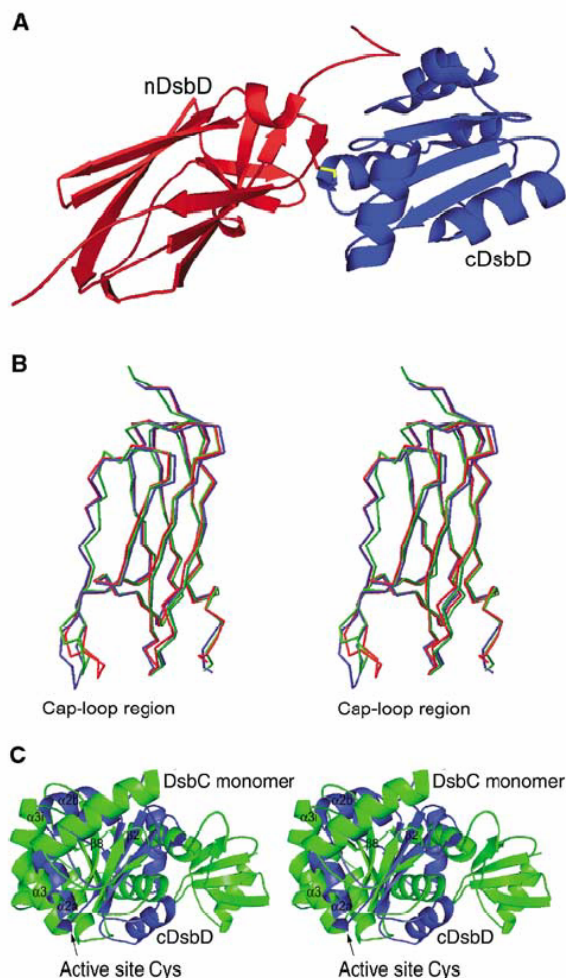[a]Last shell: 2.85–2.95 Å.
[b]Last shell: 2.85–3.03 Å.

Figure 3 (**A**) Ribbon diagram of the structure of the nDsbD-SS-cDsbD mixed disulfide. The structure of nDsbD (red) comprises residues 1–125, and that of cDsbD (blue) residues 426–545 (complex B). The disulfide bond between Cys109 and Cys461 is depicted in yellow. (**B**) Superposition of the C^α-traces of nDsbD from the nDsbD-SS-DsbC complex (1JZD, green) and nDsbD from nDsbD-SS-cDsbD (complex B, blue) onto that of monomeric nDsbD (1L6P, red) shows different conformations of the Cap-loop region (residues 68–72). (**C**) Stereo picture showing differences in the orientation of cDsbD (blue) and DsbC (green) in the complex with nDsbD (not shown), based on superposition of nDsbD from nDsbD-SS-DsbC (1JZD) onto nDsbD from the nDsbD-SS-cDsbD complex. The arrow indicates the approximate position of the active site cysteines for both complexes.

complexes, the contact areas of nDsbD for binding of cDsbD and DsbC overlap. Cys109 in isolated oxidized nDsbD is shielded by the so-called Cap-loop region (segment Asp68–Gly72) (Goulding *et al*, 2002). As reported for the nDsbD-SS-DsbC complex (Haebel *et al*, 2002), Cys109 of nDsbD becomes accessible in nDsbD-SS-cDsbD due to a conformational switch of that region. The Cap-loop region is in a more open conformation in nDsbD-SS-cDsbD than in the nDsbD-SS-DsbC complex (Figure 3B). Crystal contacts between nDsbD-SS-nDsbD complexes A and C may contribute to this difference. In the case of complex B, the Cap-loop

region is involved only in a weak crystal contact with complex A through a hydrogen bond. Electron density for residues Phe70 and Tyr71 (side chain only) in complex B is poorly defined, indicating that the Cap-loop region is flexible.

Kim *et al* (2003) previously modelled the nDsbD-SS-cDsbD complex using the nDsbD-SS-DsbC structure (Haebel *et al*, 2002) as a template. However, the orientation of cDsbD relative to nDsbD in the experimental structure of nDsbD-SS-cDsbD differs from this model (Figure 3C). For example, helix α2a and strand β2 of cDsbD have a different orientation (an angle of ∼20°) than the corresponding helix α3 and strand β8 of DsbC in the model.

The three copies of the nDsbD domain in the asymmetric unit also exhibit differences around the N-termini due to crystal contacts. In complex A, electron density is visible for residues Gly1 to Ala5, then there is a gap until Gln10. In complex B, the entire N-terminal region has well-defined electron density, whereas no clear electron density is discernible before Ser9 in complex C. These N-terminal residues in complexes A and B adopt different conformations, which again appear to be caused by crystal contacts.

A surface representation of nDsbD-SS-cDsbD shows a relatively planar region between the C-terminus of nDsbD and the N-terminus of cDsbD, which is supposed to be oriented towards the surface of the membrane (Supplementary Figure S2). The TM domain of DsbD consists of eight predicted TM helices (Stewart *et al*, 1999; Chung *et al*, 2000; Gordon *et al*, 2000). Recently, Katzen and Beckwith (2003) showed that Cys163 from the first predicted TM helix 1 can form a disulfide bridge with Cys285 from the fourth TM helix, and proposed a model for the TM domain in which helices 1 and 8 are adjacent. This model would require long linker segments to connect the TM domain with the crystallographically observed C-terminus of nDsbD and N-terminus of cDsbD, which are approximately 60 Å apart. The 20 residues separating the last observed residue of nDsbD from the first predicted residue of TM helix 1, and the 15 residues between the last residue of the predicted TM helix 8 and the first observed residue of cDsbD may span this distance. Comparison of the structure of nDsbD-SS-cDsbD with that of nDsbD-SS-DsbC suggests that a large translation of nDsbD away from cDsbD is required to allow disulfide exchange of nDsbD in the context of full-length DsbD with the active site of DsbC. In addition, there may be a rotation of nDsbD such that Cys109 is sufficiently distant from the plane of the membrane to prevent clashes between DsbD and DsbC (Figure 4).

Specific interactions stabilizing the nDsbD-SS-cDsbD complex

Besides the interdomain disulfide bond, the nDsbD-SS-cDsbD domain interface is characterized by only a limited number of specific interactions, namely four (complex B), five (complex C), or six (complex A) interdomain hydrogen bonds (Table III). The main-chain carbonyl of Cys109 is hydrogen-bonded to the amide nitrogen of Leu510, and the amide nitrogen of Cys109 is linked to the carbonyl oxygen of Leu510. A third hydrogen bond near the active cysteines is formed by the amide nitrogen of Phe531 and by the carbonyl of Gly107. The other interdomain hydrogen bonds lie in the Cap-loop region and differ in every complex in the asymmetric unit due to conformational changes induced by crystal contacts. In complexes A and C, the side-chain amine of

Lys469 and the hydroxyl group of Tyr470 are involved in a network of hydrogen bonds with the carboxylate of Glu69. In complexes A and B, the hydroxyl group of Tyr71 also interacts with the main-chain carbonyl of Asp459, while the electron density of Tyr71 in complex B is not well defined. Overall, the number of specific contacts is rather limited relative to the size of the interface area (1301 $\mathring{A}^2$, see below).

Comparison between the contact interface of nDsbD-SS-cDsbD and nDsbD-SS-DsbC

We calculated the interface areas of nDsbD-SS-cDsbD and nDsbD-SS-DsbC with the program Grasp (Nicholls *et al*, 1993) following the protocol of Janin (1997). nDsbD-SS-cDsbD has a calculated binding interface of 1301 $\mathring{A}^2$, whereas nDsbD-SS-DsbC has an interface of 2045 $\mathring{A}^2$ (Figure 5, Table III). This difference is caused by the second nDsbD interface in the nDsbD-SS-DsbC complex, which mediates additional noncovalent contacts between nDsbD and the second DsbC subunit.

The first interface of nDsbD-SS-DsbC is the active site interface; this interface strongly overlaps with the interface
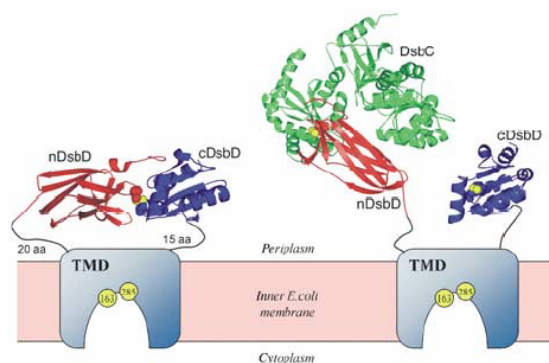

Figure 4 Electron transfer from cDsbD to DsbC via nDsbD involves large domain movements. Left: Proposed orientation of nDsbD-SS-cDsbD with respect to the transmembrane domain (TMD) in the context of full-length DsbD. Cys163 and Cys285 from the TM domain are indicted by yellow circles, and sulfur atoms of Cys109 and Cys461 are depicted by yellow spheres. The 20- and 15-residue-long linkers connecting the last structured residue of nDsbD with the first predicted TMD residue, and the last predicted TMD residue with the first structured residue of cDsbD, respectively, are indicated as black lines. Right: Model of the mixed disulfide complex between DsbD and DsbC, based on the structures of nDsbD-SS-cDsbD and nDsbD-SS-DsbC (1JZD). Disulfide exchange between nDsbD and DsbC is only possible when nDsbD and cDsbD undergo a massive domain movement.

of nDsbD-SS-cDsbD (Figure 5) and has a comparable size of 1376 $\mathring{A}^2$. In fact, the nDsbD-SS-cDsbD and the nDsbD-SS-DsbC interfaces share a common area of around 90% of their surface. Similarly to the interface between nDsbD and cDsbD (4–6 interdomain hydrogen bonds), also in the nDsbD-SS-DsbC complex there is only a limited number (7) of intersubunit hydrogen bonds (Table III). Three hydrogen bonds described for nDsbD-SS-cDsbD are located at the same position as in nDsbD-SS-DsbC. The main-chain carbonyl and the amide nitrogen of Cys109 (nDsbD) hydrogen-bond the amide nitrogen and carbonyl oxygen, respectively, of Thr182 of DsbC. The third hydrogen bond is formed by the amide nitrogen of DsbC Tyr196 and by the carbonyl of Gly107 (nDsbD).

The nDsbD-SS-DsbC complex has one residue forming intersubunit hydrogen bonds in the Cap-loop region (hydroxyl group of Tyr71 of nDsbD to the guanidinium moiety of DsbC Arg125). As mentioned above, the Cap-loop region in the nDsbD-SS-cDsbD complex is also involved in crystal contacts. In nDsbD-SS-cDsbD, the Cap-loop region exhibits a wider opening than in nDsbD-SS-DsbC.

The additional, second interface of nDsbD-SS-DsbC is stabilized by three hydrogen bonds and a specific salt bridge. Indices for planarity and shape complementarities (sc-index) were also calculated. Lower planarity and a lower sc-index are found for nDsbD-SS-cDsbD (Table III). The planarity for nDsbD-SS-cDsbD is 1.81 $\mathring{A}$ and for nDsbD-SS-DsbC 2.34 $\mathring{A}$ (first interface). Analysis of 23 optional interfaces of protein–protein complexes by Jones and Thornton (1996) updated at http://www.biochem.ucl.ac.uk/bsm/-PP/server/server_datasets.html yielded an average planarity of 2.6 $\mathring{A}$ ($\sigma = 0.6 \mathring{A}$). Compared to this value, nDsbD-SS-cDsbD shows a very low planarity, whereas nDsbD-SS-DsbC shows a value that lies in the average. Comparison of these values, the wider opening of the Cap-loop region and the additional contact area in nDsbD-SS-DsbC suggest that the interaction of nDsbD with cDsbD may be less specific than that with DsbC. This is, however, most likely compensated by the high relative effective concentrations of the periplasmic domains in the context of full-length DsbD.

Large kinetic barriers guarantee the coexistence of the DsbA/B and DsbC/D redox system

We measured the rate constants of nonfunctional disulfide exchange reactions either by tryptophan fluorescence (DsbA/DsbC, DsbA/nDsbD, DsbA/cDsbD, DsbB/DsbC) or acid-quenching after different reaction times and HPLC separation of reaction products (nDsbD/DsbC, cDsbD/DsbC). Figure 6 shows that all nonfunctional disulfide exchange reactions are

Table 3 Analysis of specific interdomain contacts formed by nDsbD

	nDsbD-SS-DsbC			nDsbD-SS-cDsbD
	First interface	*Second interface*	*Total*	
Interface area ($\mathring{A}^2$)	1376 (1268)[a]	669 (654)[a]	2045 (1922)[a]	1301
Planarity ($\mathring{A}$)[b]	2.34	1.29		1.81
Hydrogen bonds	7	3	10	4–6[d]
Salt bridges	0	1	1	0
Index of surface complementarity[c]			0.76	0.67

[a]Haebel *et al* (2002).
[b]Jones and Thornton (1997).
[c]Lawrence and Colman (1993).
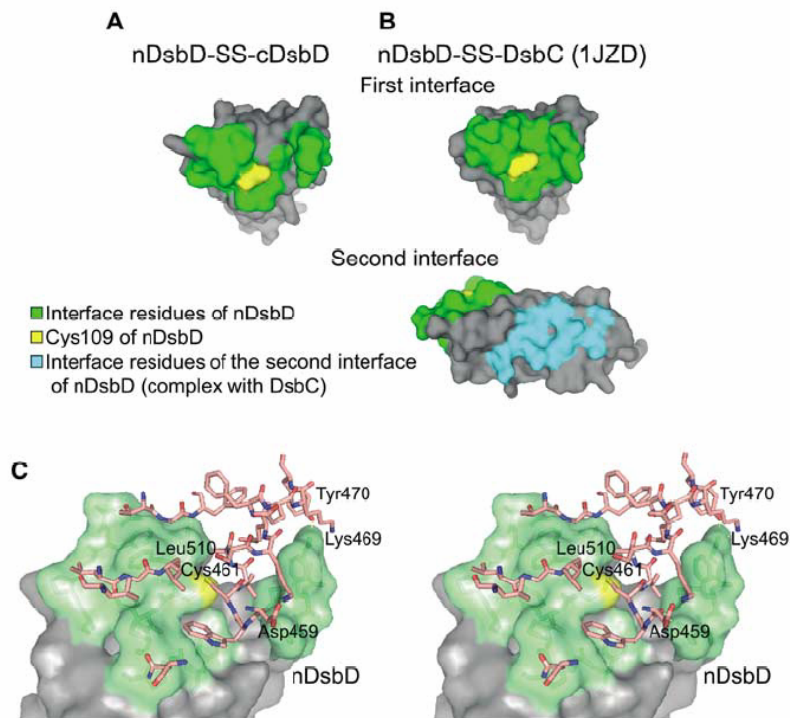[d]Depending on the respective complex in a.u.

Figure 5 Surface representations and interface analysis of the nDsbD-SS-cDsbD and nDsbD-SS-DsbC (1JZD) complexes. (**A**) Residues of nDsbD involved in the interaction with cDsbD (green). (**B**) Residues of nDsbD involved in the interaction with the first interface (green) and the second interface (cyan) of DsbC. (**C**) Details of the nDsbD-SS-cDsbD interface. Residues of nDsbD participating in the dimer interface are shown in green on the surface of the domain. The interacting residues of cDsbD appear in ball-and-stick representation in pink and atom colors.

indeed 10^3–10^7-fold slower than disulfide exchange between DsbA and DsbB, and DsbC and nDsbD, both of which have apparent second-order rate constants above $10^6 \, M^{-1} \, s^{-1}$ at pH 7.0. Among the nonfunctional reactions, oxidation of DsbC by quinone-depleted DsbB is fastest ($1.9 \times 10^3 \, M^{-1} \, s^{-1}$), albeit > 1000-fold slower than oxidation of DsbA by DsbB (Figure 6). This explains that DsbC accumulates in the oxidized form in the periplasm of *dsbD* null strains (Rietsch *et al*, 1997) and indicates that DsbC may be oxidized directly by DsbB in these strains. Conversely, DsbA is also a very poor redox partner of DsbD ($k_{app} = 900 \, M^{-1} \, s^{-1}$), again in agreement with the predominantly reduced state of DsbA in *dsbB* deletion mutants (Kishigami *et al*, 1995). Overall, the kinetic data demonstrate that large kinetic barriers for nonfunctional disulfide exchange reactions guarantee the coexistence of the DsbA/B and DsbC/D redox systems.

Conclusions

In the present work, we have gained a complete picture on the kinetics of disulfide exchange reactions that may occur between proteins from the oxidative DsbA/B and reductive DsbC/D pathway in the *E. coli* periplasm. Overall, nonfunctional reactions between oxidoreductase components from different pathways are separated by large kinetic barriers from functional reactions, such that nonfunctional disulfide exchange is 10^3–10^7 times slower than functional electron transfer. Steric hindrance of nonfunctional interactions is likely to be the main mechanism guaranteeing the indepen-

dence of the DsbA/B and DsbC/D systems. An alternative explanation would be particularly fast, functional disulfide exchange reactions mediated through very specific side-chain contacts in the contact area between functional reaction partners. We consider this mechanism less prevalent. This is best illustrated by nDsbD, which not only interacts rapidly with cDsbD and DsbC (Katzen and Beckwith, 2000; Krupp *et al*, 2001; Collet *et al*, 2002) via its nucleophilic Cys109 thiol, but is also supposed to react rapidly with DsbG (Bessette *et al*, 1999) and CcmG (Katzen *et al*, 2002) via Cys109. It is thus difficult to conceive a single binding area around Cys109 in nDsbD that simultaneously mediates highly specific recognition of four different target proteins. Indeed, the number of specific hydrogen bonds and salt bridges in the interface between nDsbD and cDsbD relative to the total binding area of about 1300 Å^2 is very small (Table III). The same holds true for the nDsbD-SS-DsbC complex, albeit there are additional contacts to the second DsbC subunit (Table III). We thus conclude that surface complementarity to the extent that disulfide interchange between active sites can occur without steric hindrance, and a limited number of specific contacts are sufficient to mediate rapid, functional disulfide exchange between intrinsically reactive Dsb proteins. A main factor determining the intrinsic reactivities of the nucleophilic active site cysteines in proteins from the thioredoxin family is the strongly lowered pK_a value of the more N-terminal active site thiols (Nelson and Creighton, 1994). For example, the pK_a values of the nucleophilic cysteines in DsbA and DsbC are 3.4 and 4.1, respectively (Nelson and Creighton, 1994; Sun
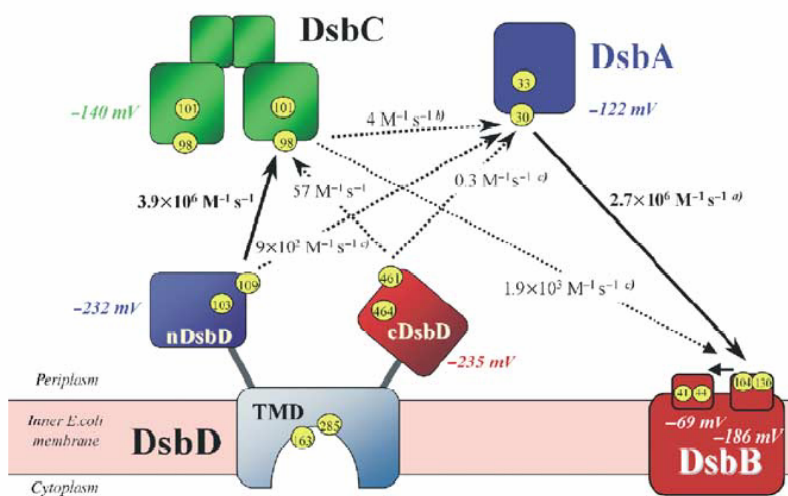
Figure 6 Large kinetic barriers separate the DsbA/B and DsbC/D redox systems. Apparent rate constants of disulfide exchange were measured at pH 7.0 and 25°C. Functional disulfide exchange reactions (bold solid arrows) have second-order rate constants above $10^6 \, M^{-1} \, s^{-1}$, while nonfunctional ('forbidden') reactions (dotted arrows) are 10^3–10^7-fold slower. Arrows indicate the direction of two-electron transfer. All measured rates have errors <30%. [a]Grauschopf *et al* (2003). [b]Zapun *et al* (1995) reported a value of $100 \, M^{-1} \, s^{-1}$ for this reaction at pH 7.5. [c]Reactions were followed by the change in tryptophan fluorescence.

and Wang, 2000), and are sufficient to explain the high reactivity of both proteins (Szajewski and Whitesides, 1980; Grauschopf *et al*, 1995; Huber-Wunderlich and Glockshuber, 1998).

We have shown that Cys109 from nDsbD and Cys461 from cDsbD form a transient mixed disulfide bond in the reaction mechanism of DsbD, and conclude that large relative domain movements between nDsbD and cDsbD are necessary to allow electrons flow from cDsbD to DsbC. The fact that nDsbD but not cDsbD can be cleaved off proteolytically from full-length DsbD (Collet *et al*, 2002) indicates that the linker segment between nDsbD and the TM domain is more flexible than that between cDsbD and the TM domain. It may therefore well be that it is essentially nDsbD that moves away from cDsbD to allow subsequent disulfide exchange between nDsbD and DsbC, DsbG, or CcmG.

If we assume that DsbD-mediated electron transfer occurs exclusively via disulfide exchange (Chung *et al*, 2000; Katzen and Beckwith, 2000; Krupp *et al*, 2001), the last mechanistic step that remains to be elucidated will be the identification of the pair of cysteines that mediate disulfide exchange between the TM domain and cDsbD. As Cys461 is the only surface-exposed residue in cDsbD, we propose that Cys461 not only reacts with Cys109 of nDsbD, but is also capable of forming a disulfide bond with either Cys163 or Cys285 from the TM domain if this mechanism holds true. This implies additional domain movements of cDsbD relative to the TM domain. Cys163 and Cys285 are both located in the predicted TM helices 1 and 4, can form a disulfide bond that connects both helices, and have been shown to be accessible from the cytoplasmic side (Chung *et al*, 2000; Katzen and Beckwith, 2003). This has led to a model according to which the TM domain of DsbD adopts a 'funnel-like' structure, with the 'funnel' opening toward the cytoplasm when the Cys163–Cys285 disulfide is formed (Katzen and Beckwith, 2003). Direct oxidation of the Cys163–Cys285 pair by oxidized cDsbD is thus only conceivable when a major structural rearrangement occurs in the TM domain such that the 'funnel' opens toward the periplasm when the Cys163–Cys285 disulfide is reduced by cytoplasmic thioredoxin. Alternatively, a protein-bound cofactor may assist electron transfer from the Cys163/Cys285 pair to the Cys461–Cys464 disulfide bond of cDsbD.

Materials and methods

Construction of expression plasmids

The plasmid pNDsbD for cytosolic expression of nDsbD (residues 1–143 of mature DsbD) under control of *trc*-promotor/*lac*-operator was constructed as follows. A 435-bp gene fragment encoding nDsbD was amplified by PCR from genomic DNA of the *E. coli* wild-type strain W3110 with primers N1 (5′-GGG AAT TCC ATA TGA TGG CTC AAC GCA TCT TTA CG-3′) and N2 (5′-CCC GGA TCC TTA TTG CGC GGT GGG CTG C-3′) and cloned into pDsbA3 (Hennecke *et al*, 1999) via *Nde*I and *Bam*HI.

For expression of cDsbD (residues 419–546 of mature DsbD) with C-terminal (His)$_6$ tag, a 399-bp fragment was amplified with primers C1 (5′-CTA GCT AGC CAG GAT TGG GCA TTT GGT GCG ACG-3′) and C2 (5′-CGC GGA TCC TTA ATG GTG ATG GTG ATG GTG CGG TTG GCG ATC GCG-3′) and cloned into pDsbA3 via *Nhe*I and *Bam*HI. In the resulting plasmid pCDsbD, the sequence encoding (His)$_6$-tagged cDsbD is fused to the DsbA signal sequence for periplasmic expression under the control of *trc*-promotor/*lac*-operator.

The Cys variants of nDsbD and cDsbD, in which one of the active site cysteines was replaced by a serine, were constructed from pNDsbD and pCDsbD using the QuikChange method (Stratagene). All constructs were verified by DNA sequencing.

Purification of nDsbD, cDsbD, DsbA, DsbB, and DsbC

All proteins were expressed in the *E. coli* BL21*Rosetta* cells (Novagene) grown in 9 l of Luria–Bertani (LB) medium containing ampicillin (100 μg/ml) at 37°C. Protein production was induced with IPTG (final concentration 100 μM) when cells had reached an optical density (OD) at 600 nm of 0.6–0.8. After further growth at 37°C for 4 h, bacteria were harvested by centrifugation. For purification of nDsbD, cells were suspended in 5 mM Tris–HCl (pH 8.0) and disrupted (Cell Cracker). After centrifugation at

50 000 *g* for 30 min at 4°C, the supernatant was dialyzed at 4°C against 5 mM Tris–HCl (pH 8.0), and applied on Fast Flow Q Sepharose pre-equilibrated with the same buffer. Proteins were eluted with a gradient of 0 to 500 mM NaCl in 5 mM Tris–HCl (pH 8.0). Fractions containing nDsbD were pooled and mixed with ammonium sulfate to a final concentration of 1.4 M. The solution was applied to Phenyl Sepharose HP equilibrated with 1.4 M ammonium sulfate and 10 mM Tris–HCl (pH 8.0). Proteins were eluted with a gradient from 1.4 to 0 M ammonium sulfate in 10 mM Tris–HCl (pH 8.0). Fractions containing pure nDsbD were dialyzed against distilled water. The final yield of purified nDsbD was 100 mg/l bacterial culture.

For purification of cDsbD, bacteria were suspended in cold PBS buffer (20 mM sodium phosphate (pH 7.5), 150 mM NaCl) containing polymyxin B (1 mg/ml) and shaken at 4°C for 90 min. After centrifugation at 50 000 *g* for 30 min at 4°C, the supernatant was mixed with imidazole–HCl (pH 7.5) to a concentration of 10 mM and applied to an Ni-NTA Superflow column equilibrated with 10 mM imidazole–HCl and PBS (pH 7.5). Proteins were eluted with a gradient from 10 to 300 mM imidazole–HCl in PBS. Fractions containing (His)$_6$-tagged cDsbD were dialyzed against distilled water. The final yield of purified protein was 20 mg/l bacterial culture.

Cysteine variants of nDsbD and (His)$_6$-tagged cDsbD were purified according to the same protocols with comparable yields. Oxidized *E. coli* DsbA (Hennecke *et al*, 1999), oxidized *E. coli* DsbC (Maskos *et al*, 2003), and oxidized, quinone-depleted *E. coli* DsbB (Grauschopf *et al*, 2003) were purified as described.

Synthesis of nDsbD-SS-cDsbD

For preparation of nDsbD-SS-cDsbD, we first prepared the mixed disulfide between the nDsbD variant C103S and nitrothiobenzoic acid (nDsbD(C103S)-NTB). The variant C103 was produced in *E. coli* and enriched by chromatography on Fast Flow Q Sepharose as described for wild-type nDsbD. Pooled fractions (in Tris–HCl (pH 8.0)) were mixed with excess dithiobisnitrobenzoic acid (DTNB) (final concentration 10 mM) and incubated at 25°C for 15 min. After addition of ammonium sulfate to a concentration of 1.2 M, the solution was applied to Phenyl Sepharose HP equilibrated with 1.2 M ammonium sulfate and 10 mM Tris–HCl (pH 8.0). The mixed disulfide was eluted with a gradient from 1.2 to 1 M ammonium sulfate. Fractions containing nDsbD(C103S)-NTB were pooled and dialyzed against PBS (pH 7.5). The (His)$_6$-tagged variant C464S of cDsbD was purified from the periplasmic extract as described for (His)$_6$-tagged wild-type cDsbD, and also dialyzed against PBS (pH 7.5).

Purified nDsbD(C103S)-NTB and cDsbD(C464S) were then mixed at equimolar concentrations (30 μM each), incubated in PBS for 30 min at 25°C, and applied to an Ni-NTA Superflow column equilibrated with PBS (pH 7.5). The column was washed with PBS and 10 mM imidazole–HCl (pH 7.5), and the nDsbD(C103S)-cDsbD(C464S) mixed disulfide (nDsbD-SS-cDsbD) was eluted with a gradient from 10 to 70 mM imidazole–HCl. Fractions containing the mixed disulfide and small amounts of cDsbD were concentrated and subjected to gel filtration on a Superdex 75 16/60 column in 100 mM sodium phosphate and 500 mM NaCl (pH 7.0). Fractions containing the pure complex were dialyzed against distilled water and concentrated.

Protein concentrations

Protein concentrations were determined according to the molar extinction coefficients at 280 nm, using values of 20 000 and 8300 M^{-1} cm^{-1} for native nDsbD and native cDsbD, respectively. For oxidized DsbA, DsbC, and DsbB, extinction coefficients of 23 250, 16 200, and 47 750 M^{-1} cm^{-1} were used, respectively. Reduced proteins were prepared by reduction with a 1000-fold molar excess of DTT at pH 8.0, followed by gel filtration in 0.1 mM EDTA. Free thiol groups in reduced proteins were quantified by Ellman's assay (Ellman, 1959) using $\varepsilon_{412\,nm} = 13\,600$ M^{-1} cm^{-1} per free thiol group.

HPLC analysis of disulfide exchange kinetics

Disulfide exchange reactions between Dsb proteins were performed at 25°C and initial protein concentrations between 0.25 and 75 μM under second-order or pseudo-first-order conditions in 100 mM sodium phosphate and 0.1 mM EDTA (pH 7.0). Samples were removed after different incubation times, and the reactions were

rapidly quenched by addition of 0.4 volumes of 30% (w/v) formic acid (final pH < 2). Reaction products were separated with an Agilent 1100 HPLC instrument equipped with a diode array detection system and a C$_{18}$ reverse-phase column (Agilent Zorbax 300 SB, 5 μM, 2.1 × 150 mm). Proteins were eluted at 55°C with a linear gradient of H$_2$O/0.1% TFA and acetonitirile/0.07% TFA, and detected by their absorbance at 220 and 280 nm.

Fluorescence measurements

Disulfide exchange between DsbC$_{red}$ and DsbB$_{ox}$, and between nDsbD$_{red}$ (or cDsbD$_{red}$) and DsbA$_{ox}$ was followed by the change in tryptophan fluorescence at 330 nm (excitation at 280 nm) in 100 mM sodium phosphate and 0.1 mM EDTA (pH 7.0). Initial protein concentrations varied between 5 and 50 μM for the individual reactions.

Redox equilibria

For determination of equilibrium constants (K_{eq}) between Dsb proteins and glutathione or DTT (cf. Grauschopf *et al*, 2003 and references cited therein), the redox state of the respective protein at different [GSH]^2/[GSSG] or DTT$_{ox}$/DTT$_{red}$ ratios was determined. Proteins were incubated for 16 h at 25°C in 100 mM sodium phosphate and 0.1 mM EDTA (pH 7.0) containing the respective thiol-disulfide mixtures. In the case of nDsbD, the fraction of reduced protein was quantified by Ellman's assay after removal of excess DTT through gel filtration. In the case of cDsbD and DsbC, the oxidized and reduced forms of the protein were separated and quantified by reverse-phase HPLC after acid quenching. cDsbD and nDsbD were equilibrated with DTT$_{ox}$/DTT$_{red}$ mixtures, while DsbC was incubated with glutathione redox buffers. To exclude air oxidation, all buffers were degassed and flushed with argon. Standard redox potentials (E_o') were calculated by the Nernst equation ($E_o'_{protein} = E_o'_{reference} - (RT/2F) \ln K_{eq}$), using E_o' values of −0.240 and −0.307 V for the redox potentials of glutathione and DTT$_{ox}$/DTT$_{red}$, respectively (Rost and Rapoport, 1964; Rothwarf and Scheraga, 1992).

Crystallization and structure determination

Purified disulfide-linked nDsbD-SS-cDsbD complex in distilled water was concentrated to 40 mg/ml. The sitting drop vapor diffusion method was used for producing crystals. A measure of 1 μl of protein solution was mixed with 1 μl of mother liquor solution (0.1 M sodium acetate (pH 4.5), 0.8 M sodium formate, 25% PEG 2K MME). Plate-like crystals grew at 4°C within a week to maximum dimensions of 130 × 500 × 30 μm. Crystals were cryo-protected by adding 15% ethylene glycol to the mother liquor solution and directly frozen in the nitrogen gas stream. Diffraction data were collected at 98.2 K on beamline X06SA at the Swiss Light Source (Paul Scherrer Institut Villigen, Switzerland) using a MAR CCD image plate at a wavelength of 0.7514 Å. The short wavelength was chosen to reduce synchrotron radiation damage to the disulfide bridge (Schlichting *et al*, 2000). Data were processed with DENZO and SCALEPACK (Otwinowski and Minor, 1997) to 2.85 Å. nDsbD-SS-cDsbD crystals belong to space group C2 with $a = 188.5$ Å, $b = 52.6$ Å, $c = 107.9$ Å, and $\beta = 100.4°$, and contain three molecules per asymmetric unit (Table II).

The structure of nDsbD-SS-cDsbD was solved by molecular replacement with AMoRe (Navaza, 1994) using the structure of nDsbD from the nDsbD-SS-DsbC structure (PDB entry 1JZD; Haebel *et al*, 2002) and a high-resolution structure of cDsbD (G Capitani and Ch U Stirnimann, unpublished data) as search models, against 12–4 Å data. Solutions for two complexes could be found using AMoRe against the data processed in C2. This corresponds to four solutions against data processed in P1. These four P1 solutions were refined in CNS (Brünger *et al*, 1998) to an *R*-factor of 0.418 and a free *R*-factor of 0.426. Nine cycles of water picking (with ARP/wARP-like picking parameters) and density modification in CNS lead to a much improved map, which was skeletonized with MAPMAN (Kleywegt and Jones, 1996). The waters introduced in the previous phase improvement step were then deleted. The structure refined to an *R*-factor of 0.308 and a free *R*-factor of 0.348 after having fitted the fifth and sixth complexes to the skeleton and to the density by hand using the program O (Jones *et al*, 1991). Molecular replacement in AMoRe worked now in C2 by picking the three corresponding P1 solutions. The nDsbD-SS-cDsbD structure was iteratively rebuilt in O and refined in CNS using NCS restraints to an *R*-factor of 0.224 and a free *R*-factor of 0.284 in space group C2

(Table II). The coordinates and structure factors of nDsbD-SS-cDsbD were deposited with the Protein Data Bank (http://www.rcsb.org/pdb/) with entry code 1SE1.

The stereochemistry of the nDsbD-SS-cDsbD structure was checked with WHAT_CHECK (Hooft *et al*, 1996) and PROCHECK (Laskowski *et al*, 1993). All figures were prepared with PyMOL (http://www.pymol.org; DeLano, 2002) except for Figure 1B, for which SwissPDB Viewer was used (http://www.expasy.org/spdbv; Guex and Peitsch, 1997). The interface areas of the nDsbD-SS-cDsbD and nDsbD-SS-DsbC complexes were calculated with the program Grasp (Nicholls *et al*, 1993). The shape complementarity of the interfaces of nDsbD-SS-cDsbD and nDsbD-SS-DsbC was calculated with the CCP4 program SC (Lawrence and Colman, 1993).

Supplementary data

Acknowledgements

References

Andersen CL, Matthey-Dupraz A, Missiakas D, Raina S (1997) A new *Escherichia coli* gene, dsbG, encodes a periplasmic protein involved in disulphide bond formation, required for recycling DsbA/DsbB and DsbC redox proteins. *Mol Microbiol* **26:** 121–132

Bader M, Muse W, Ballou DP, Gassner C, Bardwell JC (1999) Oxidative protein folding is driven by the electron transport system. *Cell* **98:** 217–227

Bader MW, Xie T, Yu CA, Bardwell JC (2000) Disulfide bonds are generated by quinone reduction. *J Biol Chem* **275:** 26082–26088

Bardwell JC, Lee JO, Jander G, Martin N, Belin D, Beckwith J (1993) A pathway for disulfide bond formation *in vivo*. *Proc Natl Acad Sci USA* **90:** 1038–1042

Bessette PH, Cotto JJ, Gilbert HF, Georgiou G (1999) *In vivo* and *in vitro* function of the *Escherichia coli* periplasmic cysteine oxidoreductase DsbG. *J Biol Chem* **274:** 7784–7792

Brünger AT, Adams PD, Clore GM, DeLano WL, Gros P, Grosse-Kunstleve RW, Jiang JS, Kuszewski J, Nilges M, Pannu NS, Read RJ, Rice LM, Simonson T, Warren GL (1998) Crystallography & NMR system: a new software suite for macromolecular structure determination. *Acta Crystallogr D* **54:** 905–921

Chung J, Chen T, Missiakas D (2000) Transfer of electrons across the cytoplasmic membrane by DsbD, a membrane protein involved in thiol-disulphide exchange and protein folding in the bacterial periplasm. *Mol Microbiol* **35:** 1099–1109

Collet JF, Bardwell JC (2002) Oxidative protein folding in bacteria. *Mol Microbiol* **44:** 1–8

Collet JF, Riemer J, Bader MW, Bardwell JC (2002) Reconstitution of a disulfide isomerization system. *J Biol Chem* **277:** 26886–26892

Dailey FE, Berg HC (1993) Mutants in disulfide bond formation that disrupt flagellar assembly in *Escherichia coli*. *Proc Natl Acad Sci USA* **90:** 1043–1047

Darby NJ, Creighton TE (1995) Catalytic mechanism of DsbA and its comparison with that of protein disulfide isomerase. *Biochemistry* **34:** 3576–3587

DeLano WL (2002) *The PyMol Molecular Graphics System*. San Carlos, CA, USA: DeLano Scientific

Ellman GL (1959) Tissue sulfhydryl groups. *Arch Biochem Biophys* **82:** 70–77

Goldstone D, Haebel PW, Katzen F, Bader MW, Bardwell JC, Beckwith J, Metcalf P (2001) DsbC activation by the N-terminal domain of DsbD. *Proc Natl Acad Sci USA* **98:** 9551–9556

Gordon EH, Page MD, Willis AC, Ferguson SJ (2000) *Escherichia coli* DipZ: anatomy of a transmembrane protein disulphide reductase in which three pairs of cysteine residues, one in each of three domains, contribute differentially to function. *Mol Microbiol* **35:** 1360–1374

Goulding CW, Sawaya MR, Parseghian A, Lim V, Eisenberg D, Missiakas D (2002) Thiol-disulfide exchange in an immunoglobulin-like fold: structure of the N-terminal domain of DsbD. *Biochemistry* **41:** 6920–6927

Grauschopf U, Fritz A, Glockshuber R (2003) Mechanism of the electron transfer catalyst DsbB from *Escherichia coli*. *EMBO J* **22:** 3503–3513

Grauschopf U, Winther JR, Korber P, Zander T, Dallinger P, Bardwell JC (1995) Why is DsbA such an oxidizing disulfide catalyst? *Cell* **83:** 947–955

Guex N, Peitsch MC (1997) SWISS-MODEL and the Swiss-PdbViewer: an environment for comparative protein modeling. *Electrophoresis* **18:** 2714–2723

Haebel PW, Goldstone D, Katzen F, Beckwith J, Metcalf P (2002) The disulfide bond isomerase DsbC is activated by an immuno-globulin-fold thiol oxidoreductase: crystal structure of the DsbC–DsbDalpha complex. *EMBO J* **21:** 4774–4784

Hennecke J, Sebbel P, Glockshuber R (1999) Random circular permutation of DsbA reveals segments that are essential for protein folding and stability. *J Mol Biol* **286:** 1197–1215

Hiniker A, Bardwell JC (2003) Disulfide bond isomerization in prokaryotes. *Biochemistry* **42:** 1179–1185

Hooft RW, Vriend G, Sander C, Abola EE (1996) Errors in protein structures. *Nature* **381:** 272

Huber-Wunderlich M, Glockshuber R (1998) A single dipeptide sequence modulates the redox properties of a whole enzyme family. *Fold Des* **3:** 161–171

Janin J (1997) Specific versus non-specific contacts in protein crystals. *Nat Struct Biol* **4:** 973–974

Jones S, Thornton JM (1996) Principles of protein–protein interactions. *Proc Natl Acad Sci USA* **93:** 13–20

Jones S, Thornton JM (1997) Prediction of protein–protein interaction sites using patch analysis. *J Mol Biol* **272:** 133–143

Jones TA, Zou J-Y, Cowan SW, Kjeldgaard M (1991) Improved methods for building protein models in electron density maps and the location of errors in these models. *Acta Crystallogr A* **47:** 110–119

Katzen F, Beckwith J (2000) Transmembrane electron transfer by the membrane protein DsbD occurs via a disulfide bond cascade. *Cell* **103:** 769–779

Katzen F, Beckwith J (2003) Role and location of the unusual redox-active cysteines in the hydrophobic domain of the transmembrane electron transporter DsbD. *Proc Natl Acad Sci USA* **100:** 10471–10476

Katzen F, Deshmukh M, Daldal F, Beckwith J (2002) Evolutionary domain fusion expanded the substrate specificity of the transmembrane electron transporter DsbD. *EMBO J* **21:** 3960–3969

Kim JH, Kim SJ, Jeong DG, Son JH, Ryu SE (2003) Crystal structure of DsbDgamma reveals the mechanism of redox potential shift and substrate specificity. *FEBS Lett* **543:** 164–169

Kishigami S, Akiyama Y, Ito K (1995) Redox states of DsbA in the periplasm of *Escherichia coli*. *FEBS Lett* **364:** 55–58

Kleywegt GJ, Jones TA (1996) xdlMAPMAN and xdlDATAMAN—programs for reformatting, analysis and manipulation of biomacromolecular electron-density maps and reflection data sets. *Acta Crystallogr D* **52:** 826–828

Kobayashi T, Ito K (1999) Respiratory chain strongly oxidizes the CXXC motif of DsbB in the *Escherichia coli* disulfide bond formation pathway. *EMBO J* **18:** 1192–1198

Krupp R, Chan C, Missiakas D (2001) DsbD-catalyzed transport of electrons across the membrane of *Escherichia coli*. *J Biol Chem* **276:** 3696–3701

Laskowski RA, MacArthur MW, Moss DS, Thornton JM (1993) PROCHECK: a program to check the stereochemical quality of protein structure. *J Appl Crystallogr* **26:** 283–291

Lawrence MC, Colman PM (1993) Shape complementarity at protein/protein interfaces. *J Mol Biol* **234:** 946–950

Maskos K, Huber-Wunderlich M, Glockshuber R (2003) DsbA and DsbC-catalyzed oxidative folding of proteins with complex disulfide bridge patterns *in vitro* and *in vivo*. *J Mol Biol* **325:** 495–513

McCarthy AA, Haebel PW, Torronen A, Rybin V, Baker EN, Metcalf P (2000) Crystal structure of the protein disulfide bond isomerase, DsbC, from *Escherichia coli*. *Nat Struct Biol* **7:** 196–199

Missiakas D, Georgopoulos C, Raina S (1994) The *Escherichia coli* dsbC (xprA) gene encodes a periplasmic protein involved in disulfide bond formation. *EMBO J* **13:** 2013–2020

Navaza J (1994) AMoRe: an automated package for molecular replacement. *Acta Crystallogr A* **50:** 157–163

Nelson JW, Creighton TE (1994) Reactivity and ionization of the active site cysteine residues of DsbA, a protein required for disulfide bond formation *in vivo*. *Biochemistry* **33:** 5974–5983

Nicholls A, Bharadwaj R, Honig B (1993) GRASP graphical representation and analysis of surface properties. *Biophys J* **64:** A166

Otwinowski Z, Minor W (1997) Processing of X-ray diffraction data collected in oscillation mode. *Methods Enzymol* **276:** 307–328

Reid E, Cole J, Eaves DJ (2001) The *Escherichia coli* CcmG protein fulfils a specific role in cytochrome *c* assembly. *Biochem J* **355:** 51–58

Rietsch A, Bessette P, Georgiou G, Beckwith J (1997) Reduction of the periplasmic disulfide bond isomerase, DsbC, occurs by passage of electrons from cytoplasmic thioredoxin. *J Bacteriol* **179:** 6602–6608

Ritz D, Beckwith J (2001) Roles of thiol-redox pathways in bacteria. *Annu Rev Microbiol* **55:** 21–48

Rost J, Rapoport S (1964) Reduction-potential of glutathione. *Nature* **201:** 185

Rothwarf DM, Scheraga HA (1992) Equilibrium and kinetic constants for the thiol-disulfide interchange reaction between glutathione and dithiothreitol. *Proc Natl Acad Sci USA* **89:** 7944–7948

Schlichting I, Berendzen J, Chu K, Stock AM, Maves SA, Benson DE, Sweet RM, Ringe D, Petsko GA, Sligar SG (2000) The catalytic pathway of cytochrome p450cam at atomic resolution. *Science* **287:** 1615–1622

Stewart EJ, Katzen F, Beckwith J (1999) Six conserved cysteines of the membrane protein DsbD are required for the transfer of electrons from the cytoplasm to the periplasm of *Escherichia coli*. *EMBO J* **18:** 5963–5971

Sun XX, Wang CC (2000) The N-terminal sequence (residues 1–65) is essential for dimerization, activities, and peptide binding of *Escherichia coli* DsbC. *J Biol Chem* **275:** 22743–22749

Szajewski RP, Whitesides GM (1980) Rate constants and equilibrium constants of thiol-disulfide interchange reactions involving oxidized glutathione. *J Am Chem Soc* **102:** 2011–2026

van Straaten M, Missiakas D, Raina S, Darby NJ (1998) The functional properties of DsbG, a thiol-disulfide oxidoreductase from the periplasm of *Escherichia coli*. *FEBS Lett* **428:** 255–258

Wunderlich M, Otto A, Seckler R, Glockshuber R (1993) Bacterial protein disulfide isomerase: efficient catalysis of oxidative protein folding at acidic pH. *Biochemistry* **32:** 12251–12256

Zapun A, Creighton TE (1994) Effects of DsbA on the disulfide folding of bovine pancreatic trypsin inhibitor and alpha-lactalbumin. *Biochemistry* **33:** 5202–5211

Zapun A, Missiakas D, Raina S, Creighton TE (1995) Structural and functional characterization of DsbC, a protein involved in disulfide bond formation in *Escherichia coli*. *Biochemistry* **34:** 5075–5089

3.2 Structural basis and kinetics of DsbD-dependent cytochrome *c* maturation

Christian U. Stirnimann, Anna Rozhkova, Ulla Grauschopf, Markus G. Grütter, Rudi Glockshuber, and Guido Capitani

Structural Basis and Kinetics of DsbD-Dependent Cytochrome *c* Maturation

Christian U. Stirnimann,[1,3] Anna Rozhkova,[2,3]
Ulla Grauschopf,[2] Markus G. Grütter,[1]
Rudi Glockshuber,[2,*] and Guido Capitani[1,*]
[1]Biochemisches Institut
Universität Zürich
Winterthurerstrasse 190
8057 Zürich
Switzerland
[2]Institut für Molekularbiologie und Biophysik
Eidgenössische Technische Hochschule Hönggerberg
8093 Zürich
Switzerland

Summary

DsbD from *Escherichia coli* transports two electrons from cytoplasmic thioredoxin to the periplasmic substrate proteins DsbC, DsbG and CcmG. DsbD consists of an N-terminal periplasmic domain (nDsbD), a C-terminal periplasmic domain, and a central transmembrane domain. Each domain possesses two cysteines required for electron transport. Herein, we demonstrate fast (3.9×10^5 M^{-1}s^{-1}) and direct disulfide exchange between nDsbD and CcmG, a highly specific disulfide reductase essential for cytochrome *c* maturation. We determined the crystal structure of the disulfide-linked complex between nDsbD and the soluble part of CcmG at 1.94 Å resolution. In contrast to the other two known complexes of nDsbD with target proteins, the N-terminal segment of nDsbD contributes to specific recognition of CcmG. This and other features, like the possibility of using an additional interaction surface, constitute the structural basis for the adaptability of nDsbD to different protein substrates.

Introduction

Disulfide bond reduction in the oxidizing *Escherichia coli* periplasm is catalyzed by the inner membrane protein DsbD. DsbD transfers electrons originating from cytoplasmic NADPH via thioredoxin reductase and thioredoxin to the periplasm (Kadokura et al., 2003). DsbD consists of a central transmembrane domain (TMD), a periplasmic N-terminal immunoglobulin-like domain (nDsbD), and a C-terminal thioredoxin-like domain (cDsbD) (Gordon et al., 2000; Goulding et al., 2002; Kim et al., 2003). Each of the domains has one pair of cysteines that is essential for electron transport (Stewart et al., 1999). It is proposed that electrons are transferred across the inner *E. coli* membrane via intramolecular disulfide exchange between the three DsbD domains (Figure 1). First, electrons are transferred from thioredoxin to the TMD, followed by reduction of cDsbD

*Correspondence: rudi@mol.biol.ethz.ch (R.G.); capitani@bioc.unizh.ch (G.C.)
[3]These authors contributed equally to this work.

and finally of nDsbD (Collet et al., 2002; Goldstone et al., 2001; Katzen and Beckwith, 2003; Krupp et al., 2000; Rozhkova et al., 2004).

DsbC, DsbG and CcmG (DsbE) are known in vivo substrate proteins of DsbD. DsbC is a homodimeric, periplasmic disulfide isomerase that catalyzes rearrangement of incorrect disulfide bonds in scrambled polypeptides to the native conformation (Maskos et al., 2003; McCarthy et al., 2000; Missiakas et al., 1994; Zapun et al., 1995). DsbG is a homodimeric homolog of DsbC of unknown function (Andersen et al., 1997; Bessette et al., 1999; van Straaten et al., 1998). CcmG is a membrane-anchored, highly specific disulfide reductase that is essential for c-type cytochrome maturation (Fabianek et al., 1998). Formation of mature cytochrome *c* requires ligation of heme to reduced thiols of a C-X-X-C-H motif of apocytochrome. Since DsbA, the periplasmic dithiol-oxidase, randomly introduces disulfide bonds in apocytochromes, bacteria have evolved a specialized redox system to revert these disulfides into reduced cysteine residues (Thony-Meyer, 1997). Besides DsbD and CcmG, CcmH is also involved in this system (Fabianek et al., 1999). Electrons are thought to be transferred from DsbD via CcmG and CcmH to apocytochrome *c* (Fabianek et al., 1999; Reid et al., 2001). The 1.14 Å crystal structure of a soluble fragment of CcmG from *Bradyrhizobium japonicum* revealed a thioredoxin fold with a characteristic groove near the C-X-X-C active site that has been proposed to interact either with DsbD and/or CcmH, and an unusual acidic environment at the active site (Edeling et al., 2004; Edeling et al., 2002).

We have recently solved the structure of the disulfide-linked complex between nDsbD and cDsbD (Rozhkova et al., 2004) that represents a trapped reaction intermediate in the intramolecular electron transfer cascade of DsbD, and we compared the structure with that of the complex between nDsbD and DsbC (Haebel et al., 2002). We also measured the kinetics of all disulfide exchange reactions for the disulfide bond formation and isomerization pathways. Here, we extend the kinetic analysis to the disulfide reduction pathway of cytochrome *c* maturation. We also present the structure of a disulfide-linked complex between nDsbD and the soluble fragment of CcmG from *E. coli*, which reveals the structural basis for the specific interaction between nDsbD and CcmG.

Results and Discussion

Rapid Disulfide Exchange Proves Direct Electron Flow from DsbD to CcmG

Two soluble leaderless CcmG constructs (CcmG$_{\Delta 19-185}$ and CcmG$_{\Delta 43-185}$) were designed for crystallization purposes, expressed in the cytoplasm of *E. coli*, and purified. We determined the redox potentials of the active site disulfides by equilibration with DTT under standard conditions. The values of −0.203 V and −0.209 V obtained for CcmG$_{\Delta 19-185}$ and CcmG$_{\Delta 43-185}$ (Figure 2), respectively, are almost identical. The previously re-
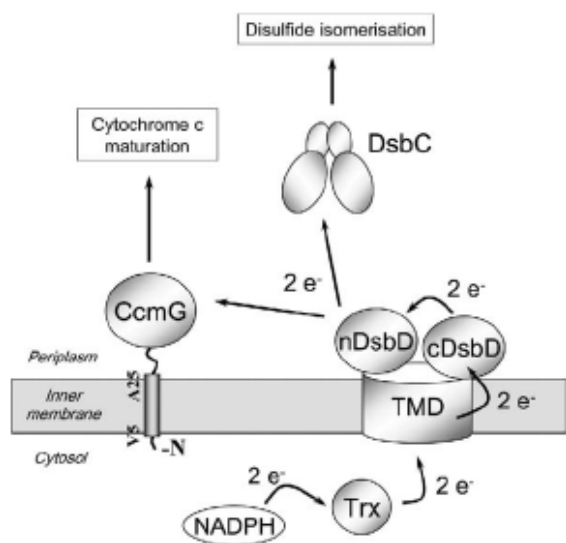
Figure 1. Proposed Electron Flow Cascade from NADPH in the Cytoplasm to DsbC and CcmG in the Periplasm via Thioredoxin and DsbD

Figure 2. Determination of the Redox Potentials of CcmG$_{\Delta19-185}$ and CcmG$_{\Delta43-185}$

A total of 2 μM CcmG$_{\Delta19-185}$ or CcmG$_{\Delta43-185}$ was incubated at 25°C and pH 7.0 in the presence of 50 mM DTT$_{ox}$ and various concentrations of DTT$_{red}$ (1.5–5 mM), and fluorescence at 335 nm was recorded. Data were normalized and fitted (solid line) according to Equation 1 (see Experimental Procedures). The calculated redox potentials of CcmG$_{\Delta19-185}$ and CcmG$_{\Delta43-185}$ are −0.203 V and −0.209 V, respectively.

ported equilibrium constant between glutathione and CcmG$_{\Delta19-185}$ is 215 mM (Li et al., 2001). Our data are in good agreement with the corresponding CcmG$_{\Delta19-185}$ redox potential of −0.220 V, when calculated by using the standard redox potential of glutathione of −0.240 V (Williams, 1992).

Although the reduction of CcmG by nDsbD (E$_o'$ = −0.232 V [Collet et al., 2002; Rozhkova et al., 2004]) would proceed just to ~70%, overall electron transfer from thioredoxin (E$_o'$ = −0.270 V [Krause et al., 1991]) via DsbD to CcmG is thermodynamically driven and guarantees effective reduction of CcmG.

The rate constants of the disulfide exchange between nDsbD and both CcmG constructs were determined by stopped flow fluorescence. Figures 3A and 3B show that reduction of CcmG$_{\Delta19-185}$ and CcmG$_{\Delta43-185}$ by nDsbD is very fast (3.0 × 10^5 M^{-1}s^{-1} and 3.9 × 10^5 M^{-1}s^{-1}, respectively) and in the range of the known functional reactions between Dsb proteins in the periplasm with rate constants of ~10^6 M^{-1}s^{-1} (Grauschopf et al., 2003; Rozhkova et al., 2004). The very similar rate constants indicate that residues A19–G42 of CcmG are not required for rapid electron transfer from nDsbD to CcmG. In addition, we showed that, as expected, no reaction between cDsbD and CcmG occurs (Figure 3C). Our kinetic data and the observation that DsbD and CcmG form a mixed disulfide in vivo (Katzen and Beckwith, 2000) support the existing model (Figure 1), according to which DsbD transfers electrons directly to CcmG (Fabianek et al., 1999; Reid et al., 2001) and not via CcmH, as proposed in an alternative model (Reid et al., 2001).

We also measured the kinetics of the direct oxidation of CcmG by DsbA. This reaction is kinetically restricted and extremely slow (0.31 M^{-1}s^{-1}), guaranteeing the resistance of the first reductive reaction step in the cytochrome c maturation pathway against oxidation in the

periplasm (Figure 4). This, together with the observation that CcmG is more stable in the reduced state (Li et al., 2001), suggests that CcmG, when overexpressed in the periplasm, will accumulate at least partially in the reduced form, even in the absence of DsbD. This explains why mature cytochrome c could be detected in vivo when Ccm proteins were overexpressed in dsbD null mutants (Stevens et al., 2004).

Structure of the Mixed-Disulfide Complex

The structure of the mixed-disulfide complex of E. coli nDsbD and CcmG$_{\Delta43-185}$ (nDsbD-SS-CcmG, Figure S1; see the Supplemental Data available with this article online) was determined at 1.94 Å resolution. The final model of nDsbD-SS-CcmG (Figure 5A) encompasses residues R8–N125 of nDsbD and R49–A184 of E. coli CcmG (EC-CcmG) and exhibits very good geometry and stereochemistry (Table 1). Its Ramachandran plot contains two outliers (nDsbD Q26 and D79), both located in a β turn with well-defined electron density. D79 assumes the same conformation in all previously reported nDsbD structures (1L6P, 1JPE, 1JZD, 1SE1); Q26 is an outlier also in 1L6P and 1JPE. The side chain of residue R8 is rather disordered and was modeled in two alternative conformations.

In the nDsbD-SS-CcmG model, nDsbD has an average B-factor of 31.7 Å^2, much lower than that of EC-CcmG (51.0 Å^2). This is probably due to the more limited participation of EC-CcmG in crystal contacts compared to nDsbD.

As already described, nDsbD possesses an immunoglobulin-like fold (Goulding et al., 2002). EC-CcmG possesses the same thioredoxin-like secondary structure motif found in B. japonicum CcmG (BJ-CcmG): β$_1$α$_A$β$_2$α$_B$β$_3$α$_C$β$_4$β$_5$α$_D$, preceded by an N-terminal extension that is seven residues shorter than in BJ-CcmG.

Figure 3. Kinetics of the Disulfide Exchange at pH 7.0 and 25°C between the Periplasmic Domains of DsbD and CcmG

(A and B) All reactions were performed in a stopped-flow fluorescence instrument under pseudo-first-order conditions, with initial protein concentrations of 10 μM for nDsbD$_{red}$ or cDsbD$_{red}$ and of 1 μM for CcmG$_{Δ10-185}$ $_{ox}$ or CcmG$_{Δ43-185}$ $_{ox}$. The fit (solid line) yields rate constants of 3.0 × 105 M$^{-1}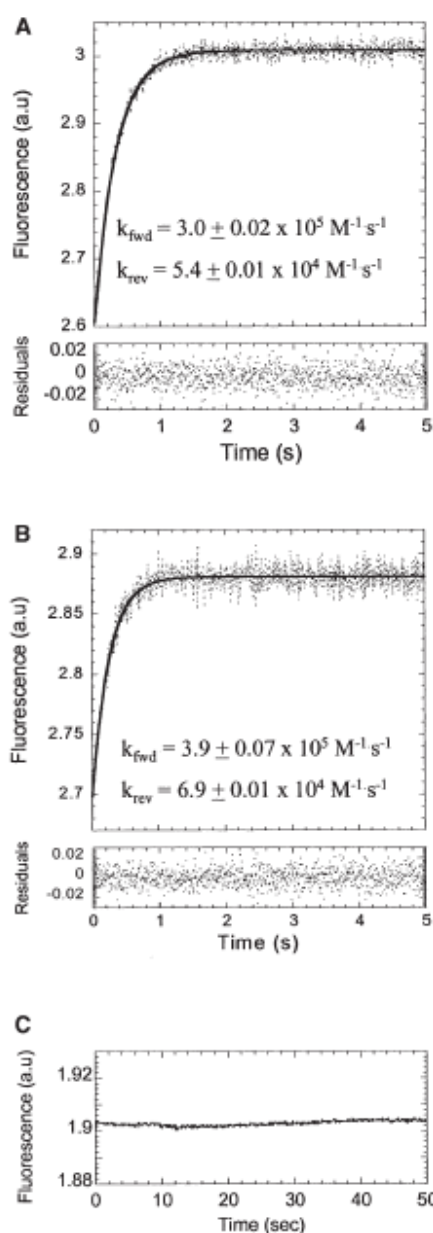$s^{-1} and 3.9 × 105 M^{-1}s^{-1} for the reduction of (A) CcmG$_{Δ10-185}$ and (B) CcmG$_{Δ43-185}$, respectively. Rate constants for the reverse reaction were calculated from the equilibrium constant (K_{eq} = 6.0) for the reduction of CcmG by nDsbD.

(C) No reduction of CcmG$_{Δ43-185}$ by cDsbD is observed during 50 s after stopped-flow mixing.

This N-terminal extension shows a more similar overall conformation to that of CcmG from *Mycobacterium tuberculosis* (*MT*-CcmG) than to that of *BJ*-CcmG. Other differences reside in loop regions: the loop between
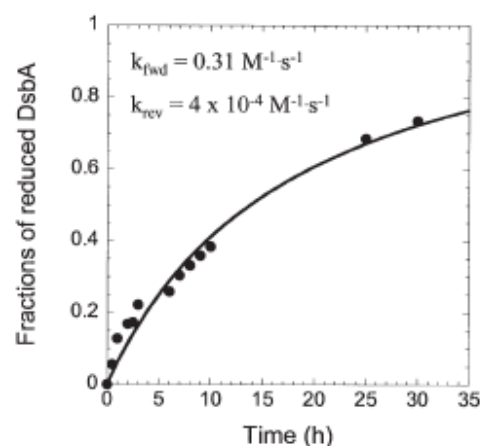
Figure 4. Oxidation of CcmG$_{Δ43-185}$ by DsbA at pH 7.0 and 25°C Is Very Slow

Measurements were performed under second-order conditions with initial protein concentrations of 50 μM. The fit (solid line) yields a rate constant of 0.31 M^{-1}s^{-1}. The rate constant for the reverse reaction was calculated from the equilibrium constant (K_{eq} = 750) for the reduction of DsbA by CcmG$_{Δ43-185}$.

EC-CcmG α helix A and β strand 2 is one residue longer than in *BJ*-CcmG; the loop between β strands 4 and 5 in *EC*-CcmG (β strands 6 and 7 in *MT*-CcmG) takes up a different conformation in *MT*-CcmG. The loop between β strand 5 and α helix D in *EC*-CcmG (β strand 7 and α helix 6 in *MT*-CcmG) is two residues shorter than in *MT*-CcmG. Notably, in a hypothetical complex of *MT*-CcmG with *E. coli* nDsbD, this loop would cause steric clashes. This is presumably not the case in the complex of *MT*-CcmG with the proposed homolog of DsbD from *M. tuberculosis* (called *MT*-DsbD or DipZ, SwissProt: Q10801) (Juarez et al., 2001). The structure of *MT*-DsbD or its individual domains has not been determined yet (only a crystallization report of the C-terminal domain has been published [Goldstone et al., 2005]).

The *EC*-CcmG structure is very similar to that of *BJ*-CcmG ([Edeling et al., 2002], rmsd Cα atoms 1.4 Å) and, to a lesser extent (rmsd 2.1 Å), to CcmG from the Gram-positive bacterium *M. tuberculosis* (Goulding et al., 2004) (Figure 5C). A DALI search (Holm and Sander, 1993) against the Protein Data Bank (www.pdb.org) identified two other periplasmic proteins from the thio-redoxin superfamily that are structurally highly related to *EC*-CcmG: *Bacillus subtilis* ResA (rmsd 2.1 Å) (Crow et al., 2004), also involved in cytochrome *c* maturation, and *B. japonicum* TlpA (rmsd 2.4 Å) (Capitani et al., 2001), which is required for the stability and assembly of cytochrome *aa3*, a heme-copper terminal oxidase of the respiratory chain.

The crystal structure of *BJ*-CcmG revealed a characteristic groove near the active site that has been proposed to interact either with DsbD and/or CcmH (Edeling et al., 2004; Edeling et al., 2002). This groove is mainly formed by the already mentioned seven additional residues in the N-terminal extension of *BJ*-CcmG. *EC*-CcmG does not possess this characteristic groove. Superposition of *EC*-CcmG onto *BJ*-CcmG and analy-
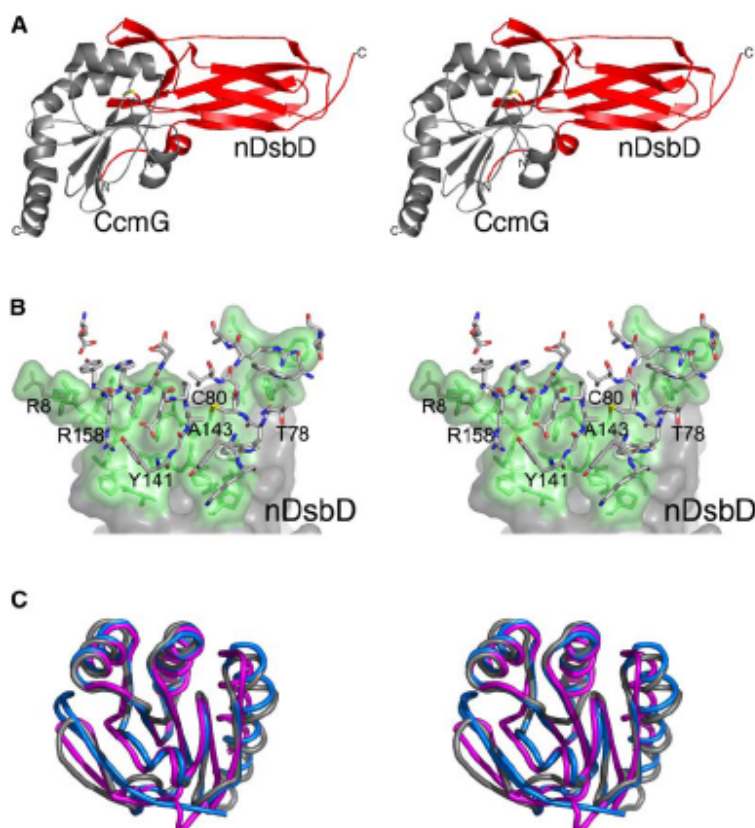
Figure 5. Structural Overview and Details of nDsbD-SS-CcmG

(A) Ribbon diagram of the mixed-disulfide complex nDsbD-SS-CcmG. nDsbD is shown in red, *EC*-CcmG in gray, and the disulfide linkage in yellow.

(B) Close-up view of the nDsbD-SS-CcmG interface. nDsbD residues involved in the dimer interface are mapped in green onto the nDsbD surface. Interacting residues of *EC*-CcmG are shown in light gray and atom colors. Hydrogen bonds appear as yellow, dotted lines. R8 exhibits a double conformation.

(C) Superposition of the Cα atoms of *BJ*-CcmG (marine) and *MT*-CcmG (violet) onto *EC*-CcmG (gray), in tube representation.

sis of the residues of *EC*-CcmG interacting with nDsbD show that the binding interface is not located near the groove region of *BJ*-CcmG.

nDsbD exhibits essentially the same binding orientation in the complexes with CcmG and with cDsbD. Also, the cap-loop region (D68–G72) of nDsbD (Goulding et al., 2002) assumes a similar conformation in the two complexes. On the other hand, based on the electron density and B factors, the cap-loop region is more flexible in nDsbD-SS-CcmG, with the side chain of F70 being not at all defined.

In addition to the active site disulfide bridge, the binding interface of nDsbD-SS-CcmG involves five intermolecular hydrogen bonds (Figure 5B, Table S1). nDsbD F11 undergoes a conformational change upon complex formation (Haebel et al., 2002). It is involved in hydrophobic interactions in all three structurally known complexes of nDsbD, but only in nDsbD-SS-CcmG does the main chain carbonyl of F11 form a hydrogen bond (Table S1) with CcmG Y141, a highly conserved residue (Figure S2). Also, nDsbD S9 hydrogen bonds CcmG Y141 and assumes a conformation that, among all known nDsbD structures, is similar only to that in complex B of nDsbD-SS-cDsbD, in which S9 is involved in a crystal contact. This additional feature suggests that nDsbD S9 and F11 contribute to the specific recognition of *EC*-CcmG. Alanine mutation studies (Edeling et al., 2004) showed that the acidic residues E86, E145, and D162 of *EC*-CcmG are required for efficient cytochrome *c* maturation. Our data demonstrate

that both E145 and D162, but not E86, contribute to the nDsbD-SS-CcmG binding interface. Part of the side chain of CcmG E145 (especially the Cγ methylene) forms a hydrophobic cluster with nDsbD F108, CcmG Y141, and CcmG A160 (Figure 6). The side chain carbonyl of *EC*-CcmG D162 interacts with the main chain carbonyl of nDsbD G107 through a bridging water molecule. *EC*-CcmG E86 contributes to the surface with its main chain, while its side chain is buried. Its carboxyl group is involved in a network of hydrogen bonds (*EC*-CcmG N74, *EC*-CcmG L163, and three bridging waters) stabilizing a region behind the interface with nDsbD. Similar long-range effects were already observed in other protein-protein interactions (de Vos et al., 1992). Overall, the decreased level of mature cytochrome *c* in CcmG$_{E86A/E145A}$ and CcmG$_{E86A/E145A/D162A}$ mutants can be explained by an impaired interaction of CcmG with nDsbD.

Helix α$_B$ of CcmG, which is present in all CcmG homologs and in TlpA but not in thioredoxin, is essential for cytochrome *c* maturation (Edeling et al., 2002). This helix would be a candidate for specific substrate recognition by CcmG, but it hardly interacts with nDsbD in the nDsbD-SS-CcmG complex; it only makes two long-range contacts with flexible side chains (F70 and Y71) of the nDsbD cap-loop region, amounting to less than 1.0% of the interface area.

The binding interface area of the nDsbD-SS-CcmG complex (1432 Å^2 and 1322 Å^2, respectively, depending on which conformation of R8 is chosen) is similar to

Table 1. Crystallographic Data and Refinement Statistics

Data Collection

Radiation source	SLS Villigen, CH beamline X06SA
Wavelength (Å)	0.9004
Space group	$P2_1$
Unit cell	a = 53.57 Å, b = 53.17 Å,
	c = 63.83 Å, β = 104.88°
Asymmetric unit content	1 nDsbD-SS-CcmG complex
Resolution range (Å)	50–1.94
Number of reflections	98,887
Number of unique reflections	26,430
Completeness (%)	99.9 (99.9)
R_{sym}	6.8 (33.2)[a]
Average I/σ	19.0 (4.0)[a]
Redundancy	3.7

Refinement Statistics

Resolution (Å)	40–1.94
Number of reflections (test)	25,833 (1902)
Number of atoms	
nDsbD	1020
CcmG	1129
Water molecules	253
Chloride ions[b]	3
Ethylene glycol[c]	16
R-factor	0.235 (0.306)[d]
R_{free}	0.270 (0.332)[d]
Rmsd bonds (Å)	0.008
Rmsd angles (°)	1.4
Average B factor ($Å^2$)	43.3
Ramachandran plot regions (%)	
Most favored	90.3
Additionally allowed	8.8
Generously allowed	0.0
Disallowed region	0.9

[a] Last shell: 2.01–1.94 Å.
[b] Contained in crystallization conditions.
[c] Contained in cryo buffer.
[d] Last shell: 2.01–1.94 Å.

that in nDsbD-SS-cDsbD (1301 $Å^2$) and in nDsbD-SS-DsbC (1376 $Å^2$, primary interface only) (Rozhkova et al., 2004). nDsbD-SS-CcmG has a surface complementarity index of 0.82 (Table 2), which is higher than those of nDsbD-SS-cDsbD and nDsbD-SS-DsbC (Rozhkova et al., 2004). Figure 7 shows surface (top) and full-atom representations (bottom) of nDsbD in the complexes with EC-CcmG ([A] and [B]), DsbC ([C] and [D]), and cDsbD ([E] and [F]). Notably, the majority of the nDsbD residues involved in the binding with thioredoxin-like partner interfaces are common (depicted in green in Figure 7). Only a few residues form contacts that are specific to one nDsbD-substrate complex (depicted in

blue). As already mentioned, two flexible regions of nDsbD are involved in the recognition of thioredoxin-like substrates: the cap-loop region and the N-terminal segment. The latter one especially exhibits a great adaptability, as can be seen from the position of R8 and S9 in nDsbD-SS-CcmG (Figures 7A and 7B) and in nDsbD-SS-DsbC (Figures 7C and 7D): the violet area indicating R8 is found in two very different positions in the two cases, and, for nDsbD-SS-DsbC, this residue is partly disordered (Haebel et al. [2002] only modeled it to Cβ). In fact, in nDsbD-SS-cDsbD, the N-terminal segment (S9 and F11) participates only to a modest amount and without hydrogen bonding to the binding interface (for this comparison, one has to use complex C of nDsbD-SS-cDsbD, which, in contrast to the other two in the asymmetric unit, is not influenced by crystal contacts in the N-terminal region [Rozhkova et al., 2004]). In nDsbD-SS-DsbC, the N-terminal segment also has a very modest interaction with the binding partner DsbC; S9 and F11 participate marginally to the interface. As mentioned above, in this case R8 is partly disordered and also has very high B factors.

While nDsbD is connected by a 20 residue long linker to the transmembrane domain of DsbD, EC-CcmG is connected by a linker of similar size (23 residues if one considers $CcmG_{\Delta43-185}$, for which the first well-defined residue is R49) to a single transmembrane helix (Figure 1). We previously proposed (Rozhkova et al., 2004) a likely orientation of nDsbD-SS-cDsbD relative to the membrane and pointed out that a large rotational motion of the nDsbD domain must occur for the interaction with DsbC. The nDsbD-SS-CcmG structure allows us to expand this model. The N termini of EC-CcmG, BJ-CcmG, B. subtilis ResA, and B. japonicum TlpA all point in the same direction, most likely toward the membrane: in fact, in the nDsbD-SS-CcmG complex, the N-terminal segment of the folded thioredoxin domain of CcmG is located close to a large relatively planar region, likely parallel to the membrane (Figure S3). According to this model, nDsbD must undergo a large displacement from its position in nDsbD-SS-cDsbD in order to access the active site disulfide of EC-CcmG (Figure 8). This mobility of nDsbD is essential for disulfide exchange between nDsbD and its substrates.

We demonstrate an intriguing ability of the N-terminal domain of DsbD to interact specifically and very rapidly with different target proteins such as the periplasmic dimer DsbC and the membrane-anchored monomer CcmG. The structural basis for this feature is at least 2-fold: first, nDsbD possesses two different interaction surfaces, one of which is only used for the reaction with
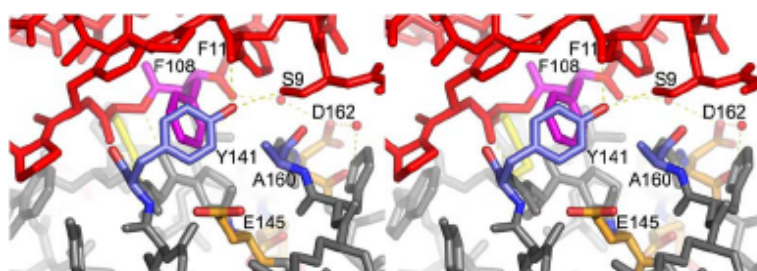

Figure 6. Detail of the Complex Interface around Y141 of CcmG

CcmG Y141 and A160 appear in cobalt and atom colors, the two acidic residues E145 and D162 in yellow and atom colors, and other residues in gray. F108 of nDsbD is depicted in violet; other nDsbD residues are depicted in red.

Table 2. Analysis of the Dimer Interface

	nDsbD-SS-DsbC		nDsbD-SS-cDsbD[a]	nDsbD-SS-CcmG
	First Interface	Second Interface		
Interface area (Å²)	1376[a]	669[a]	1296–1337[d]	1432/1322[e]
Planarity (Å)[b]	2.34[a]	1.29[a]	1.77–1.90[d]	2.44/2.13[e]
Index of surface complementarity[c]	0.76[a]	0.68	0.62–0.71[d]	0.82/0.82[e]
Hydrogen bonds	7[a]	3[a]	4–6[a,d]	5

[a] Rozhkova et al., 2004.
[b] Jones and Thornton, 1996.
[c] Lawrence and Colman, 1993.
[d] Depending on the respective complex in a.u.
[e] Depending on the respective conformation of nDsbD R8.

a dimeric partner, DsbC. In the nDsbD-SS-CcmG complex, the N-terminal segment of nDsbD also contributes to the recognition of CcmG (Figure 6, Figure S4). In addition, the main interaction surface around the active site disulfide of nDsbD, which is used in all three structures of nDsbD complexes (Figure S4), combines a comparatively small area with excellent adaptability to various thioredoxin-like partner interfaces (Figure 7). These unusual properties of nDsbD enable the inner membrane redox catalyst DsbD to provide two different systems, the disulfide bond isomerization and cytochrome c maturation pathways, with reducing equivalents.

Experimental Procedures

Construction of Expression Plasmids

For cytosolic expression of CcmG$_{\Delta 19-185}$ (residues 19–185) and CcmG$_{\Delta 43-185}$ (residues 43–185) with C-terminal (His)$_6$ tag, two plasmids were constructed: pCcmG$_{\Delta 19-185}$ and pCcmG$_{\Delta 43-185}$, respectively. The corresponding 519 bp or 447 bp gene fragment was amplified by PCR from the plasmid pEC86 (Arslan et al., 1998) encoding the *E. coli ccm* gene region with primers E1a (5′-CCCAAT

CCATATGGCGCTGCTGTGGCAGC-3′) or E1b (5′-CCCAATCCATAT GAAGCCTGTGCCGAAGTTTCG-3′) and E2 (5′-CGCGGATCCTTA ATGGTGATGGTGATGGTGTTGTGCGGCCTCCTTACT-3′) and was cloned into pET11a via NdeI and BamHI (Novagen).

The Cys variants of CcmG$_{\Delta 19-185}$ and CcmG$_{\Delta 43-185}$, in which the second active site cysteine was replaced by serine, were constructed from pCcmG$_{\Delta 19-185}$ and pCcmG$_{\Delta 43-185}$ by using Quik-Change (Stratagene). All constructs were verified by DNA sequencing.

Purification of CcmG$_{\Delta 19-185}$, CcmG$_{\Delta 43-185}$, nDsbD, cDsbD and DsbA (His)$_6$-tagged CcmG$_{\Delta 19-185}$ and CcmG$_{\Delta 43-185}$ were expressed in *E. coli* BL21Tuner (DE3) cells (Novagen) grown in Luria-Bertani (LB) medium containing ampicillin (100 μg/ml) at 37°C. Protein production was induced with IPTG to a final concentration of 100 μM when cells reached an O.D. of 0.7–0.8 at 600 nm. After further growth at 37°C for 3 hr, bacteria were harvested by centrifugation. Cells were suspended in ice-cold PBS buffer (20 mM sodium phosphate [pH 7.5], 150 mM NaCl) and disrupted with a Cell Cracker (Avestin). After centrifugation at 45,000 × g for 30 min at 4°C, the supernatant was mixed with imidazole-HCl (pH 7.5) to a concentration of 10 mM and was applied to a Ni-NTA SuperFlow column (Qiagen) equilibrated with PBS containing 10 mM imidazole-HCl (pH 7.5). Proteins were eluted with a gradient of imidazole-HCl from 10 mM to 200 mM. Fractions containing CcmG were pooled, mixed
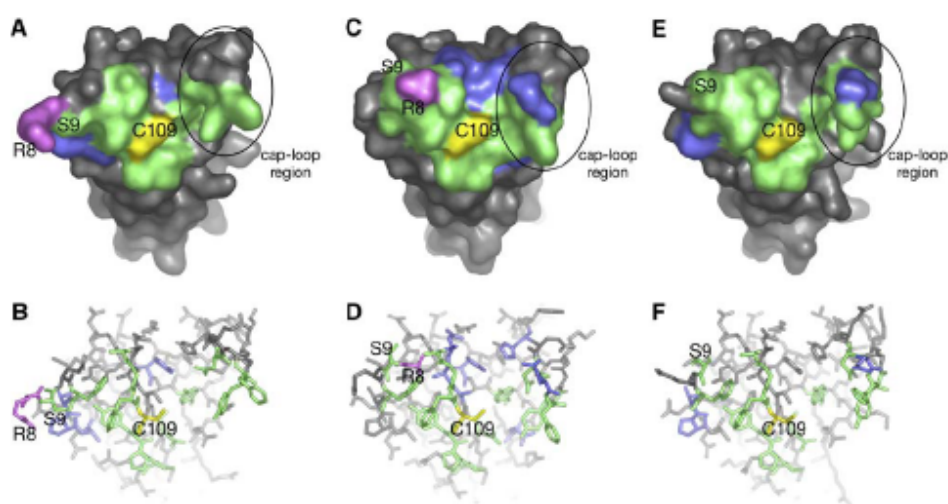
Figure 7. Dimer Interface Comparison in the Three Known Complexes of nDsbD

(A–F) Surface (top) and ball-and-stick representations (bottom) of nDsbD in ([A] and [B], respectively) nDsbD-SS-CcmG, ([C] and [D], respectively) nDsbD-SS-DsbC (1JZD), and ([E] and [F], respectively) nDsbD-SS-cDsbD (1SE1 chain C). nDsbD residues involved in the interaction with the partner in all three complexes are depicted in green; residues involved in interactions specific to one complex are depicted in blue. R8 is shown in violet (in nDsbD-SS-CcmG, only one conformation is chosen; R8 in 1JZD is only partially defined, up to Cβ; R8 is not defined at all in 1SE1 chain C).

Crystal Structure of nDsbD-SS-CcmG
991

Figure 8. A Model for Domain Movement in Reductive Electron Transfer Mediated by DsbD

Left: proposed relative orientation of nDsbD-SS-CcmG to the membrane. Right: relative orientation of the nDsbD-SS-cDsbD model to the transmembrane domain full-length DsbD. EC-CcmG C80, nDsbD C109, and cDsbD C461 are depicted as yellow spheres; TMD C163 and C285 are indicated by yellow circles. Residues predicted to form flexible linkers are depicted as black lines.

with oxidized DTT (final concentration 50 mM), and incubated at room temperature for 30 min. After concentration, the protein pool was applied to a gel filtration column Superdex 75 16/60, equilibrated with 50 mM sodium phosphate, 300 mM NaCl (pH 7.0). Fractions containing pure CcmG were dialyzed against distilled water. Both CcmG constructs were fully oxidized after purification, as confirmed by Ellman's assay (Ellman, 1959) under denaturing conditions. The final yields of purified $CcmG_{\Delta 10-185}$ and $CcmG_{\Delta 43-185}$ were 100 and 120 mg/L bacterial culture, respectively.

The (His)$_6$-tagged variant C83S of $CcmG_{\Delta 43-185}$ was expressed and purified according to the same protocol with comparable yields. nDsbD wild-type and its C103S variant, (His)$_6$-tagged cDsbD, and DsbA were expressed and purified as described (Rozhkova et al., 2004; Wunderlich and Glockshuber, 1993).

Synthesis of the nDsbD-SS-CcmG Complex

First, we prepared the mixed disulfide between nDsbD variant C103S and nitrothiobenzoic acid as described (Rozhkova et al., 2004). The purified, NTB-modified nDsbD variant C103S and the (His)$_6$-tagged variant C83S of $CcmG_{\Delta 43-185}$ were dialyzed separately against PBS (pH 7.5), were then mixed at equimolar concentrations (50 μM each), incubated at 25°C for 30 min, and applied to a Ni-NTA SuperFlow column (Qiagen), equilibrated with PBS (pH 7.5). Proteins were eluted with a gradient of imidazole-HCl from 0 to 150 mM. Fractions containing the mixed-disulfide complex were pooled, conc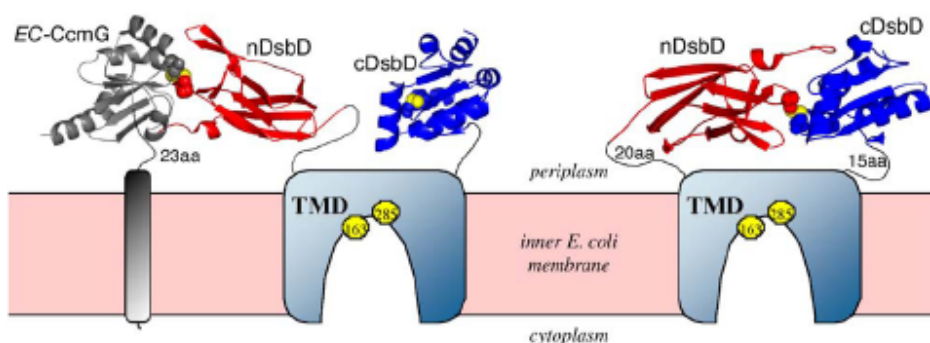entrated, and applied to a gel filtration column Superdex 75 16/60, equilibrated with 50 mM sodium phosphate, 300 mM NaCl (pH 7.0). Fractions containing pure nDsbD-SS-CcmG complex (Figure S1) were dialyzed against 20 mM HEPES-NaOH, 50 mM NaCl (pH 7.0) and were concentrated.

Protein Concentrations

Protein concentrations of $CcmG_{\Delta 10-185}$ and $CcmG_{\Delta 43-185}$ were determined by using the extinction coefficients at 280 nm of 43,100 $M^{-1}s^{-1}$ and 37,530 $M^{-1}s^{-1}$, respectively. For nDsbD, cDsbD, and DsbC, the same extinction coefficients at 280 nm as in previous work were used (Rozhkova et al., 2004).

Redox Potential Determination

For determination of equilibrium constants (K_{eq}) between $CcmG_{\Delta 10-185}$ or $CcmG_{\Delta 43-185}$ and DTT, the redox state of the proteins at different DTT_{red}/DTT_{ox} ratios was determined by the change in the fluorescence at 335 nm. Proteins (2 μM) were incubated for 15 hr at 25°C in 100 mM sodium phosphate, 0.1 mM EDTA (pH 7.0) containing 50 mM DTT_{ox} and different amounts of DTT_{red} (1.5–5 mM). To exclude air oxidation, all buffers were degassed and flushed with argon. Data were fitted according to:

$$R = ([DTT_{red}]/[DTT_{ox}])/(K_{eq} + [DTT_{red}]/[DTT_{ox}]),\qquad(1)$$

where R is the fraction of reduced CcmG at equilibrium. Standard redox potentials (E_0') were calculated by the Nernst equation:

$$E_{0\ protein}' = E_{0\ reference}' - [RT/2F]\ln K_{eq},\qquad(2)$$

by using a value of –0.307 V for the redox potential of DTT_{red}/DTT_{ox} (Rothwarf and Scheraga, 1992).

Stopped-Flow Experiments

The kinetics of the reduction of $CcmG_{\Delta 10-185}$ and $CcmG_{\Delta 43-185}$ by nDsbD in 100 mM sodium phosphate, 0.1 mM EDTA (pH 7.0) were monitored at 25°C by the change in fluorescence at 335 nm by using stopped-flow mixing in an Applied Photophysics SX-17MV instrument (1:1 volume mixing ratio). Measurements were performed under pseudo-first-order conditions with initial protein concentrations of 1 μM for the oxidized CcmG constructs and 10 μM for reduced nDsbD. Reduced nDsbD was prepared by reduction with a 1000-fold molar excess of DTT at pH 8.0, followed by removal of DTT by gel filtration in degassed buffer. Data from ten independent measurements were averaged and evaluated according to pseudo-first-order kinetics.

HPLC Analysis of Disulfide Exchange between DsbA and CcmG

To determine the second-order rate constants of the reduction of DsbA by $CcmG_{\Delta 10-185}$ or $CcmG_{\Delta 43-185}$, proteins were mixed at equimolar concentrations (50 μM of each) and incubated at 25°C in 100 mM sodium phosphate, 0.1 mM EDTA (pH 7.0). Samples were removed at different incubation times, and the reaction was stopped by the addition of formic acid to a final concentration of 10% (v/v). Reaction products were separated on an Agilent Zorbax 300 SB C$_{18}$ reverse-phase column (5 mM, 2.1 × 150 mm) at 55°C with a linear gradient from 39% to 44% (v/v) of acetonitrile in 0.1% TFA and were detected by their absorbance at 220 nm and 280 nm. The amounts of the reduced and oxidized forms of DsbA were quantified by integration of the peak areas. The data were evaluated according to second-order kinetics.

Crystallization

Purified, disulfide-linked nDsbD-SS-CcmG complex in 20 mM HEPES-NaOH [pH 7.0] and 50 mM NaCl was concentrated to 70 mg/ml. Crystals were produced by using the sitting drop vapor diffusion method. Protein solution (2.25 μl) was mixed with 1.5 μl precipitant solution (0.1 M sodium acetate [pH 4.5], 0.2 M MgCl$_2$, 15% PEG 4000). nDsbD-SS-CcmG crystals grew within 3 days at 4°C.

Data Collection and Structure Solution

Crystals were cryoprotected by adding 22.5% ethylene glycol to the mother liquid and were directly frozen in a nitrogen gas stream. Using a MAR CCD 165 image plate, diffraction data were measured on beamline X06SA at the Swiss Light Source (Paul Scherrer Institut Villigen, Switzerland) at a wavelength of 0.9004 Å with an aluminum filter (I = 0.79 I$_0$). Data were processed with DENZO and SCA-LEPACK (Otwinowski and Minor, 1997) to a resolution of

1.94 Å. nDsbD-SS-CcmG crystals belong to the monoclinic space group P2$_1$, with a = 53.57 Å, b = 53.17 Å, c = 63.83 Å, β = 104.88°, and contain one complex per asymmetric unit.

The structure was solved by molecular replacement with Phaser-1.2 (Storoni et al., 2004). Model rebuilding was carried out with the program O (Jones and Kjeldgaard, 1991), and the model was finally refined with CNS to an R-factor of 0.235 and an R$_{free}$ of 0.271. The geometry and stereochemistry of the nDsbD-SS-CcmG structure were checked with WHAT_CHECK (Hooft et al., 1996) and PRO-CHECK (Laskowski et al., 1993). The interface area of the nDsbD-SS-CcmG complex was calculated with the program GRASP (Nicholls et al., 1993) by following the method published by Janin (1997). The surface complementarity of the interfaces of nDsbD-SS-CcmG was calculated by using the CCP4 program SC (Lawrence and Colman, 1993). All structural figures were prepared with PyMOLv0.97 (http://www.pymol.org).

Supplemental Data

Supplemental Data including a hydrogen bonding table and three additional figures are available at http://www.structure.org/cgi/content/full/13/7/985/DC1/.

References

Andersen, C.L., Matthey-Dupraz, A., Missiakas, D., and Raina, S. (1997). A new *Escherichia coli* gene, dsbG, encodes a periplasmic protein involved in disulfide bond formation, required for recycling DsbA/DsbB and DsbC redox proteins. Mol. Microbiol. *26*, 121–132.

Arslan, E., Schulz, H., Zufferey, R., Kunzler, P., and Thony-Meyer, L. (1998). Overproduction of the *Bradyrhizobium japonicum* c-type cytochrome subunits of the cbb3 oxidase in *Escherichia coli*. Biochem. Biophys. Res. Commun. *251*, 744–747.

Bessette, P.H., Cotto, J.J., Gilbert, H.F., and Georgiou, G. (1999). In vivo and in vitro function of the *Escherichia coli* periplasmic cysteine oxidoreductase DsbG. J. Biol. Chem. *274*, 7784–7792.

Capitani, G., Rossmann, R., Sargent, D.F., Grutter, M.G., Richmond, T.J., and Hennecke, H. (2001). Structure of the soluble domain of a membrane-anchored thioredoxin-like protein from *Bradyrhizobium japonicum* reveals unusual properties. J. Mol. Biol. *311*, 1037–1048.

Collet, J.F., Riemer, J., Bader, M.W., and Bardwell, J.C. (2002). Reconstitution of a disulfide isomerization system. J. Biol. Chem. *277*, 26886–26892.

Crow, A., Acheson, R.M., Le Brun, N.E., and Oubrie, A. (2004). Structural basis of redox-coupled protein substrate selection by the cytochrome c biosynthesis protein ResA. J. Biol. Chem. *279*, 23654–23660.

de Vos, A.M., Ultsch, M., and Kossiakoff, A.A. (1992). Human growth hormone and extracellular domain of its receptor: crystal structure of the complex. Science *255*, 306–312.

Edeling, M.A., Guddat, L.W., Fabianek, R.A., Thony-Meyer, L., and Martin, J.L. (2002). Structure of CcmG/DsbE at 1.14 Å resolution: high-fidelity reducing activity in an indiscriminately oxidizing environment. Structure *10*, 973–979.

Edeling, M.A., Ahuja, U., Heras, B., Thony-Meyer, L., and Martin, J.L. (2004). The acidic nature of the CcmG redox-active center is important for cytochrome c maturation in *Escherichia coli*. J. Bacteriol. *186*, 4030–4033.

Ellman, G.L. (1959). Tissue sulfhydryl groups. Arch. Biochem. Biophys. *82*, 70–77.

Fabianek, R.A., Hennecke, H., and Thony-Meyer, L. (1998). The active-site cysteines of the periplasmic thioredoxin-like protein CcmG of *Escherichia coli* are important but not essential for cytochrome c maturation in vivo. J. Bacteriol. *180*, 1947–1950.

Fabianek, R.A., Hofer, T., and Thony-Meyer, L. (1999). Characterization of the *Escherichia coli* CcmH protein reveals new insights into the redox pathway required for cytochrome c maturation. Arch. Microbiol. *171*, 92–100.

Goldstone, D., Haebel, P.W., Katzen, F., Bader, M.W., Bardwell, J.C., Beckwith, J., and Metcalf, P. (2001). DsbC activation by the N-terminal domain of DsbD. Proc. Natl. Acad. Sci. USA *98*, 9551–9556.

Goldstone, D., Baker, E.N., and Metcalf, P. (2005). Crystallization and preliminary diffraction studies of the C-terminal domain of the DipZ homologue from *Mycobacterium tuberculosis*. Acta Crystallogr. F *61*, 243–245.

Gordon, E.H., Page, M.D., Willis, A.C., and Ferguson, S.J. (2000). *Escherichia coli* DipZ: anatomy of a transmembrane protein disulphide reductase in which three pairs of cysteine residues, one in each of three domains, contribute differentially to function. Mol. Microbiol. *35*, 1360–1374.

Goulding, C.W., Sawaya, M.R., Parseghian, A., Lim, V., Eisenberg, D., and Missiakas, D. (2002). Thiol-disulfide exchange in an immunoglobulin-like fold: structure of the N-terminal domain of DsbD. Biochemistry *41*, 6920–6927.

Goulding, C.W., Apostol, M.I., Gleiter, S., Parseghian, A., Bardwell, J., Gennaro, M., and Eisenberg, D. (2004). Gram-positive DsbE proteins function differently from Gram-negative DsbE homologs. A structure to function analysis of DsbE from *Mycobacterium tuberculosis*. J. Biol. Chem. *279*, 3516–3524.

Grauschopf, U., Fritz, A., and Glockshuber, R. (2003). Mechanism of the electron transfer catalyst DsbB from *Escherichia coli*. EMBO J. *22*, 3503–3513.

Haebel, P.W., Goldstone, D., Katzen, F., Beckwith, J., and Metcalf, P. (2002). The disulfide bond isomerase DsbC is activated by an immunoglobulin-fold thiol oxidoreductase: crystal structure of the DsbC-DsbDalpha complex. EMBO J. *21*, 4774–4784.

Holm, L., and Sander, C. (1993). Structural alignment of globins, phycocyanins and colicin A. FEBS Lett. *315*, 301–306.

Hooft, R.W., Vriend, G., Sander, C., and Abola, E.E. (1996). Errors in protein structures. Nature *381*, 272.

Janin, J. (1997). Specific versus non-specific contacts in protein crystals. Nat. Struct. Biol. *4*, 973–974.

Jones, S., and Thornton, J.M. (1996). Principles of protein-protein interactions. Proc. Natl. Acad. Sci. USA *93*, 13–20.

Jones, T.A., and Kjeldgaard, M. (1991). Manual for O (Uppsala, Sweden: Uppsala University).

Juarez, M.D., Torres, A., and Espitia, C. (2001). Characterization of the *Mycobacterium tuberculosis* region containing the mpt83 and mpt70 genes. FEMS Microbiol. Lett. *203*, 95–102.

Kadokura, H., Katzen, F., and Beckwith, J. (2003). Protein disulfide bond formation in prokaryotes. Annu. Rev. Biochem. *72*, 111–135.

Katzen, F., and Beckwith, J. (2000). Transmembrane electron transfer by the membrane protein DsbD occurs via a disulfide bond cascade. Cell *103*, 769–779.

Katzen, F., and Beckwith, J. (2003). Role and location of the unusual redox-active cysteines in the hydrophobic domain of the transmembrane electron transporter DsbD. Proc. Natl. Acad. Sci. USA *100*, 10471–10476.

Kim, J.H., Kim, S.J., Jeong, D.G., Son, J.H., and Ryu, S.E. (2003). Crystal structure of DsbDgamma reveals the mechanism of redox potential shift and substrate specificity(1). FEBS Lett. *543*, 164–169.

Krause, G., Lundstrom, J., Barea, J.L., Pueyo de la Cuesta, C., and Holmgren, A. (1991). Mimicking the active site of protein disulfide-isomerase by substitution of proline 34 in Escherichia coli thioredoxin. J. Biol. Chem. *266*, 9494–9500.

Krupp, R., Chan, C., and Missiakas, D. (2000). DsbD-catalyzed transport of electrons across the membrane of *Escherichia coli*. J. Biol. Chem. *20*, 3696–3701.

Laskowski, R.A., MacArthur, M.W., Moss, D.S., and Thornton, J.M. (1993). PROCHECK: a program to check the stereochemical quality of protein structure. J. Appl. Crystallogr. *26*, 283–291.

Lawrence, M.C., and Colman, P.M. (1993). Shape complementarity at protein/protein interfaces. J. Mol. Biol. *234*, 946–950.

Li, Q., Hu, H.Y., Wang, W.Q., and Xu, G.J. (2001). Structural and redox properties of the leaderless DsbE (CcmG) protein: both active-site cysteines of the reduced form are involved in its function in the *Escherichia coli* periplasm. Biol. Chem. *382*, 1679–1686.

Maskos, K., Huber-Wunderlich, M., and Glockshuber, R. (2003). DsbA and DsbC-catalyzed oxidative folding of proteins with complex disulfide bridge patterns in vitro and in vivo. J. Mol. Biol. *325*, 495–513.

McCarthy, A.A., Haebel, P.W., Torronen, A., Rybin, V., Baker, E.N., and Metcalf, P. (2000). Crystal structure of the protein disulfide bond isomerase, DsbC, from *Escherichia coli*. Nat. Struct. Biol. *7*, 196–199.

Missiakas, D., Georgopoulos, C., and Raina, S. (1994). The *Escherichia coli* dsbC (xprA) gene encodes a periplasmic protein involved in disulfide bond formation. EMBO J. *13*, 2013–2020.

Nicholls, A., Bharadwaj, R., and Honig, B. (1993). GRASP graphical representation and analysis of surface properties. Biophys. J. *64*, A166.

Otwinowski, Z., and Minor, W. (1997). Processing of X-Ray Diffraction Data Collected in Oscillation Mode (San Diego: Academic Press).

Reid, E., Cole, J., and Eaves, D.J. (2001). The *Escherichia coli* CcmG protein fulfils a specific role in cytochrome *c* assembly. Biochem. J. *355*, 51–58.

Rothwarf, D.M., and Scheraga, H.A. (1992). Equilibrium and kinetic constants for the thiol-disulfide interchange reaction between glutathione and dithiothreitol. Proc. Natl. Acad. Sci. USA *89*, 7944–7948.

Rozhkova, A., Stirnimann, C.U., Frei, P., Grauschopf, U., Brunisholz, R., Grutter, M.G., Capitani, G., and Glockshuber, R. (2004). Structural basis and kinetics of inter- and intramolecular disulfide exchange in the redox catalyst DsbD. EMBO J. *23*, 1709–1719.

Stevens, J.M., Gordon, E.H., and Ferguson, S.J. (2004). Overproduction of CcmABCDEFGH restores cytochrome *c* maturation in a DsbD deletion strain of *E. coli*: another route for reductant? FEBS Lett. *576*, 81–85.

Stewart, E.J., Katzen, F., and Beckwith, J. (1999). Six conserved cysteines of the membrane protein DsbD are required for the transfer of electrons from the cytoplasm to the periplasm of *Escherichia coli*. EMBO J. *18*, 5963–5971.

Storoni, L.C., McCoy, A.J., and Read, R.J. (2004). Likelihood-enhanced fast rotation functions. Acta Crystallogr. D Biol. Crystallogr. *60*, 432–438.

Thony-Meyer, L. (1997). Biogenesis of respiratory cytochromes in bacteria. Microbiol. Mol. Biol. Rev. *61*, 337–376.

van Straaten, M., Missiakas, D., Raina, S., and Darby, N.J. (1998). The functional properties of DsbG, a thiol-disulfide oxidoreductase from the periplasm of *Escherichia coli*. FEBS Lett. *428*, 255–258.

Williams, C.H. (1992). Lipoamide dehydrogenase, glutathione reductase, thioredoxin reductase, and mercuric ion reductase—a family of flavoenzyme transhydrogenases. In Chemistry and Biochemistry of Flavoenzymes, F. Müller, ed. (Boca Raton, FL: CRC Press), pp. 121–211.

Wunderlich, M., and Glockshuber, R. (1993). Redox properties of protein disulfide isomerase (DsbA) from *Escherichia coli*. Protein Sci. *2*, 717–726.

Zapun, A., Missiakas, D., Raina, S., and Creighton, T.E. (1995). Structural and functional characterization of DsbC, a protein involved in disulfide bond formation in *Escherichia coli*. Biochemistry *34*, 5075–5089.

Accession Numbers

The coordinates and structure factors of nDsbD-SS-CcmG have been deposited with the Protein Data Bank (http://www.rcsb.org/pdb/) with entry code 1Z5Y.

3.3 High resolution structural studies of oxidized, reduced and photo-reduced Escherichia coli cDsbD (paper in preparation)

Christian U. Stirnimann[†], Anna Rozhkova[†], Ulla Grauschopf, Markus G. Grütter, Rudi Glockshuber, and Guido Capitani

Running title: Structural studies of cDsbD

[†]These authors contributed equally to this work

Introduction

Dsb proteins catalyse oxidative protein folding in the periplasm of *Escherichia coli*. Formation of native disulfide bonds involves two independent pathways: the oxidative DsbA/B pathway and the reductive DsbC/D pathway.[1; 2] The strong dithiol oxidase DsbA very rapid and randomly introduces disulfide bonds into reduced polypeptides.[3; 4; 5] Upon oxidation of substrate proteins DsbA becomes reduced and is re-oxidized by the inner membrane protein DsbB, that transfers electrons from DsbA to ubiquinone.[6; 7; 8; 9] Since DsbA has no "proofreading" activity, rearrangement of wrong disulfide bonds in scrambled polypeptides to the native disulfide pattern is catalyzed by the periplasmic disulfide isomerase DsbC.[10; 11; 12; 13] The inner membrane protein DsbD is required for maintenance of DsbC in its active, reduced state in the highly oxidizing periplasm. DsbD also supplies two other periplasmic proteins with reducing power: DsbG, a homologue of DsbC of unknown function[14; 15; 16], and CcmG, a specialyzed thiol reductase, essential for cytochrome *c* maturation.[17]

DsbD consists of three domains: a N-terminal periplasmic domain (nDsbD) with an immunoglobulin fold,[18; 19] a central transmembrane domain (TMD), composed of eight predicted transmembrane helices,[20] and a C-terminal periplasmic thioredoxin-like domain (cDsbD).[21] Each domain has two conserved cysteine residues, essential for electron transport.[22] It is proposed that intramolecular electron transfer within DsbD proceeds exclusively through sequential disulfide exchange reactions between its three domains.[23; 24; 25; 26] The electron cascade starts with the reduction of TMD by thioredoxin, then cDsbD shuttles electrons from TMD to nDsbD, and finally reduced nDsbD passes electrons to DsbC, DsbG or CcmG.

The 1.9 Å crystal structure of oxidized cDsbD (residues 423–546 of mature *Escherichia coli* DsbD) revealed a thioredoxin fold with an extended N-terminal stretch.[21] We have recently determined the structure of a disulfide-linked complex between cDsbD and nDsbD (2.85 Å resolution), which represents an important reaction intermediate in the catalytic cycle of DsbD.[27]

For better understanding of the redox mechanism of cDsbD, we determined four high-resolution structures of cDsbD: chemically reduced (1.3 Å), pH-shifted chemically reduced (0.99 Å), photo-reduced (1.1 Å), and oxidized (1.65 Å) cDsbD. The structure of reduced cDsbD revealed that the active site Cys461 is protonated at pH 7.0. In order to determine the pKa value of Cys461, we studied the pH-dependent reactivity of Cys461 with the alkylating reagent iodoacetamide and also the pH-dependent thiolate-specific absorbance at 240 nm.

These experiments showed that cDsbD active site Cys461 has an unexpectedly high p*Ka* value of 9.3 for a thioredoxin-like protein with a redox potential of –235 mV.[27; 28; 29]

RESULTS AND DISCUSSION

Thermodynamic stabilities of the redox forms of cDsbD

Guanidinium chloride (GdmCl) induced unfolding and refolding transitions of the oxidized and reduced cDsbD at 25°C and pH 7.0 were followed by fluorescence at 345 nm (excitation at 280 nm). The transitions were cooperative and fully reversible (Fig. 1A). Evaluation of the data according to the two-state model yielded ΔG-values of $- 43.9 (\pm 2.9)$ kJ mol^{-1} for cDsbD$_{ox}$ and $- 45.5 (\pm 5.0)$ kJ mol^{-1} for cDsbD$_{red}$, indicating that at pH 7.0 both redox forms are equally stable.

pK_a of the active site Cys461 and reactivity with DTT

To determine the pK_a of the nucleophilic active-site Cys461, we first investigated the pH-dependent reactivity of Cys461 with iodoacetamide (IAM).[6; 7; 8; 9] cDsbD$_{red}$ (5 μM) was mixed with an excess of IAM (between 0.1 mM and 10 mM) in the range of pH 4-10. Samples were removed after different incubation times, and the reaction was quenched with acid. The reaction products were separated by reversed-phase HPLC, and amounts of reduced and IAM-modified cDsbD were quantified by integration of the peak areas. Figure 1B shows the pH-dependence of the apparent second-order rate constant (k_{IAM}) of the alkylation of Cys461 in reduced cDsbD by IAM. The transition appeared to be biphasic as it had previously been described for thioredoxin.[6; 7; 8; 9] Although this method did not provide an exact pK_a value, we can conclude that the pK_a of Cys461 is above 8.0. We then investigated the pH-dependence of the thiolate-specific absorbance at 240 nm.[30; 31; 32] The protein solution (initial concentration of 30 μM) was titrated in the range of pH 4-12 and the absorbance at 240 nm and 280 nm was recorded. Far-UV CD measurements proved that the secondary structure of cDsbD is not changed in this pH-range (data not shown). The titration curves of cDsbD$_{red}$ (circles) and its single cysteine variant cDsbD-Cys464Ser (squares) are depicted in Figure 1C. Both cDsbD$_{red}$ and cDsbD-Cys464Ser showed a single transition with a midpoint at pH 9.2-9.5. From these data we can conclude that Cys461 has an unusually high pK_a of about 9.3 that is similar to the pK_a of a normal cysteine thiol. It has been shown that the pK_a of the nucleophilic active site thiols in DsbA and thioredoxin variants is lowered and correlates with the redox potential of these enzyme.[30; 31; 32] cDsbD has a redox potential of -235 mV.[27; 28] Accordingly, the corresponding theoretical pKa of Cys461 lies between 6 and 7. Although the determined pK_a of cDsbD Cys461 deviates significantly from theory, it is consistent with our results obtained by the IAM-modification method (Fig. 1B) and the identical stabilities of both redox forms.

We also studied the reactivity of $cDsbD_{ox}$ with DTT at 25°C and pH 7.0. Measurements were carried out under pseudo-first order conditions with initial concentrations of $cDsbD_{ox}$ and DTT of 5 μM and 1 mM, respectively. Samples were removed at different incubation times, and the reaction was quenched with acid. Reaction products were separated by reverse-phase HPLC, and amounts of $cDsbD_{ox}$ and $cDsbD_{red}$ were quantified by integration of the peak areas. Figure 1C shows that the reduction of $cDsbD_{ox}$ by DTT is in contrast to electron transfer between other Dsb proteins very slow, with an apparent second order rate constant (15 $M^{-1}s^{-1}$) typical for the thiol-disulfide exchange between small organic molecules.[33]

Crystallization of cDsbD

Oxidized and chemically reduced cDsbD (termed $cDsbD_{ox}$ and $cDsbD_{red}$ from now on) crystallized under the same conditions. The first dataset collected for $cDsbD_{ox}$ turned out to be photoreduced (termed $cDsbD_{pr}$ from now on). A dataset of cDsbD in an intact oxidized state ($cDsbD_{ox}$) was measured from a crystal grown under similar conditions (see experimental part). In both cases the crystals grew within 3 to 5 days. cDsbD formed plate-like crystals with dimensions of about 100 x 650 x 30 μm which were arranged in bundles and star-like structures. Before being removed from the drop the crystal bundles were separated into single-crystal fragments. All crystals belong to the orthorhombic space group $P2_12_12_1$ with similar cell parameters and contain one molecule per asymmetric unit. In comparison, the lower-resolution SeMet cDsbD crystals reported by Kim *et al.* (2003)[21] exhibited the same unit cell (resolution 2.3 Å) and the native crystals contained two molecules per asymmetric unit (resolution 1.9 Å).

X-ray structure determination of cDsbD and structural quality

The X-ray structure of $cDsbD_{ox}$ was first solved by molecular replacement using data from a crystal that diffracted to 1.1 Å and turned out to be photoreduced by synchrotron radiation ($cDsbD_{pr}$). The crystal packing is extremely dense with a very low Matthews-parameter of 1.7 $Å^3Da^{-1}$.

$cDsbD_{pr}$ was refined anisotropically to a resolution of 1.1 Å (Table 1). Given the high resolution of the data, hydrogen atoms could be included into the final stage of refinement. The final R factor is 0.148 and the free R-factor 0.174.

To protect the catalytic disulfide bridge of $cDsbD_{ox}$ from radiation damage, a second dataset was measured using an aluminium filter that decreased the beam intensity to 70.3 % of the original value. A shorter wavelength (0.751 Å) was chosen to reduce radiation damage to the

disulfide bridge.[34] The crystal diffracted to 1.65 Å and the disulfide bridge was found to be intact: no positive or negative difference density is visible at this site (Table 1). $cDsbD_{red}$ data were collected at a wavelength of 1.000 Å to a resolution of 1.3 Å.

The fourth dataset (termed $cDsbD_{red/pH7}$ from now on) was collected from a chemically reduced crystal with a shift to pH 7 at a wavelength of 0.86 Å to a resolution of 0.99 Å using the same aluminium filter as described for $cDsbD_{ox}$ $cDsbD_{red/pH7}$ was anisotropically refined to a resolution of 0.99 Å. Since mostly all main-chain and several side-chain hydrogen atoms were already visible after the fourth refinement cycle they were included into the refinement. All four final atomic models exhibit excellent Ramachandran plot statistics with all residues found in most favoured and additionally allowed regions (Table 1).

Overall structure and comparison of different cDsbD structures

cDsbD possesses a thioredoxin-like fold as already described. In the following we use the nomenclature introduced by Kim *et al.* (2003).[21]

The structure of cDsbD is very rigid. Except for the active-site region, systematic superposition of $cDsbD_{ox}$, $cDsbD_{pr}$ $cDsbD_{red}$ and $cDsbD_{red/pH7}$ reveals no significant structural change. Rmsd-values for all pairs of structures lie in the 0.17 - 0.36 Å range. The sulfur of Cys464 moves by 0.5 Å towards the interior of the protein upon reduction (comparing $cDsbD_{ox}$ and $cDsbD_{red}$). This corresponds to a change by 11° in the $\chi 1$ angle of Cys464. For the accessible Cys461, the φ angle changes by 7° and the $\chi 1$ angle by 9°. The S-S distance in $cDsbD_{red}$ is 3.6 Å.

Upon superposition of the cDsbD domain from the nDsbD-SS-cDsbD complex (termed $cDsbD_{co}$ from now on)[27] onto unliganded cDsbD, only helix α2a (including the two active site cysteines) and Thr529 exhibit differences. In the complex, helix α2a is slightly pulled towards the Cap-loop region of nDsbD (Asp68-Gly72)[18] probably as a consequence of the Cys461 (cDsbD) - Cys109 (nDsbD) disulfide bond formation. The main chain carbonyl of Thr529 is forced by direct van der Waals interactions of the two side chains of Phe11 and Phe108 of nDsbD to take up a different conformation with respect to unbound cDsbD: φ and ϕ change by approximately 10° and 100°, respectively (Figure 2).

In general, compared to nDsbD that undergoes a huge opening of the Cap-loop region upon complex formation,[27] cDsbD exhibits only small structural rearrangements.

Radiation driven disulfide-reduction of cDsbD$_{pr}$

The most radiation-sensitive moieties in proteins are disulfide bonds.[35; 36; 37] The first step of the radiation-driven opening of a disulfide bond is the trapping of an electron (RSSR$^{\bullet-}$). Spontaneous and reversible bond rupture to RS$^{\bullet}$ and RS^{-} can then occur. The protonation of this radical (RSSRH$^{\bullet}$) shifts the equilibrium towards the broken state upon bond rupture to a thiol (RSH) and a thiyl radical (RS$^{\bullet}$). Figure 3 shows an overview of the disulfide opening mechanism.[38; 39; 40; 41]

Analysis of the cDsbD$_{pr}$ data set shows that opening of the Cys461-Cys464 disulfide bridge occurs during data collection. We analysed this phenomenon by partitioning the dataset into eight incremental reflection files. In the first reflection file 150 diffraction images were included. For every additional reflection file, the number of diffraction frames included was increased by 50. An independent refinement with CNS[42] at 1.4 Å resolution was than carried out for each dataset. In all cases, van der Waals interactions between the two sulfur atoms of the active site cysteines were made to be ignored during refinement in CNS. The refined S-S distances were found to increase at each step: from 2.44 Å for the first 150-frames reflection file to 2.65 Å for that containing 500 data-frames. Already for the first reflection file, opening of the disulfide bridge is clearly visible. The observed disulfide distance is 0.39 Å higher than that observed for cDsbD$_{ox}$ (2.05 Å). To analyse the state of the disulfide bridge at the end of the measurement two additional reflection files were created, encompassing frames 349 to 559 (refined S-S distance of 2.96 Å) and of frames 420 to 676 (refined S-S distance of 2.99 Å). These values clearly indicate that even after full crystal exposure the disulfide bridge is not fully reduced (for comparison: cDsbD$_{red}$ shows a distance of 3.56 Å). The analysis is summarized in Table 2.

Comparison with cDsbD in other prokaryotic organisms

18 entries for DsbD were found in a SwissProt database[43] search (www.expasy.org/sprot/). A multiple sequence alignment of the cDsbD domains from those sequences was carried out. Identical sequences were ignored for the alignment. The cDsbD sequence of *Salmonella typhi*, differing from that of *Salmonella typhimurium* by only four residues, all found in highly variable regions, was also ignored. As shown in Figure 4A, *E. coli* has the shortest cDsbD-sequence. Highly conserved regions (Figure 4A) are visible in the multiple sequence alignment. Except for *Campylobacter jejuni* cDsbD, the active site motif is YADW**C**(V,I)(A,S)**C**K. *C. jejuni* exhibits the active site pattern: TASW**C**EN**C**K. This is consistent with the fact that cDsbD of *C. jejuni* has the lowest sequence identity and the

second last similarity of all sequences used. The more distant relationship of *C. jejuni* cDsbD to the rest of the group is also indicated by phylogenetic analysis of the DsbD family and their homologs by Kimbal *et al.*[44] Their tree was built using multiple sequence alignments of the DsbD transmembrane helices 1 to 6 using homolog sequences from all Gram-negative (G-) protobacteria, G-bacteria, Gram positve (G+) bacteria, Archaea, Thermatoga and Cyanobacteria. According to the different branches of the tree, the authors defined the different Dsb-family sequences in 17 clusters. G- proteobacteria Dsb-family proteins and homologs resulted in 5 clusters whereas cluster 1 consists of G- proteobacterial DsbDs. Cluster contains two mean branches. The first branch contains the DsbD protein from *N. meningitidis* and *C. jejuni* whereas the mean branch consists of all the others (Kimbal *et al.* did not include *Vibrio parahaemolyticus*, *Vibrio vulnificus*, *Salmonella typhimurium* and *Ralstonia solanacearum* in the analysis).

The conserved residues were mapped onto the cDsbD structure. Figure 4B indicates that most residues located in the binding interface of cDsbD to nDsbD are highly conserved. Not surprisingly, hardly any conserved residue can be found on the opposite site of the cDsbD surface (Figure 4C).

MATERIALS AND METHODS

Protein purification

(His)$_6$-tagged cDsbD and its single cysteine variant cDsbD-Cys464Ser (a.a numbering corresponds to the mature full length DsbD) were overexpressed in *E. coli*, purified, and protein concentration was determined as described.[27]

Stability measurements

GdmCl-induced unfolding and refolding of oxidized and reduced forms of cDsbD were performed at 25°C in 20 mM HEPES, 170 mM NaCl, 0.1 mM EDTA (pH 7.0). In the case of reduced cDsbD, 0.5 mM DTT was included. For unfolding, 2.5 μM protein was incubated for 15 h with various concentrations of GdmCl. For refolding, 125 μM protein was first denatured with 6 M GdmCl for 3 h at 25°C, then diluted 1:50 into refolding buffer with various concentrations of GdmCl and incubated for 15 h. The transitions were followed by the fluorescence at 345 nm (excitation at 280 nm). Data were evaluated according to the two-state model with a six-parameter fit.[45]

HPLC measurements

HPLC analysis was performed on an Agilent 1100 HPLC instrument equipped with a diode array detection system and an Agilent Zorbax 300 SB C_{18} reversed-phase column (5 mM, 2.1 x 150 mm). Different species of cDsbD were separated at 55°C with a linear gradient from 35 % to 55 % (v/v) of acetonitrile in 0.1 % TFA, and detected by their absorbance at 220 nm and 280 nm. The amounts of reduced, oxidized or IAM-modified forms of cDsbD were quantified by integration of the peak areas.

Determination of the pK_a of the active site Cys461

All experiments were performed at 25°C in the reaction buffer (200 mM KCL, 10 mM disodium hydrogen phosphate, 10 mM boric acid, 10 mM succinic acid, 0.1 mM EDTA), adjusted with HCl or NaOH to pH 4–12. Reduced cDsbD was prepared by reduction with a 1000-fold molar excess of DTT at pH 8.0 for 30 min at room temperature, followed by removal of DTT by gel filtration in degassed buffer.

The ionization of Cys461 was measured by the pH-dependent reactivity with iodoacetamide (IAM).[30; 46] Reactions were performed under pseudo-first order conditions with initial cDsbD$_{red}$ concentration of 5 μM, and IAM concentrations between 0.1 mM and 10 mM. Samples were removed after different incubation times. The reaction was stopped by addition of 0.4 volumes of 30 % (v/v) formic acid (final pH < 2), and HPLC analysis were performed as described. Data were evaluated according to pseudo-first order kinetics. The apparent second-order rate constants (k_{IAM}) were calculated and plotted against pH.

The pK_a of Cys461 in cDsbD or cDsbD-Cys464 was alternatively measured by the pH-dependent thiolate-specific absorbance at 240 nm.[30; 31; 32] Initial protein concentration was 30 μM. The sample absorbance was measured against air and was corrected for the dilution caused by pH adjustment and for the absorbance of a protein-free reference solution, titrated in the same manner. The data was evaluated according to the Henderson-Hasselbach equation as described previously.[31]

HPLC analysis of the reactivity with DTT

Measurements were performed under pseudo-first order conditions with an initial concentration of oxidized cDsbD of 5 μM and 1 mM of DTT at 25°C in 100 mM sodium phosphate, 0.1 mM EDTA (pH 7.0). Samples were removed after different incubation times, and reaction was stopped by addition of 0.4 volumes of 30 % (v/v) formic acid (final pH < 2).

HPLC analyses were performed as described. Data were evaluated according to pseudo-first order kinetics and the apparent second order rate constants were calculated.

Crystallization of cDsbD

Purified cDsbD was concentrated to 19.3 mg/ml. The sitting drop vapour diffusion method was used for producing crystals. In the case of $cDsbD_{pr}$ and $cDsbD_{red}$ 1.4 µl of protein solution were mixed with 2 µl of precipitant solution (0.1 M ammonium acetate, 0.2 sodium acetate pH 4.6, 0.1 M sodium iodide, 40 % PEG 4K and for $cDsbD_{red}$ additionally 0.3 mM TCEP HCl). The crystals used for $cDsbD_{pH7}$ grew under the same condition as that the one used for $cDsbD_{pr}$ and $cDsbD_{red}$, but the drop size was 2 µl (1 µl in protein + 1 µl precipitant solution) each. The second $cDsbD_{ox}$-crystal measured was crystallized in 0.3 M sodium acetate pH 4.6, 0.1 M sodium iodide and 40 % PEG 4K whereas 0.8 µl of protein solution were mixed with 2 µl of precipitant solution. In both cases plate-like crystals grew at 4 °C within three to five days to maximum dimensions for a single crystal of 130 x 500 x 30 µm. Reduced cDsbD was obtained by adding 3 mM Tris(2-carboxyethyl)phosphine (TCEP HCl) to oxidized cDsbD. Crystals grew under the same conditions as described for the oxidized form.

Data collection and structure solution

cDsbD crystals were directly frozen in the nitrogen gas stream. No addition of cryoprotectant was necessary. The first diffraction data of oxidized cDsbD were collected at 90.9 K on beamline X06SA at the Swiss Light Source (Paul Scherrer Institut Villigen, Switzerland) using a MAR CCD image plate at a wavelength of 0.860 Å. This crystal was soaked in saturated cis-$Pt(NH_2)_2Cl_2$ for around 24 hours before mounting. Data were processed with XDS[47] to a resolution of 1.1 Å. To obviate a problem with the spindle acceleration the processed data were corrected with the program check_spindleshutter (Kai Diederichs, personal communication). The structure of cDsbD was solved by molecular replacement with AMoRe[48] using a truncated thioredoxin model[49] (PDB-code: 2TRX) against 12 to 4 Å data. The truncated search model was aptly modified by visual inspection of a stereo picture of cDsbD superimposed on *E. coli* thioredoxin as published by Kim *et al.*, 2003.[21] The cDsbD structure was auto-built using ARP/wARP v6[50] and iteratively rebuilt in O.[51] The structure was first isotropically refined to 1.4 Å using CNS[42] and then anisotropically refined in SHELXL[52] to a R-factor of 0.148 and a free R-factor of 0.175 (Table 1).

Since the oxidized cDsbD dataset exhibits photo reduction of the disulfide bridge (see Results and Discussion), a second dataset was collected using an aluminium filter (reducing intensity to 70.3 % of the original value) with 0.751 Å wavelength and at 98.2 K temperature. Oxidized cDsbD data were processed with DENZO and SCALEPACK[53] to 1.65 Å, respectively.

Diffraction data for TCEP-reduced cDsbD were collected at a temperature of 100 K with a wavelength of 1.000 Å. Data were processed DENZO and SCALEPACK to a resolution of 1.3 Å.

A second TCEP-reduced crystal was soaked for ten minutes at room temperature in a mixture containing 300 µl precipitant solution (0.1 M ammonium acetate, 0.2 sodium acetate, 0.1 M sodium iodide pH 4.6, 40 % PEG 4K and 3 mM TCEP HCl) and 167.5 µl titration solution (0.3 M HEPES base, 0.1 M NaI, 40 % PEG 4K and 3 mM TCEP HCl) with the final pH of 7.0. Diffraction data for TCEP-reduced and pH shifted cDsbD (cDsbD$_{red/pH7}$) were collected at a temperature of 100 K with a wavelength of 0.9718 Å. The dataset was processed with DENZO and SCALEPACK to a resolution of 0.99 Å. All cDsbD crystals (oxidized and TCEP-reduced) belong to space group P2$_1$2$_1$2$_1$ and contain one molecule per asymmetric unit (Table 1).

The position of iodide ions from NaI (in the model of cDsbD$_{ox}$, cDsbD$_{red}$ and cDsbD$_{red/pH7}$) were identified by analysis of Bijvoet difference Fourier map taking also in account of the environment of the major difference peaks.

Stereochemical analysis

The stereochemistry of all four cDsbD structures was checked with WHAT_CHECK[54] and PROCHECK.[55] The photo-reduced and the pH shifted TCEP reduced stuructures were additionally checked with the Protein Anisotropic Refinement Validation and Analysis Tool (PARVATI[56], http://www.bmsc.washington.edu/parvati/parvati.html). All structural figures were prepared using PyMOL[57] (http://www.pymol.org).

Analysis of the disulfide opening

The opening of the active site disulfide bridge was analysed by partitioning the cDsbD$_{pr}$-dataset into eight reflection files. In the first reflection file 150 diffraction images were included. An increment of 50 frames was used for every additional reflection file. Every dataset was then independently refined with CNS[42] and van der Waals interactions between the two sulfurs of Cys461 and Cys464 were made to be ignored. For each model the S-S

distance was measured using the program O.[58]

Acknowledgements

References

1.   Collet, J. F. & Bardwell, J. C. (2002). Oxidative protein folding in bacteria. *Mol Microbiol* 44, 1-8.

2.   Ritz, D. & Beckwith, J. (2001). Roles of thiol-redox pathways in bacteria. *Annu Rev Microbiol* 55, 21-48.

3.   Darby, N. J. & Creighton, T. E. (1995). Catalytic Mechanism of Dsba and Its Comparison with That of Protein Disulfide-Isomerase. *Biochemistry* 34, 3576-3587.

4.   Wunderlich, M., Otto, A., Seckler, R. & Glockshuber, R. (1993). Bacterial protein disulfide isomerase: efficient catalysis of oxidative protein folding at acidic pH. *Biochemistry* 32, 12251-6.

5.   Zapun, A. & Creighton, T. E. (1994). Effects of Dsba on the Disulfide Folding of Bovine Pancreatic Trypsin-Inhibitor and Alpha-Lactalbumin. *Biochemistry* 33, 5202-5211.

6.   Bader, M. W., Xie, T., Yu, C. A. & Bardwell, J. C. (2000). Disulfide bonds are generated by quinone reduction. *J Biol Chem* 275, 26082-8.

7.   Bardwell, J. C., Lee, J. O., Jander, G., Martin, N., Belin, D. & Beckwith, J. (1993). A pathway for disulfide bond formation in vivo. *Proc Natl Acad Sci U S A* 90, 1038-42.

8.   Dailey, F. E. & Berg, H. C. (1993). Mutants in disulfide bond formation that disrupt flagellar assembly in Escherichia coli. *Proc Natl Acad Sci U S A* 90, 1043-7.

9.   Grauschopf, U., Fritz, A. & Glockshuber, R. (2003). Mechanism of the electron transfer catalyst DsbB from Escherichia coli. *Embo J* 22, 3503-13.

10.   Maskos, K., Huber-Wunderlich, M. & Glockshuber, R. (2003). DsbA and DsbC-catalyzed oxidative folding of proteins with complex disulfide bridge patterns in vitro and in vivo. *J Mol Biol* 325, 495-513.

11.   McCarthy, A. A., Haebel, P. W., Torronen, A., Rybin, V., Baker, E. N. & Metcalf, P. (2000). Crystal structure of the protein disulfide bond isomerase, DsbC, from Escherichia coli. *Nat Struct Biol* 7, 196-9.

12.   Missiakas, D., Georgopoulos, C. & Raina, S. (1994). The Escherichia coli dsbC (xprA) gene encodes a periplasmic protein involved in disulfide bond formation. *Embo J* 13, 2013-20.

13.   Zapun, A., Missiakas, D., Raina, S. & Creighton, T. E. (1995). Structural and Functional-Characterization of Dsbc, a Protein Involved in Disulfide Bond Formation in Escherichia-Coli. *Biochemistry* 34, 5075-5089.

14.   Andersen, C. L., Matthey-Dupraz, A., Missiakas, D. & Raina, S. (1997). A new
        Escherichia coli gene, dsbG, encodes a periplasmic protein involved in disulphide
        bond formation, required for recycling DsbA/DsbB and DsbC redox proteins. *Mol
        Microbiol* 26, 121-32.

15.   Bessette, P. H., Cotto, J. J., Gilbert, H. F. & Georgiou, G. (1999). In vivo and in vitro
        function of the Escherichia coli periplasmic cysteine oxidoreductase DsbG. *J Biol
        Chem* 274, 7784-92.

16.   van Straaten, M., Missiakas, D., Raina, S. & Darby, N. J. (1998). The functional
        properties of DsbG, a thiol-disulfide oxidoreductase from the periplasm of Escherichia
        coli. *FEBS Lett* 428, 255-8.

17.   Fabianek, R. A., Hennecke, H. & Thony-Meyer, L. (1998). The active-site cysteines
        of the periplasmic thioredoxin-like protein CcmG of Escherichia coli are important but
        not essential for cytochrome c maturation in vivo. *J Bacteriol* 180, 1947-50.

18.   Goulding, C. W., Sawaya, M. R., Parseghian, A., Lim, V., Eisenberg, D. & Missiakas,
        D. (2002). Thiol-disulfide exchange in an immunoglobulin-like fold: structure of the
        N-terminal domain of DsbD. *Biochemistry* 41, 6920-7.

19.   Haebel, P. W., Wichman, S., Goldstone, D. & Metcalf, P. (2001). Crystallization and
        initial crystallographic analysis of the disulfide bond isomerase DsbC in complex with
        the alpha domain of the electron transporter DsbD. *J Struct Biol* 136, 162-6.

20.   Gordon, E. H., Page, M. D., Willis, A. C. & Ferguson, S. J. (2000). Escherichia coli
        DipZ: anatomy of a transmembrane protein disulphide reductase in which three pairs
        of cysteine residues, one in each of three domains, contribute differentially to
        function. *Mol Microbiol* 35, 1360-74.

21.   Kim, J. H., Kim, S. J., Jeong, D. G., Son, J. H. & Ryu, S. E. (2003). Crystal structure
        of DsbDgamma reveals the mechanism of redox potential shift and substrate
        specificity. *FEBS Letters* 543, 164-169.

22.   Stewart, E. J., Katzen, F. & Beckwith, J. (1999). Six conserved cysteines of the
        membrane protein DsbD are required for the transfer of electrons from the cytoplasm
        to the periplasm of Escherichia coli. *Embo J* 18, 5963-71.

23.   Chung, J., Chen, T. & Missiakas, D. (2000). Transfer of electrons across the
        cytoplasmic membrane by DsbD, a membrane protein involved in thiol-disulphide
        exchange and protein folding in the bacterial periplasm. *Mol Microbiol* 35, 1099-109.

24.   Krupp, R., Chan, C. & Missiakas, D. (2001). DsbD-catalyzed transport of electrons
        across the membrane of Escherichia coli. *J Biol Chem* 276, 3696-701.

25. Rietsch, A., Bessette, P., Georgiou, G. & Beckwith, J. (1997). Reduction of the periplasmic disulfide bond isomerase, DsbC, occurs by passage of electrons from cytoplasmic thioredoxin. *J Bacteriol* 179, 6602-8.

26. Katzen, F. & Beckwith, J. (2000). Transmembrane electron transfer by the membrane protein DsbD occurs via a disulfide bond cascade. *Cell* 103, 769-79.

27. Rozhkova, A., Stirnimann, C. U., Frei, P., Grauschopf, U., Brunisholz, R., Grutter, M. G., Capitani, G. & Glockshuber, R. (2004). Structural basis and kinetics of inter- and intramolecular disulfide exchange in the redox catalyst DsbD. *Embo J* 23, 1709-19.

28. Collet, J. F., Riemer, J., Bader, M. W. & Bardwell, J. C. (2002). Reconstitution of a disulfide isomerization system. *J Biol Chem* 277, 26886-92.

29. Huber-Wunderlich, M. & Glockshuber, R. (1998). A single dipeptide sequence modulates the redox properties of a whole enzyme family. *Fold Des* 3, 161-71.

30. Nelson, J. W. & Creighton, T. E. (1994). Reactivity and ionization of the active site cysteine residues of DsbA, a protein required for disulfide bond formation in vivo. *Biochemistry* 33, 5974-83.

31. Grauschopf, U., Winther, J. R., Korber, P., Zander, T., Dallinger, P. & Bardwell, J. C. (1995). Why is DsbA such an oxidizing disulfide catalyst? *Cell* 83, 947-55.

32. Kortemme, T. & Creighton, T. E. (1995). Ionisation of cysteine residues at the termini of model alpha-helical peptides. Relevance to unusual thiol pKa values in proteins of the thioredoxin family. *J Mol Biol* 253, 799-812.

33. Rothwarf, D. M. & Scheraga, H. A. (1992). Equilibrium and kinetic constants for the thiol-disulfide interchange reaction between glutathione and dithiothreitol. *Proc Natl Acad Sci U S A* 89, 7944-8.

34. Schlichting, I., Berendzen, J., Chu, K., Stock, A. M., Maves, S. A., Benson, D. E., Sweet, R. M., Ringe, D., Petsko, G. A. & Sligar, S. G. (2000). The catalytic pathway of cytochrome p450cam at atomic resolution. *Science* 287, 1615-1622.

35. Burmeister, W. P. (2000). Structural changes in a cryo-cooled protein crystal owing to radiation damage. *Acta Crystallogr D Biol Crystallogr* D56, 328-341.

36. Ravelli, R. B. & McSweeney, S. M. (2000). The 'fingerprint' that X-rays can leave on structures. *Structure Fold Des* 15, 315-328.

37. Schrøder Leiros, H. K., McSweeney, S. M. & Smalås, A. O. (2001). Atomic Resolution structures of trypsin provide insight into structural radiation damage. *Acta Crystallogr D Biol Crystallogr* D57, 488-497.

38.   Weik, M., Berges, J., Raves, M. L., Gros, P., McSweeney, S., Silman, I., Sussman, J. L., Houee-Levin, C. & Ravelli, R. B. (2002). Evidence for the formation of disulfide radicals in protein crystals upon X-ray irradiation. *Journal of Synchrotron Radiation* 9, 342-346.

39.   Armstrong, D. A. (1990). *Sulfur-centered reactive intermediates in chemistry and biology*. NATO ASI series. Series A, Life sciences (Chatgilialoglu, C. & Asmus, K.-D., Eds.), Plenum Press, New York.

40.   von Sonntag, C. (1990). *Sulfur-centered reactive intermediates in chemistry and biology*. NATO ASI series. Series A, Life sciences (Chatgilialoglu, C. & Asmus, K.-D., Eds.), Plenum Press, New York.

41.   Favaudon, V., Tourbez, H., Houee-Levin, C. & Lhoste, J. M. (1990). CO2.- radical induced cleavage of disulfide bonds in proteins. A gamma-ray and pulse radiolysis mechanistic investigation. *Biochemistry* 29, 10978-10989.

42.   Brünger, A. T., Adams, P. D., Clore, G. M., DeLano, W. L., Gros, P., Grosse-Kunstleve, R. W., Jiang, J. S., Kuszewski, J., Nilges, M., Pannu, N. S., Read, R. J., Rice, L. M., Simonson, T. & Warren, G. L. (1998). Crystallography & NMR system: A new software suite for macromolecular structure determination. *Acta Crystallogr D Biol Crystallogr* 54, 905-21.

43.   Boeckmann, B., Bairoch, A., Apweiler, R., Blatter, M. C., Estreicher, A., Gasteiger, E., Martin, M. J., Michoud, K., O'Donovan, C., Phan, I., Pilbout, S. & Schneider, M. (2003). The SWISS-PROT protein knowledgebase and its supplement TrEMBL in 2003. *Nucleic Acids Res.* 31, 365-370.

44.   Kimball, R. A., Martin, L. & Saier, M. H., Jr. (2003). Reversing transmembrane electron flow: the DsbD and DsbB protein families. *J Mol Microbiol Biotechnol* 5, 133-49.

45.   Santoro, M. M. & Bolen, D. W. (1988). Unfolding free energy changes determined by the linear extrapolation method. 1. Unfolding of phenylmethanesulfonyl alpha-chymotrypsin using different denaturants. *Biochemistry* 27, 8063-8068.

46.   Yang, Y. & Wells, W. W. (1991). Identification and characterization of the functional amino acids at the active center of pig liver thioltransferase by site directed mutagenesis. *J Biol Chem* 19, 12759-12765.

47.   Kabsch, W. (1993). Automatic processing of rotation diffraction data from crystals of initially unknown symmetry and cell constants. *J. Appl. Crystallog.* 26, 795-800.

48.   Navaza, J. (1994). AMoRe: an automated package for molecular replacement. *Acta Crystallogr A* A50, 157-163.

49.   Katti, S. K., LeMaster, D. M. & Eklund, H. (1990). Crystal structure of thioredoxin from Escherichia coli at 1.68 Å resolution. *J. Mol. Biol.* 212, 167-84.

50.   Lamzin, V. S. & Wilson, K. S. (1993). Automated refinement of protein models. *Acta cryst.* D49, 129-147.

51.   Jones, T. A., Zou, J.-Y., Cowan, S. W. & Kjeldgaard, M. (1991). Improved methods for building protein models in electron density maps and the location of errors in these models. *Acta Cryst.* A47, 110-119.

52.   Sheldrick, G. M. & Schneider, T. R. (1997). SHELXL: High Resolution Refinement. *Methods in Enzymology*, 319-343.

53.   Otwinowski, Z. & Minor, W., Eds. (1997). Processing of X-ray diffraction data collected in oscillation mode. Vol. 276. Methods in Enzymology. Edited by Carter, C. W. & Sweet, R. M.: Academic Press.

54.   Hooft, R. W. W., Vriend, G., Sander, C. & Abola, E. E. (1996). Errors in protein structures. *Nature* 381, 272-272.

55.   Laskowski, R. A., MacArthur, M. W., Moss, D. S. & Thornton, J. M. (1993). PROCHECK: a program to check the stereochemical quality of protein structures. *Journal of Applied Crystallography* 26, 283-291.

56.   Merritt, E. A. (1999). Comparing anisotropic displacement parameters in protein structures. *Acta Crystallogr D Biol Crystallogr* 55, 1997-2004.

57.   DeLano, W. L. (2002). The PyMol Molecular Graphics System. DeLano Scientific, San Carlos, CA, USA.

58.   Jones, E. Y., Walker, N. P. C. & Stuart, D. I. (1991). Methodology employed for the structure determination of tumour necrosis factor, a case of high non-crystallographic symmetry. *Acta Cryst.* A47, 753-770.

59.   Thompson, J. D., Higgins, D. G. & Gibson, T. J. (1994). CLUSTAL W: improving the sensitivity of progressive multiple sequence alignment through sequence weighting, positions-specific gap penalties and weight matrix choice. *Nucleic Acids Research* 22, 4673-4680.
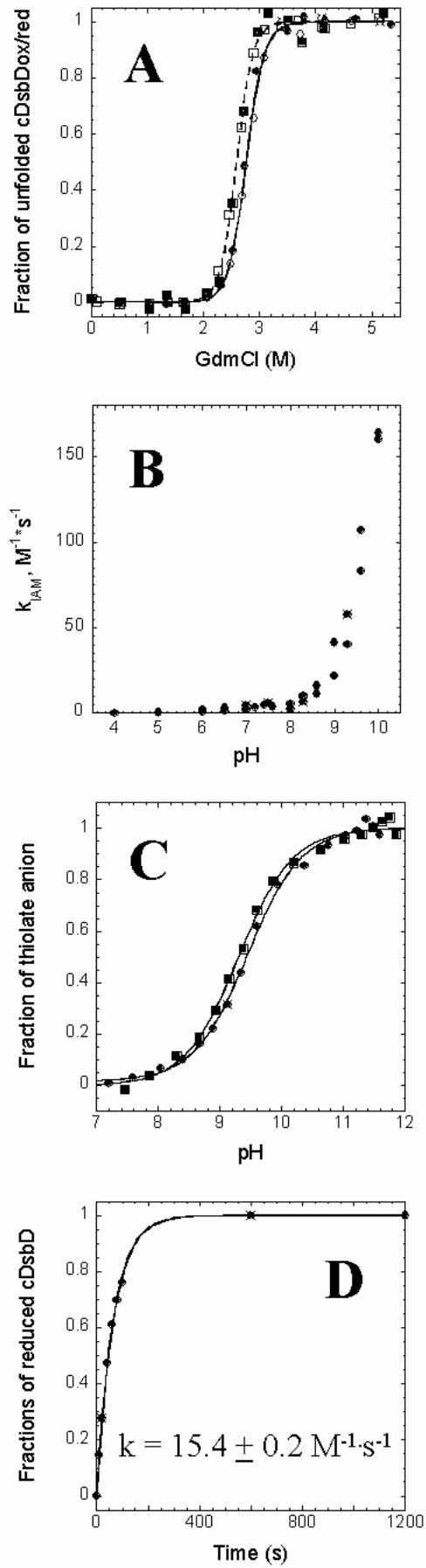
Figure 1. Biophysical properties of cDsbD. (**A**) GdmCl-induced folding and unfolding transitions of oxidized (circles) and reduced (squares) cDsbD at 25°C and pH 7.0. Unfolding (filled symbols) and refolding (open symbols) were followed by the fluorescence at 345 nm (excitation at 280 nm). Original data were evaluated according to the two-state model and normalized. Solid and dashed lines represent the fit for $cDsbD_{ox}$ and $cDsbD_{red}$, respectively. The obtained m-values of 15.9($\pm$ 1.1) kJ mol^{-1} M^{-1} and 17.5($\pm$ 1.9) kJ mol^{-1} M^{-1} and ΔG of – 43.9($\pm$ 2.9) kJ mol^{-1} and –45.5($\pm$ 5.0) kJ mol^{-1} for the oxidized and reduced forms, respectively, are very similar. (**B**) pH-dependence of the active site Cys461 reactivity with IAM. The apparent second-order rate constants (k_{IAM}) were determined by HPLC analysis as described in Methods. (**C**) The pH-dependence of the ionization of the Cys461 thiol of cDsbD (circles) and cDsbD-Cys464Ser (squares). The thiolate-specific absorbance was monitored at 240 nm and the fraction of the thiolate anion was calculated as described in Methods. The fit (solid line) yields a pK_a value of 9.4 for cDsbD and 9.3 for cDsbD-Cys464Ser. (D) Very low reactivity of cDsbD with DTT at 25°C and pH 7.0. The reduction of cDsbD by DTT was performed under pseudo-first order conditions with initial concentrations of 5 μM for $cDsbD_{ox}$ and 1 mM for DTT. The amounts of the reduced and oxidized cDsbD species after different incubation times were quantified by reversed-phase HPLC. The fit (solid line) yields a pseudo-first order rate constant of 0.0154 s^{-1} that corresponds to a second-order rate constant of 15.4 M^{-1}s^{-1}.
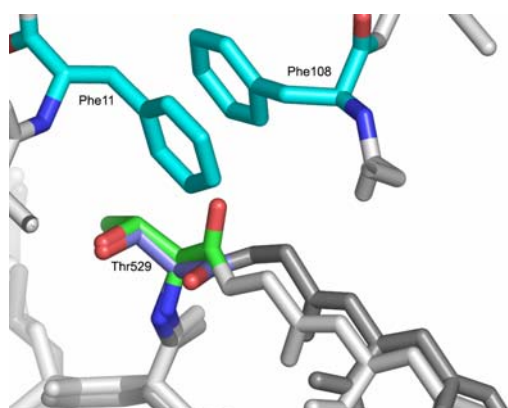
Figure 2. Superposition of cDsbD from the nDsbD-SS-cDsbD complex (light gray, Rozhkova et al., 2004) onto cDsbD$_{pr}$ (dark grey). Conformational change of the main chain carbonyl of Thr529 in cDsbD$_{pr}$ (green) to cDsbD$_{co}$: (blue) forced by direct van der Waals interactions of the two side chains of Phe11 and Phe108 of nDsbD$_{co}$ (cyan) upon complex formation of cDsbD with nDsbD.

RSSR + e$^-$ —> RSSR$^{\bullet-}$ (spontaneous and reversible bond rupture)

or

CO$_2$$^{\bullet-}$ + RSSR —> CO$_2$ + RSSR$^{\bullet-}$ (CO$_2$$^{\bullet-}$ from decarboxylation of Glu)

RSSR$^{\bullet-}$ + H$^+$ —> RSSRH$^{\bullet}$ (disulfide radical with equilibrium towards broken state)

RSSRH$^{\bullet}$ —> RSH + RS$^{\bullet}$ (thiol and thiyl radical)

Figure 3. Mechanism of the disulfide opening in crystals upon synchrotron radiation exposure.[38; 41]

(A)


```
                                                  β1        α1              β2
                        *         20        *         40        *         60        *
DsbD_EC  : ------------------------------THTAQ-TQTHLNETQIKTVDELNQALVEAK--GKPVMLDL : 456
DsbD_ST  : QARRAWMRIVQIILLAAALISVRPLQDWAFGSPSAQ-APAHLNETAISTVDELNQALAQAK--GKPVMLDF : 435
DsbD_STi : QARRAWMRIVQIILLAAALISVRPLQDWAFGSPSAQ-APAHLNETAISTVDELNQALAQAK--GKPVMLDF : 435
DsbD_PC  : ------------------------------PGVTAS-QEQALPEQNIGTVADLQQQLSQAQ--GKITMVDL : 465
DsbD_YP  : ----------------------RPLQDWAFNGNTQQNAVKHINEQPVANLPQLQAVLAQAQ--GKPVMLDL : 478
DsbD_VP  : --------------------------------NHETQAQQTTVSETRIANVAELEEQLALAKAAGKPVMLDF : 481
DsbD_VV  : -------------------------------TDSSQQTQTSEVSEIKIRNVEELQQQLALAKQAKKPVMLDF : 482
DsbD_VC  : --------------------SAQPLLNHWLAPTQTAQQVKQIQETRIANLSELQSALAEAKAQGKSVMLDL : 489
DsbD_HI  : --------------------QNWIWQTQTTTQSAVENMPVSQVKEKQIKNTEELDRTLAENP--HSIAMLDL : 471
DsbD_PM  : --------------------------NRHTPAHQTTSLSQEERITSYAQLQQVLSKNP--NSLAMLDL : 461
DsbD_RS  : -----------------GRDPLQPLAGVMRASAGAQPDARGVVEQRVKSVSEVDEAVRAATAT GRPVMLDF : 457
DsbD_PS  : --------------GGSDDLMKPLQVYSASNSSSAANPVSHDAETTIKDPAALQRELDEAQAGGQWVLLDY : 468
DsbD_PA2 : -------------AAGADDPWRPLQVYAAANRGATPTASAHEAELTVSQPAEIDRQLAAAKAEGQWVLLDY : 477
DsbD_PA1 : --------------QGESDPIHPLGRSVPSIHAGPP--STPGEWQNLTTPAQLDAALAEARQAGKPVLLDW : 481
DsbD_CJ  : ----------------------KNFLNPLNFNTISASKHALSYDYINNFEQLKQEIQTNT---KPIMLDF : 467
DsbD_NM  : -------------NGKTTALHHFLTLNPPAEAGKSSEHGKMFADTAALKAAMDTALKEHP--DKPVVLDL : 494
                                                          6         6              66D
```



```
                 α2a           α2b        β3           α3          β4           β4
                      80        *         100       *         120       *         140
DsbD_EC  : YADWCVACKEFEKYTFSDPQVQKALADTVLLQANVTANDAQDVALLKHLNVLGLPTILFFDGQGQEHPQAR : 527
DsbD_ST  : YADWCVACKEFEKYTFSDPRVQQALGDTVLLQANVTANNAQDVALLKHLQVLGLPTILFFNTQGGQEQPQSR : 506
DsbD_STi : YADWCVACKEFEKYTFSDPRVQQVLGDTVLLQANVTANNAQDVALLKHLQVLGLPTILFFDAQGQEQPQAR : 506
DsbD_PC  : YADWCVACKEFEKYTFTDPQVRQEFSQFRLVQANVTANSAQDNALITHLNVLGLPTILFFDANGHEIPDSR : 536
DsbD_YP  : YADWCVACKEFEKYTFSDDKVQRQLANTLLLQADVTANNAEHATLLKKFNVLGLPTILFFDSQGNEITAAR : 549
DsbD_VP  : YADWCVACKEFEKYTFHDPKVEAKLQDFVLLQADVTKNQVQDIELLKHMNVLGLPTIEFWDAKGEHVSNAR : 552
DsbD_VV  : YADWCVACKEFEKYTFHDPAVAAQLKQFVLLQADVTRNQAQDIELLQAQQVLGLPTIDFWDAQGNPVSNAR : 553
DsbD_VC  : YADWCVACKEFEKYTFHAKQVENKLSGFVLLQADVTKNQPQDIELLKALNVLGLPTIEFWNAQGEPVPNAR : 560
DsbD_HI  : YADWCVACKEFEKLTFSDPQVQQQFQNILLLQVSMTKNSPENKALMERFNVMGLPTILFFDQQNNEIKGSR : 542
DsbD_PM  : YADWCVACKEFETHTFSDVAVQKAFTDVLLQVDMTKNSEANRELMQKLHVIGLPTLIFFNQQGGQEIEGSR : 532
DsbD_RS  : YADWCVSCKEMERLTFTDARVRAALADVVLLQADVTADGADDRALLKRFSLFGPPATIFFDAQGNQAP-VR : 527
DsbD_PS  : YADWCVSCKVMEKQVFGKAHVMEALSDVRLLRLDVTADNAASRELLGRYKVPGPPSLLWIGADGIERRSQR : 539
DsbD_PA2 : YADWCVSCRIMEKQVFAKPDVLAALQGVRLLRLDVTADNAASRELLHRYQVPGPPSLIWIGPEGEERRARR : 548
DsbD_PA1 : YADWCISCKVIERQVLTDPTVQARLPAYRLLRFDITESNPAQRGLLDRYNLFGPPAILFFAPGGDEWSDLR : 552
DsbD_CJ  : TASWCENCKLLDELTFSDERIIQKMQNYKLIKVDVSENNNEQIKTMKEFNVFGPPVLIFFE---NGKEKLK : 535
DsbD_NM  : YADWCISCKEMAAYTLNQPEVHQAVDMERFFQIDVTANTPEHQALLKEYGLFGPEGVFVVRSDGSRSE--P : 563
             yAdWC  C4  e   tf     6         1     63       16     6 G P        g
```
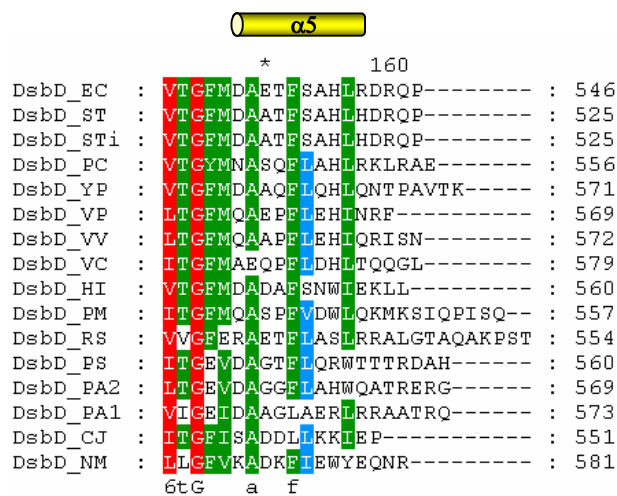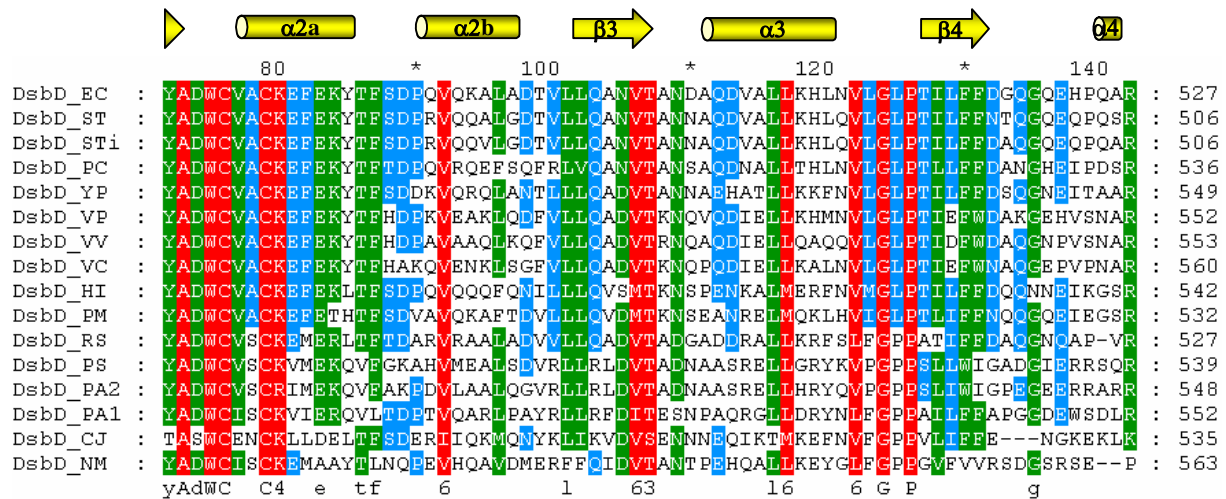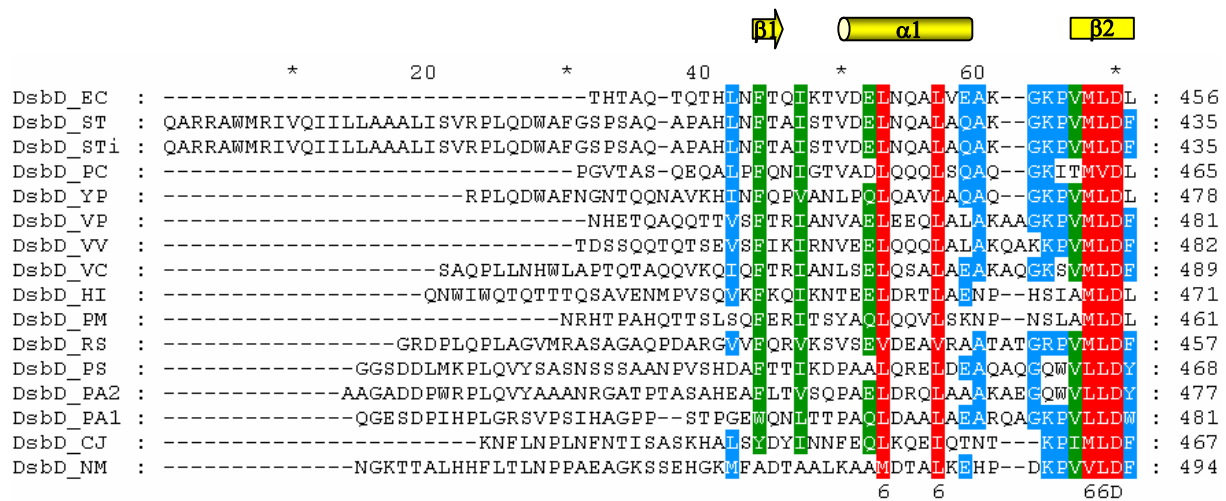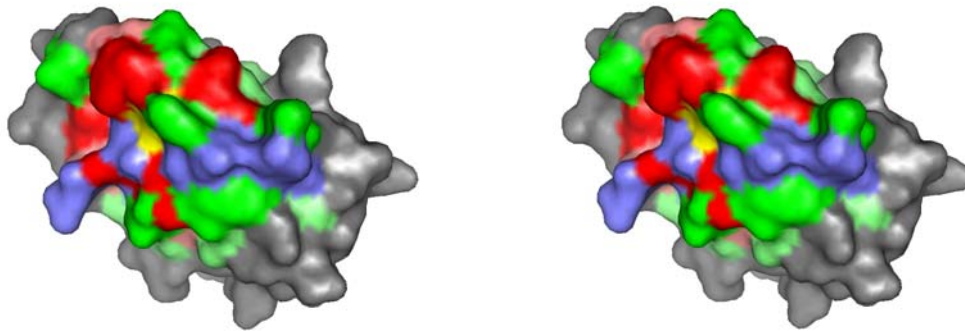


```
                 α5
                      *         160
DsbD_EC  : VTGFMDAETFSAHLRDRQP-------- : 546
DsbD_ST  : VTGFMDAATFSAHLHDRQP-------- : 525
DsbD_STi : VTGFMDAATFSAHLHDRQP-------- : 525
DsbD_PC  : VTGYMNASQFLAHLRKLRAE------- : 556
DsbD_YP  : VTGFMDAAQFLQHLQNTPAVTK----- : 571
DsbD_VP  : LTGFMQAEPFLEHINRF---------- : 569
DsbD_VV  : LTGFMQAAPFLEHIQRISN-------- : 572
DsbD_VC  : ITGFMAEQPFLDHLTQQGL-------- : 579
DsbD_HI  : VTGFMDADAFSNWIEKLL--------- : 560
DsbD_PM  : ITGFMQASPFVDWLQKMKSIQPISQ-- : 557
DsbD_RS  : VVGFERAETFLASLRRALGTAQAKPST : 554
DsbD_PS  : ITGEVDAGTFLQRWTTTRDAH------ : 560
DsbD_PA2 : LTGEVDAGGFLAHWQATRERG------ : 569
DsbD_PA1 : VIGEIDAAGLAERLRRAATRQ------ : 573
DsbD_CJ  : ITGFISADDLLKKIEP----------- : 551
DsbD_NM  : LLGFVKADKFIEWYEQNR--------- : 581
             6tG    a  f
```
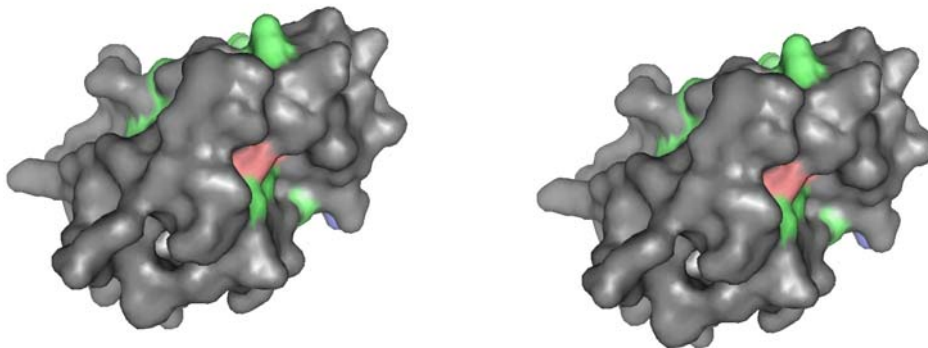
(B)

(C)

Figure 4. (A) Multiple Sequence Alignment of 14 cDsbD sequences from SwissProt[43] using CLUSTALW[59]. Conserved residues are indicated in red, residues >80 % conserved in green and >60 % in blue. On the top the relative alignment numbering and on the right the absolute numbering for all cDsbD sequences is indicated. Abbreviations: EC: *Escherichia coli* cDsbD; ST: *Salmonella typhimurium* cDsbD (66 % sequence identity and 72 % similarity to EC); STi: *Salmonella typhi* cDsbD (67 %, 72 %); PC*: Pantoae citrea* cDsbD (59 %, 72 %); YP*: Yersinia pestis* cDsbD (55 %, 67%); VP: *Vibrio parahaemolyticus* cDsbD (58 %, 70 %); VV: *Vibrio vulnificus* cDsbD (52 %, 64 %); VC: *Vibrio cholerae* cDsbD (49 %, 60 %); HI: *Haemophilus influenzae* cDsbD (45 %, 60 %); PM: *Pasteurella multodica* cDsbD (42 %, 59 %); RS: *Ralstonia solanacearum* cDsbD (42 %, 58 %); PS: *Pseudonomas species* cDsbD (33 %, 47 %); PA2: *Pseudonomas aeruginosa* cDsbD2 (30 %, 45 %); PA1: *Pseudonomas aeruginosa* cDsbD1 (31 %, 45 %); CM: *Camptylobacter jejuni* cDsbD (24 %, 52 %); NM: *Nesseria meningitidis serotype A&B* cDsbD (25 % , 43 %). Secondary structure elements of E. coli cDsbD are shown above aligned sequences in yellow. **(B)** Stereo surface representation of cDsbD mapped by conserved residues. Conserved residues in the binding interface are shown in red, other conserved residues in light red, residues in the binding interface >80 % conserved in green, other residues >80 % conserved in aquamarine, other residues of the binding interface in light blue and the only accessible Cys461 in yellow. **(C)** Stereo surface representation of the cDsbD backside mapped by conserved residues (for colour code see above).

Table 1: Crystallographic data and refinement statistics

Data collection:

Radiation source	SLS Villigen, CH beamline X06SA			
Dataset	$cDsbD_{ox}$	$cDsbD_{pr}$	$cDsbD_{red}$	$cDsbD_{red/H7}$
Wavelength (Å)	0.7514	0.8600	1.0000	0.9718
Space group	$P2_12_12_1$	$P2_12_12_1$	$P2_12_12_1$	$P2_12_12_1$
Unit cell (Å^3)	30.3 46.0 73.8	30.17 45.97 73.82	30.36 46.08 74.14	30.29 46.07 74.07
Resolution range (Å)	20 – 1.65	16 – 1.1	20 – 1.3	15 – 0.99
No. of reflections	88321	166079	138741	337860
No. of unique reflections	13029	42360	25864	58388
Completeness (%)	99.5 (97.7)[§]	99.7 (99.5)[†]	98.2 (87.0)[¥]	99.6 (96.9)[Δ]
R_{sym}	9.3 (44.7)[§]	12.4 (42.9)[†]	9.1 (28.8)[¥]	7.9 (44.5)[Δ]
Average I/σ	19.0 (3.3)[§]	6.9 (3.0)[†]	20.8 (3.1)[¥]	18.8 (2.6)[Δ]
Redundancy	6.8	3.9	5.4	5.8

last shell: [§]1.71 - 1.65 Å [†]1.15 - 1.10 Å [¥]1.35 - 1.30 Å [Δ]1.03 – 0.99

Refinement statistics:

Resolution (Å)	20 – 1.65	15 – 1.1	15 – 1.3	20 – 0.99
No. of reflections (test)	11933 (950)	41402 (953)	25027 (778)	56885 (1437)
R factor	0.1646	0.1488 (a8)	0.1686	0.1227 (a5b)
free R factor	0.2363	0.1738 (a8)	0.1989	0.1677 (a5b)

Table 2: Sulfur-sulfur distances in different datasets

Dataset	distance
cDsbD$_{ox}$	2.05 Å
cDsbD$_{pr}$ (1 150) *	2.44 Å
cDsbD$_{pr}$ (1 200)	2.47 Å
cDsbD$_{pr}$ (1 250)	2.48 Å
cDsbD$_{pr}$ (1 300)	2.51 Å
cDsbD$_{pr}$ (1 350)	2.54 Å
cDsbD$_{pr}$ (1 400)	2.59 Å
cDsbD$_{pr}$ (1 450)	2.62 Å
cDsbD$_{pr}$ (1 500)	2.65 Å
cDsbD$_{pr}$ (349 559)	2.96 Å
cDsbD$_{pr}$ (420 676)	2.99 Å
cDsbD$_{red}$ (TCEP)	3.56 Å
cDsbD$_{pH7}$ (TCEP)	3.55 Å

3.4 Rapid reduction of DsbG by nDsbD (unpublished results)

To gain the complete picture on the kinetics of the disulfide exchange reactions performed by nDsbD, we also determined kinetic parameters of the reduction of DsbG by nDsbD. As in the case of DsbC (3.9×10^6 $M^{-1}s^{-1}$), the reaction is extremely fast, with a rate constant of 1.9×10^6 $M^{-1}s^{-1}$ (Fig. 10, 11). To test whether the fast electron transfer from nDsbD to DsbC or DsbG is due to their dimerization state, we measured kinetics of the disulfide exchange between
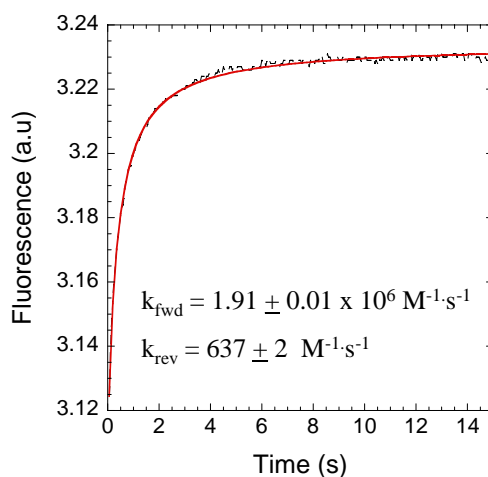

Figure 10. Reduction of DsbG by nDsbD. $(His)_6$-tagged DsbG was overexpressed and purified as described (Bessette *et al.*, 1999). The kinetics of the reduction of DsbG (1 µM) by nDsbD (1 µM) were monitored at 25°C by the change in DsbG fluorescence at 340 nm using stopped-flow mixing in an Applied Photophysics SX-17MV instrument (1:1 mixing ratio). Measurements were performed in 100 mM sodium phosphate, 0.1 mM EDTA, pH 7.0. Data from 20 independent measurements were averaged and evaluated according to second order kinetics. The fit (red solid line) yields a rate constant of 1.9×10^6 $M^{-1}s^{-1}$. Rate constant for the reverse reaction was calculated from the equilibrium constant ($K_{eq} = 3000$) for the reduction of DsbG by nDsbD.

nDsbD and the isolated catalytic domain of DsbC (DsbC-C) or DsbG (DsbG-C). Reduction of DsbG-C by nDsbD proved to be 10 times slower (2.0×10^5 $M^{-1}s^{-1}$, Fig. 12 B) than the reaction between DsbG and nDsbD, which could be caused by lowered effective concentration of the active site cysteines in DsbG-C compared to DsbG. Surprisingly, disulfide exchange between DsbC-C and nDsbD is an extremely slow process with a second-order rate constant of 3.6×10^3 $M^{-1}s^{-1}$ (Fig. 12 A, the data were provided by Patrick Frei). Thus, dimerization of DsbC is likely required for its efficient reduction by nDsbD *in vivo*, rather than for protection active sites of DsbC from DsbB-mediated oxidation as it was proposed earlier (Bader *et al.*, 2001). Overall, through dimerization DsbC gains the second binding site that interacts with the same nDsbD molecule (Fig. 8B) (Haebel *et al.*, 2002), which dramatically increases the affinity.
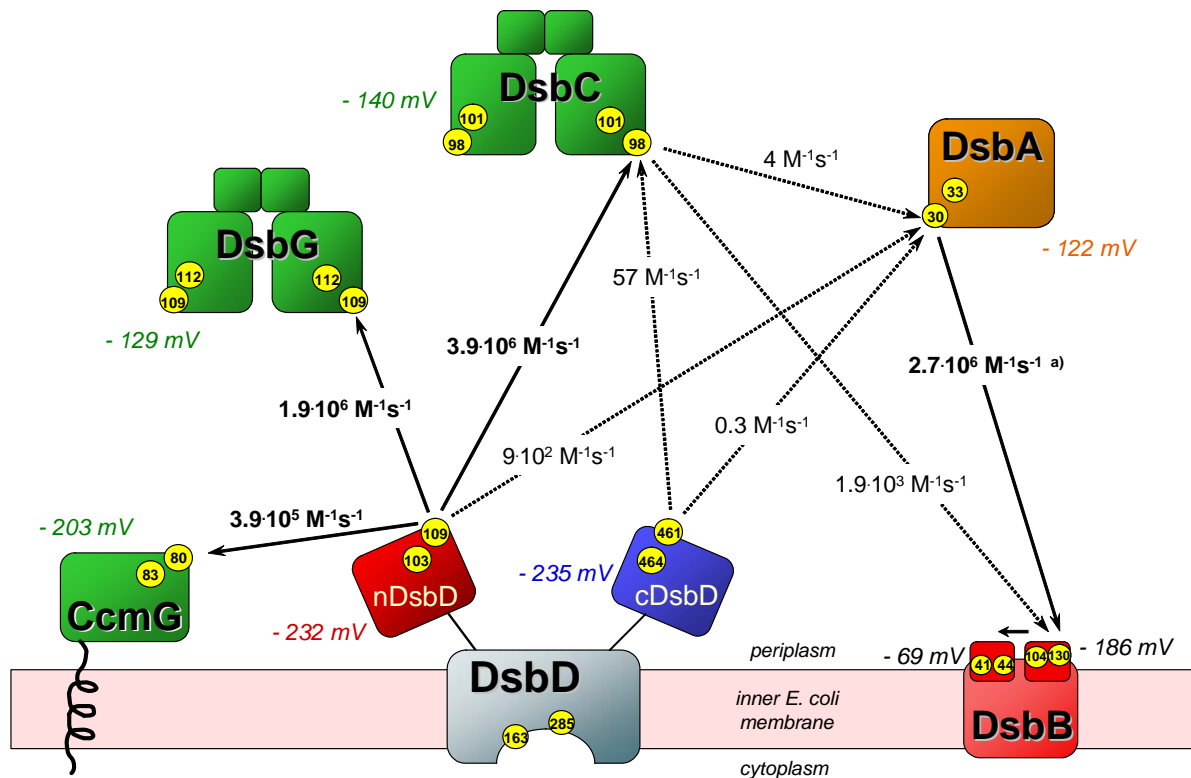
Figure 11. Complete kinetic picture of functional and non-functional disulfide exchange reactions between components of the oxidizing DsbB pathway and the reducing DsbD pathway. Arrows indicate the direction of two-electron transfer. Functional disulfide exchange reactions (solid bold arrows) have second-order rate constants above $10^5 \, M^{-1}s^{-1}$, while non-functional reactions (dotted arrows) are 10^2-10^7-fold slower. [a] (Grauschopf *et al.*, 2003)
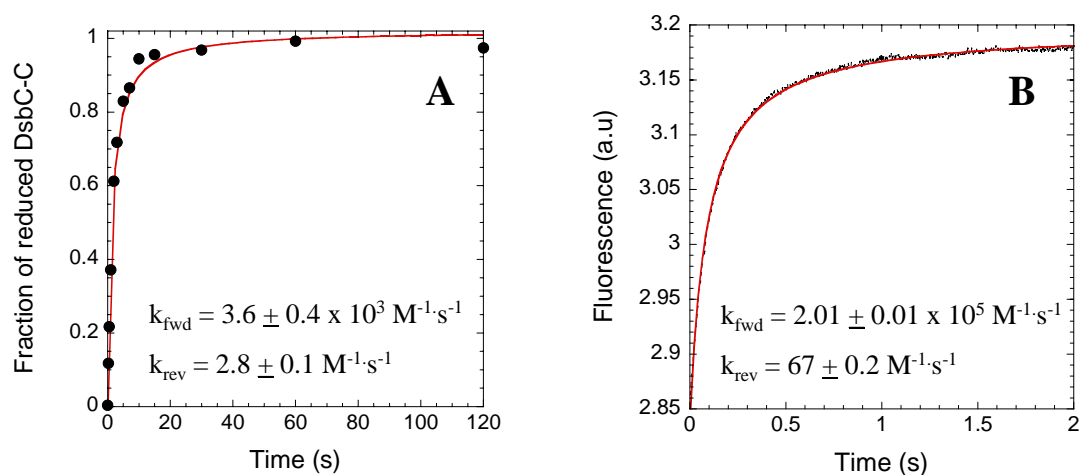

Figure 12. Reduction of DsbC-C and DsbG-C by nDsbD. DsbC-C and DsbG-C were overexpressed and purified according to the protocol used for the wild-type proteins (Bessette *et al.*, 1999; Maskos *et al.*, 2003). **A.** The kinetics of the reduction of DsbC-C$_{ox}$ (3.5 μM) by nDsbD$_{red}$ (3.5 μM) were measured by reversed-phase HPLC as described for DsbC (Rozhkova *et al.*, 2004). **B.** Reduction of DsbG-C$_{ox}$ (1 μM) by nDsbD$_{red}$ (1 μM) was followed by stopped-flow as described above for DsbG. All measurements were performed in 100 mM sodium phosphate, 0.1 mM EDTA, pH 7.0. Data were evaluated according to second-order kinetics. The fit (red solid line) yields rate constants of $3.6 \times 10^3 \, M^{-1}s^{-1}$ and of $2.0 \times 10^5 \, M^{-1}s^{-1}$ for the reduction of DsbC-C and DsbG-C, respectively. Rate constants for the reverse reactions were calculated from the equilibrium constants for the reduction of DsbC ($K_{eq} = 1300$) or DsbG ($K_{eq} = 3000$) by nDsbD, respectively.

References

Bader, M.W., Hiniker, A., Regeimbal, J., Goldstone, D., Haebel, P.W., Riemer, J., Metcalf, P., and Bardwell, J.C. (2001) Turning a disulfide isomerase into an oxidase: DsbC mutants that imitate DsbA. *Embo J* **20**: 1555-1562.

Bessette, P.H., Cotto, J.J., Gilbert, H.F., and Georgiou, G. (1999) In vivo and in vitro function of the Escherichia coli periplasmic cysteine oxidoreductase DsbG. *J Biol Chem* **274**: 7784-7792.

Grauschopf, U., Fritz, A., and Glockshuber, R. (2003) Mechanism of the electron transfer catalyst DsbB from Escherichia coli. *Embo J* **22**: 3503-3513.

Haebel, P.W., Goldstone, D., Katzen, F., Beckwith, J., and Metcalf, P. (2002) The disulfide bond isomerase DsbC is activated by an immunoglobulin-fold thiol oxidoreductase: crystal structure of the DsbC-DsbDalpha complex. *Embo J* **21**: 4774-4784.

Maskos, K., Huber-Wunderlich, M., and Glockshuber, R. (2003) DsbA and DsbC-catalyzed oxidative folding of proteins with complex disulfide bridge patterns in vitro and in vivo. *J Mol Biol* **325**: 495-513.

Rozhkova, A., Stirnimann, C.U., Frei, P., Grauschopf, U., Brunisholz, R., Grutter, M.G., Capitani, G., and Glockshuber, R. (2004) Structural basis and kinetics of inter- and intramolecular disulfide exchange in the redox catalyst DsbD. *Embo J* **23**: 1709-1719.

4. Oxidative protein folding in eukaryotes versus *E. coli*: analogies and differences

In eukaryotes, folding and assembly of secretory and membrane proteins containing disulfide bonds take place in the endoplasmic reticulum (ER). The environment of the ER lumen provides the pH and redox conditions required for folding. A growing family of ER thioredoxin-like oxidoreductases is thought to be responsible for the formation of native disulfide bonds in the ER. Protein disulfide isomerase (PDI) is the most prominent and best characterized member of this family and an essential enzyme in all eukaryotes. PDI was discovered by Anfinsen's group in early 1960's as a component of microsomal extracts that assisted the refolding of RNAse A and lysozyme (Goldberger *et al.*, 1963, 1964). PDI is composed of four thioredoxin-like domains (**a**-**b**-**b′**-**a′**), followed by the acidic **c** domain. There is an extensive internal sequence similarity between the **a** domain and the **a′** domain as well as between the **b** domain and the **b′** domain. The two redox active site sequences of PDI (C-G-H-C) are located in the **a** and **a′** domains, and the active site cysteine residues are required for PDI activity (Laboissiere *et al.*, 1995; Vuori *et al.*, 1992). PDI is a multifunctional enzyme capable of catalyzing formation, reduction and isomerization of disulfide bonds in proteins *in vitro*. The oxidative activity of PDI is also established *in vivo*. For example, oxidative folding of the secretory marker protein carboxypeptidase Y (CPY) depends on direct oxidation by PDI in yeast (Frand and Kaiser, 1999; Holst *et al.*, 1997). The capture of mixed-disulfides between PDI and CPY indicates direct thiol-disulfide exchange between PDI and the substrate protein in the ER (Frand and Kaiser, 1999). Upon oxidation of thiols in substrate proteins, PDI becomes reduced and must be re-oxidized. Since glutathione is the major redox buffer in the ER, and the ratio of reduced (GSH) to oxidized (GSSG) glutathione in the ER (between 1:1 and 3:1) provides optimal conditions for oxidative refolding of proteins *in vitro*, it was believed that glutathione was responsible for re-oxidation of the PDI active sites. However, elimination of glutathione from the yeast cell by removal of the enzyme involved in the first step of synthesis, γglutamylcysteine synthetase, did not prevent disulfide bond formation, but rendered the cells more prone to hyperoxidation, suggesting that glutathione functions as a net reductant in the ER (Cuozzo and Kaiser, 1999). Both genetic and biochemical approaches in yeast showed that the conserved membrane-associated ER protein Ero1 is responsible for the oxidation of PDI (Chakravarthi and Bulleid, 2004; Frand and Kaiser, 1998; Tu *et al.*, 2000; Tu and Weissman, 2002). Defects in Ero1 lead to a lack of disulfide bond formation, whereas overexpression of Ero1 accelerates the rate of

oxidative protein folding and the acquisition of a native structure, demonstrating that Ero1 is an essential component of the oxidative folding machinery (Chakravarthi and Bulleid, 2004; Frand and Kaiser, 1998; Pollard *et al.*, 1998; Sevier and Kaiser, 2002). Ero1 is an FAD-dependent enzyme that is able to oxidize PDI directly through disulfide exchange and pass electrons to the terminal electron acceptor, molecular oxygen (Frand and Kaiser, 1999; Tu *et al.*, 2000). Ero1 can catalyze oxidation of PDI also under anaerobic conditions, indicating that alternative electron acceptors could be used in the absence of oxygen (Sevier *et al.*, 2001). It has been shown that PDI / Ero1-catalyzed disulfide bond formation proceeds independent of glutathione both *in vivo* and *in vitro* (Cuozzo and Kaiser, 1999; Tu *et al.*, 2000). Thus Ero1 and PDI constitute an oxidative pathway (Fig. 13), analogous to the DsbA/B pathway in *E. coli*, that independently of the bulk redox environment catalyzes rapid disulfide formation in eukaryotes. An important implication of this finding is that the flow of oxidizing equivalents
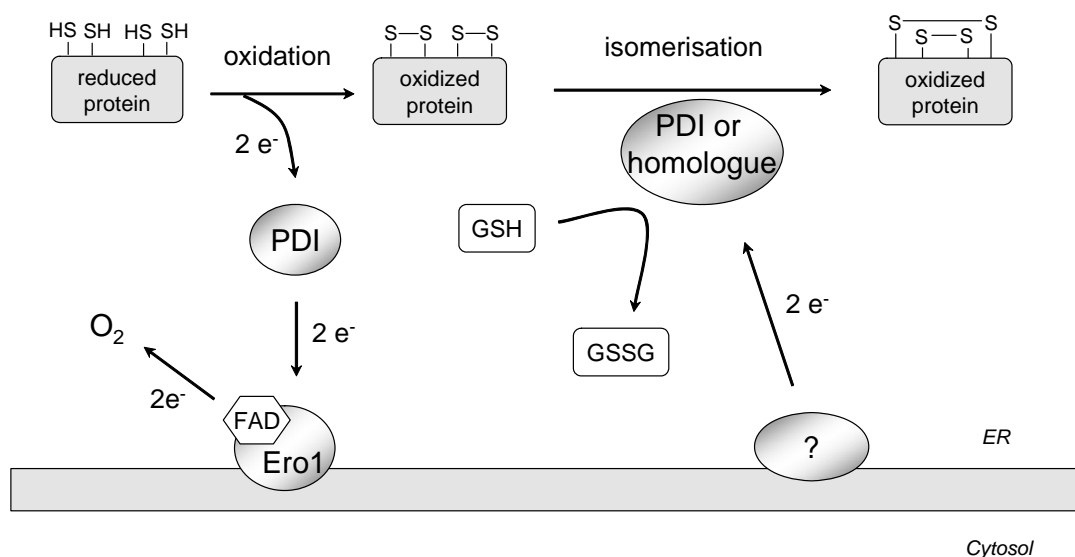

Figure 13. Schematic model of oxidative protein folding in the ER. The formation of disulfide bonds in the ER is catalyzed by PDI and Ero1. Disulfide isomerization may be performed by PDI or some of its homologues that are possibly kept in the active reduced state by GSH or by a not yet identified redox catalyst. (Tu and Weissman, 2004)

in the ER is controlled by the kinetics of the disulfide exchange between proteins rather than by equilibration of protein thiols and disulfides with glutathione redox buffer.

The formation of native disulfide bonds not only involves oxidative pairing of free thiols, but also isomerization of wrongly formed disulfides in proteins with multiple disulfide bonds. Eukaryotic secretory proteins typically contain more disulfide bonds than their prokaryotic counterparts, indicating that there is an even greater need for disulfide bond isomerization function in the ER than in the periplasm. Although many proteins are able to

fold spontaneously in a glutathione buffer in the absence of oxidoreductases, the folding rate is dramatically increased in the presence of PDI (Weissman and Kim, 1993). In addition to a kinetic advantage, the catalyzed reduction or isomerization of disulfide bonds in proteins has the advantage that the enzymes favour the formation of native over non-native disulfides. The most obvious candidate for the role of the disulfide isomerase in the ER is PDI that is by far the most active disulfide isomerase *in vitro*. An attractive model is that PDI catalyzes all types of reactions important for oxidative protein folding *in vivo*, namely disulfide bond formation, reduction and isomerization. Combination of the oxidase, the reductase and the isomerase activities requires that redox active sites of PDI would either alternatively exist in the oxidized or reduced state, or that one of them would be kept in the oxidized state and the other in the reduced state *in vivo*. Recently, Tai and Rapoport (2005) showed that Ero1 oxidizes only the **a′** domain (Tsai and Rapoport, 2002). Moreover, Ero1 seems to be more efficient in oxidizing substrate-associated PDI compared to free PDI (Tsai and Rapoport, 2002). This would prevent futile redox cycles of PDI in the absence of substrate, in which free oxidized PDI would be reduced by GSH. Since the **a** domain is not a substrate of Ero1, it could be kept in reduced state for example by the glutathione redox buffer and function as an isomerase or a reductase. This assumption is consistent with the observation that PDI is partially reduced in the ER of yeast (Xiao *et al.*, 2004).

Another possibility is that individual members of the PDI family might be dedicated to the catalysis of disulfide bond formation, reduction or isomerization *in vivo*, just as DsbA and DsbC work in separate pathways to catalyze disulfide bond formation and isomerization in the bacterial periplasm. In this context, it is not surprising that there are four PDI homologues in the ER of yeast and dozens more are found in higher eukaryotes. Several of these oxidoreductases exist in a predominantly reduced form in the cell and therefore could act as substrate-specific reductases or isomerases (Mezghrani *et al.*, 2001; Tu and Weissman, 2004). In yeast, one or more of the PDI homologues appeared to contribute to the maturation of CPY that requires disulfide bond isomerization *in vitro* (Xiao *et al.*, 2004).

Since disulfide bond isomerization can be catalyzed by oxidoreductases only in reduced state, there must be a reductive pathway in the ER. The existing data indicate that glutathione plays a role in the formation of native disulfide bonds in the ER (Chakravarthi and Bulleid, 2004; Jessop *et al.*, 2004). Chacravarthi and Bulleid (2004) showed that a normal level of intracellular glutathione is required to prevent the formation of non-native disulfide bonds during the post-translational folding in the ER of human tissue type plasminogen activator that contains 17 disulfide bonds. The detection of a mixed disulfide between

glutathione and Erp57, an analogue of PDI, led to the conclusion that GSH can reduce the ER oxidoreductases directly (Jessop *et al.*, 2004). However, these data do not prove that the direct reduction of the ER oxidoreductases by glutathione is the only existing or main reductive pathway in the ER. It could well be that glutathione contributes to the overall redox equilibrium in the eukaryotic cell, rather than directly participating in the disulfide reduction in the ER proteins. In this case, the reducing equivalents required for the disulfide bond isomerization in the ER could come through a separate enzyme-catalyzed pathway, analogous to the reductive DsbC/DsbD pathway in *E. coli*. In this model, glutathione (or another low molecular weight reductant) could serve as a source of reducing power in the eukaryotic cell that would be transferred by a redox catalyst to the ER oxidoreductases (Fig. 13).

Dependence of the formation of native disulfides in proteins both in prokaryotes and eukaryotes on oxidative and reductive reactions, and therefore requirement of catalytic pathways for maintaining the appropriate redox state of the oxidoreductases, raises the question of how the two seemingly opposing pathways can coexist within the same intracellular compartment. Appling the principles discovered in prokaryotes, the segregation of the oxidative and the reductive pathways could be explained by kinetic barriers between the two pathways. Indeed, fast and specific oxidation of PDI by Ero1 well explains effective disulfide bond formation in the ER in the presence of GSH. On the other hand, the inability of Ero1 to oxidize the a domain and some of PDI homologues (Mezghrani *et al.*, 2001; Tu and Weissman, 2004) can cause their accumulation in the reduced state such that they function as disulfide isomerases or reductases in the presence of glutathione redox buffer. However, the reduction of these enzymes by glutathione may be not rapid enough to support protein folding in the cell, and not yet identified redox catalyst(s), analogous to DsbD, could be required. In this context, complete kinetic analysis of the possible disulfide exchange reactions between the ER components involved in native disulfide bond formation would provide important information about the intracellular role of glutathione and the mechanism of oxidative protein folding in eukaryotes.

References

Chakravarthi, S., and Bulleid, N.J. (2004) Glutathione is required to regulate the formation of native disulfide bonds within proteins entering the secretory pathway. *J Biol Chem* **279**: 39872-39879.

Cuozzo, J.W., and Kaiser, C.A. (1999) Competition between glutathione and protein thiols for disulphide-bond formation. *Nat Cell Biol* **1**: 130-135.

Frand, A.R., and Kaiser, C.A. (1998) The ERO1 gene of yeast is required for oxidation of protein dithiols in the endoplasmic reticulum. *Mol Cell* **1**: 161-170.

Frand, A.R., and Kaiser, C.A. (1999) Ero1p oxidizes protein disulfide isomerase in a pathway for disulfide bond formation in the endoplasmic reticulum. *Mol Cell* **4**: 469-477.

Goldberger, R.F., Epstein, C.J., and Anfinsen, C.B. (1963) Acceleration of reactivation of reduced bovine pancreatic ribonuclease by a microsomal system from rat liver. *J Biol Chem* **238**: 628-635.

Goldberger, R.F., Epstein, C.J., and Anfinsen, C.B. (1964) Purification and Properties of a Microsomal Enzyme System Catalyzing the Reactivation of Reduced Ribonuclease and Lysozyme. *J Biol Chem* **239**: 1406-1410.

Holst, B., Tachibana, C., and Winther, J.R. (1997) Active site mutations in yeast protein disulfide isomerase cause dithiothreitol sensitivity and a reduced rate of protein folding in the endoplasmic reticulum. *J Cell Biol* **138**: 1229-1238.

Jessop, C.E., Chakravarthi, S., Watkins, R.H., and Bulleid, N.J. (2004) Oxidative protein folding in the mammalian endoplasmic reticulum. *Biochem Soc Trans* **32**: 655-658.

Laboissiere, M.C., Sturley, S.L., and Raines, R.T. (1995) The essential function of protein-disulfide isomerase is to unscramble non-native disulfide bonds. *J Biol Chem* **270**: 28006-28009.

LaMantia, M.L., and Lennarz, W.J. (1993) The essential function of yeast protein disulfide isomerase does not reside in its isomerase activity. *Cell* **74**: 899-908.

Mezghrani, A., Fassio, A., Benham, A., Simmen, T., Braakman, I., and Sitia, R. (2001) Manipulation of oxidative protein folding and PDI redox state in mammalian cells. *Embo J* **20**: 6288-6296.

Pollard, M.G., Travers, K.J., and Weissman, J.S. (1998) Ero1p: a novel and ubiquitous protein with an essential role in oxidative protein folding in the endoplasmic reticulum. *Mol Cell* **1**: 171-182.

Sevier, C.S., Cuozzo, J.W., Vala, A., Aslund, F., and Kaiser, C.A. (2001) A flavoprotein oxidase defines a new endoplasmic reticulum pathway for biosynthetic disulphide bond formation. *Nat Cell Biol* **3**: 874-882.

Sevier, C.S., and Kaiser, C.A. (2002) Formation and transfer of disulphide bonds in living cells. *Nat Rev Mol Cell Biol* **3**: 836-847.

Tsai, B., and Rapoport, T.A. (2002) Unfolded cholera toxin is transferred to the ER membrane and released from protein disulfide isomerase upon oxidation by Ero1. *J Cell Biol* **159**: 207-216.

Tu, B.P., Ho-Schleyer, S.C., Travers, K.J., and Weissman, J.S. (2000) Biochemical basis of oxidative protein folding in the endoplasmic reticulum. *Science* **290**: 1571-1574.

Tu, B.P., and Weissman, J.S. (2002) The FAD- and O(2)-dependent reaction cycle of Ero1-mediated oxidative protein folding in the endoplasmic reticulum. *Mol Cell* **10**: 983-994.

Tu, B.P., and Weissman, J.S. (2004) Oxidative protein folding in eukaryotes: mechanisms and consequences. *J Cell Biol* **164**: 341-346.

Vuori, K., Myllyla, R., Pihlajaniemi, T., and Kivirikko, K.I. (1992) Expression and site-directed mutagenesis of human protein disulfide isomerase in Escherichia coli. This

multifunctional polypeptide has two independently acting catalytic sites for the isomerase activity. *J Biol Chem* **267**: 7211-7214.

Weissman, J.S., and Kim, P.S. (1993) Efficient catalysis of disulphide bond rearrangements by protein disulphide isomerase. *Nature* **365**: 185-188.

Xiao, R., Wilkinson, B., Solovyov, A., Winther, J.R., Holmgren, A., Lundstrom-Ljung, J., and Gilbert, H.F. (2004) The contributions of protein disulfide isomerase and its homologues to oxidative protein folding in the yeast endoplasmic reticulum. *J Biol Chem* **279**: 49780-49786.

5. Outlook

The most intriguing and difficult question about the catalytic mechanism of DsbD is electron transfer across the inner membrane. Despite the intensive studies on DsbD during last 10 years, its TM domain remains poorly characterized. For example, such a basic property as the redox potential is not yet determined. We do not know whether DsbD needs a co-factor for its function, and if not, how could a single pair of cysteine residues be sufficient for electron transfer across ~60 Å membrane space? It is also not clear, which cysteine in the TM domain mediates the disulfide exchange between the TM domain and cDsbD.

One of the difficulties in the characterizing the disulfide exchange reaction between DsbD domains is the fact that the wild type domains of DsbD show no change in fluorescence upon reduction/oxidation. To solve this problem, we engineered a Trp-variant of cDsbD (cDsbD-Y457W), which doubles its fluorescence signal upon reduction. This amino acid replacement does not affect stability, redox potential and reactivity of the protein. Based on the Y457W mutation, spectroscopically active DsbD constructs can be designed. For example, a truncated DsbD variant lacking nDsbD and bearing the Y457W replacement would be a useful tool for investigation of the disulfide exchange between the TM domain and cDsbD. A fusion construct with nDsbD and cDsbD-Y457W linked *via* a flexible linker of different length can be used to estimate the rate of the intramolecular disulfide exchange between the periplasmic domains of DsbD and their effective concentrations in the context of full-length DsbD.

In vitro reconstitution of the entire electron flow from NADPH, thioredoxin reductase and thioredoxin to DsbC *via* DsbD is an important and necessary proof of the proposed mechanism. However, the reconstitution could not be achieved simply by mixing the purified components in solution, as there is comparably fast direct electron transfer from thioredoxin to nDsbD, cDsbD or DsbC (circumventing electron flow through the TM domain). Incorporation of DsbD into liposomes thus seems to be a very attractive approach. First of all, the membrane protein would be in the environment close to the natural and could adopt proper conformation. Second, it would allow separation of the cytosolic and periplasmic components of the pathway by the membrane and therefore would exclude the above-mentioned side reactions. Third, presence of the membrane gives a possibility to adjust the pH and ionic strength conditions corresponding to the cytosol and the periplasm.

Finally, determination of the X-ray structure of full-length DsbD is of high interest. The X-ray structure of the nDsbD-SS-cDsbD mixed disulfide, which was determined in this work, could be used to solve the structure of DsbD through molecular replacement.

6. Curriculum vitae

Name: Anna Rozhkova

Date of birth: March 27, 1979

Place of birth: Moscow

Nationality: Russian Federation

Education:

1985-1995:   School, Moscow, Russian Federation

1995-2000:   Studies at Moscow State University, Russian Federation

2000:   Diplom in Biochemistry

2000-2001:   Trainings in Biophysics in group of Prof. Victor Tsetlin, Institute of
                         Bioorganic Chemistry, RAS, Moscow, Russian Federation

2001-2005:   PhD thesis at the Institut für Molekularbiologie und Biophysik,
                         Eidgenössische Technische Hochschule Zürich, Switzerland, under
                         supervision of Prof. Rudi Glockshuber

7. Acknowledgments

First of all, many thanks to my supervisor Prof. Rudi Glockshuber for the opportunity to work on this PhD project, for all ideas and discussions, and for being a perfect Boss.

Thanks to Prof. Linda Thöny-Meyer for waking up my interest to the cytochrome *c* maturation.

Dr. Guido Capitani, Christian Stirnimann, and Prof. Markus Grütter, I thank for the fruitful collaboration in crystallization and structure determination.

I also thank all members of the group of Prof. Glockshuber. I say my especial thanks to Dr. Ulla Grauschopf for the excellent permanent help during the whole PhD work, for the perfect advises and suggestions, for all the knowledge, shared with me, and for critical reading of this thesis. Thanks to Patrick Frei and Goran Malojčić for many fruitful discussions and collaboration. I thank Andrea Fritz for cloning of some constructs and for being a source of sparkling life energy in the lab. Thanks to Dr. Eva Künnemann-Zobeley for the introduction into the stopped-flow technique. Dr. Michael Vetsch and Prof. EilikaWeber-Ban, I thank for the introduction into kinetics, for the help with data analysis, and for being my co-examiner. Thanks to Dr. John Grimshaw for critical reading of this thesis.

Finally, I would like to thank the members of the Protein Service Lab, Dr. René Brunisholz for a lot of help with HPLC experiments and for Edman sequencing, and Helene Rechsteiner for MALDI-MS measurements.